Department of Communications and Networking

Backhaul Link Enhancement and Radio Resource Management for Relay Deployments

Ömer Bulakçı

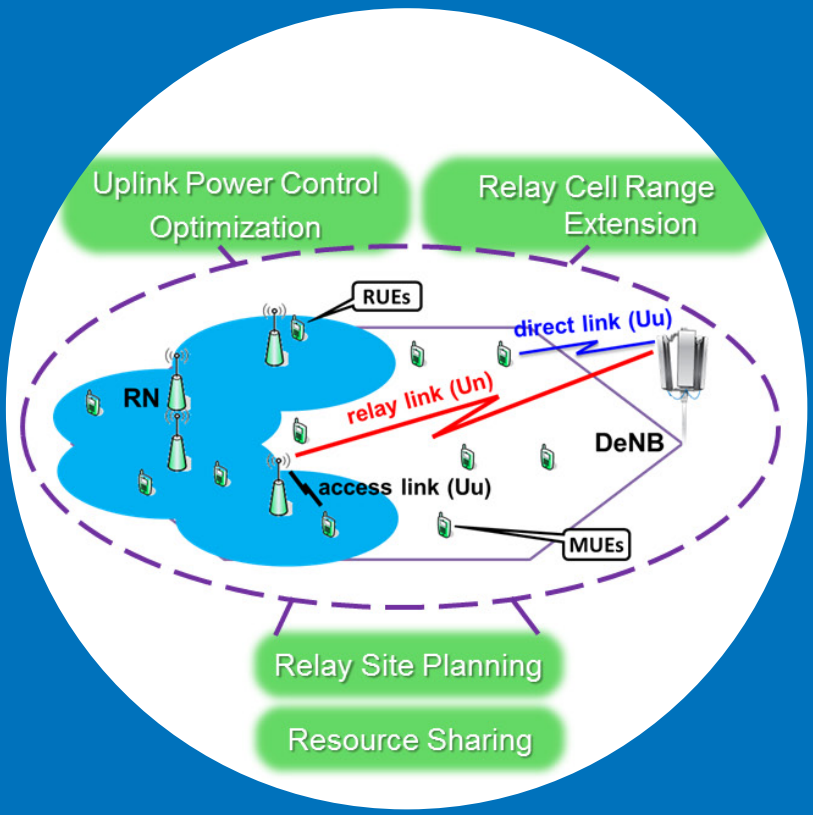

Aalto University

DOCTORAL DISSERTATIONS

Aalto University publication series
DOCTORAL DISSERTATIONS 103/2013

Backhaul Link Enhancement and Radio Resource Management for Relay Deployments

Ömer Bulakçı

A doctoral dissertation completed for the degree of Doctor of Science (Technology) to be defended, with the permission of the Aalto University School of Electrical Engineering, at a public examination held at the lecture hall S3 of the school on the 14th of June 2013 at 12 o'clock (at noon).

Aalto University
School of Electrical Engineering
Department of Communications and Networking

Supervising professor
Prof. Jyri Hämäläinen (Aalto University, Finland)

Thesis advisor
Dr. Simone Redana (Nokia Siemens Networks, Germany)

Preliminary examiners
Prof. S. Ben Slimane (KTH Royal Institute of Technology, Sweden)
Dr. Antti Tölli (University of Oulu, Finland)

Opponent
Prof. Mikko Valkama (Tampere University of Technology, Finland)

Aalto University publication series
DOCTORAL DISSERTATIONS 103/2013

ISBN 978-952-60-5222-9 (printed)
ISBN 978-952-60-5223-6 (pdf)
ISSN-L 1799-4934
ISSN 1799-4934 (printed)
ISSN 1799-4942 (pdf)
http://urn.fi/URN:ISBN:978-952-60-5223-6

Unigrafia Oy
Helsinki 2013

Finland

441 697
Printed matter

Aalto University

Abstract

Aalto University, P.O. Box 11000, FI-00076 Aalto www.aalto.fi

Author
Ömer Bulakçı

Name of the doctoral dissertation
Backhaul Link Enhancement and Radio Resource Management for Relay Deployments

Publisher School of Electrical Engineering

Unit Department of Communications and Networking

Series Aalto University publication series DOCTORAL DISSERTATIONS 103/2013

Field of research Communications Engineering

Manuscript submitted 31 January 2013 **Date of the defence** 14 June 2013

Permission to publish granted (date) 30 April 2013 **Language** English

☐ **Monograph** ☒ **Article dissertation (summary + original articles)**

Abstract

Mobile networks are experiencing a dramatic increase in the data traffic. Besides, a continuously growing number of users expect mobile broadband access with the utmost in quality and ubiquitous connectivity. In this regard, multi-hop decode-and-forward relaying is a promising enhancement to existing radio access networks to fulfill the challenging requirements in a cost-efficient way and, thus, is an integral part of the Fourth Generation (4G) standards. Nevertheless, in order to fully exploit the potential benefits of relay deployments, proper radio resource management (RRM) is necessary.

The research in this thesis has contributed to cellular relay deployments for future mobile networks. Concretely, we have developed key RRM concepts with a particular focus on the uplink (UL) system performance to complement the existing literature. We have demonstrated the performance of these concepts by taking Third Generation Partnership Project (3GPP) Long-Term Evolution (LTE) Release 10 and beyond (LTE-Advanced) Type 1 inband relaying as a practical framework, and by considering urban and suburban scenarios. First, by performing relay site planning (RSP) we aim at improving the quality of the wireless backhaul which is crucial for the end-to-end user performance. Then, we analyze UL power control (PC) and verify its importance and applicability in relay deployments. In this context, we propose manual and automated optimizations to tune PC parameters on all links to further enhance the system performance. Moreover, we study the energy efficiency by taking into account throughput (TP) per power consumption. Further, we investigate various resource sharing strategies among and within the links. Via proposed approaches, performance enhancement is targeted along with higher system fairness and more flexible resource allocation. In addition, we address a key issue regarding the small coverage area of an RN cell in the overlaying macrocell, which results in load imbalances, inefficient resource utilization, and increased UL inter-cell interference. Specifically, we apply practical cell range extension (CRE) techniques to cope with these drawbacks.

Performance evaluations reveal that relay deployments clearly outperform macrocell-only deployments in terms of TP as well as TP per power consumption provided that proper RRM is performed. Our results also verify that the use of RSP yields substantial improvements. Furthermore, our results show that the proposed RRM concepts and the associated joint optimization strategies can fulfill the aforementioned goals while achieving significant system performance enhancements.

Keywords Decode-and-Forward, Inband Relay, Mobile Networks, RRM, Site Planning

ISBN (printed) 978-952-60-5222-9 **ISBN (pdf)** 978-952-60-5223-6

ISSN-L 1799-4934 **ISSN (printed)** 1799-4934 **ISSN (pdf)** 1799-4942

Location of publisher Espoo **Location of printing** Helsinki **Year** 2013

Pages 257 **urn** http://urn.fi/URN:ISBN:978-952-60-5223-6

Preface

The research work for this doctoral thesis has been carried out at the Department of Communications and Networking (ComNet) of Aalto University School of Electrical Engineering (formerly known as Helsinki University of Technology), Espoo, Finland, in collaboration with the Department of Radio Systems, Nokia Siemens Networks (NSN), Munich, Germany during 2009-2012. This work was funded by NSN.

First of all, I would like to express my deepest gratitude to my supervisor Prof. Jyri Hämäläinen for his continuous support, encouragement, for many enlightening discussions throughout this work and, especially, for availing me this opportunity. I would also like to sincerely thank my advisor Dr. Simone Redana from NSN who has provided me with the necessary support and guidance at all phases of this work. It has been a pleasure and a great honor to work with them.

Special thanks to Abdallah Bou Saleh with whom I had numerous fruitful discussions, authored multiple publications presented in this thesis, and handled various challenges together. I would also like to thank my co-author Bernhard Raaf for the delightful discussions on relaying and patents, which clearly influenced my work. Next, I would like to thank my co-author Ahmad Awada for fruitful teamwork and thoughtful discussions.

I acknowledge my M.Sc. thesis students Dereje W. Kifle, Andrei S. Nedelcu, and Zhe Ren for their contributions. Special thanks to my co-author Dr. Ingo Viering for the fruitful discussions on various topics presented in this thesis and for his encouragement. I would like to thank my other co-authors Aydin Karaer, Dr. Bernhard Wegmann, and Prof. Fabrizio Granelli for their contributions. I acknowledge Michael Färber, Peter Merz, Rüdiger Halfmann, and Andreas Lobinger for facilitating the necessary resources at NSN to conduct this work. I would like to thank my

other colleagues at NSN for the good time and support, including Federica Vitiello, Isil Burcu Barla, and Wolfgang Mennerich.

I would like to thank the thesis pre-examiners Prof. S. Ben Slimane and Dr. Antti Tölli for their comments and suggestions. I am grateful to Prof. Risto Wichman for being in charge of my supplementary field. I am also grateful to my ComNet colleagues Dr. Alexis Dowhuszko especially for his help during the preparations for my thesis writing, Osman N. C. Yilmaz, Furqan Ahmad and Anzil A. Rasheed for making my stays in Helsinki pleasant, and resource manager Viktor Nässi and financial secretary Sanna Patana for their continuous assistance. Also, I would like to express my appreciation to my friends Scott Steeg and Katherine McGinley for their useful tips for the thesis writing.

I would like to take this opportunity to pay my gratitude to people who are close to me for their unique support throughout this work during both the high and low times: Anna Neudecker, Volkan Öztürk, Onur Ucaner, Onurcan Iscan, Furkan Dayi, A. Eray Topak, Can Uz, Dr. Matthias Schuster, M. Fatih Aksoy, Evren Sahin, and Daniils Dikanskis.

My special intimate thanks go to my family for the love and encouragement they have given me over the years.

Munich, May 22, 2013,

Ömer Bulakçı

Contents

List of Publications

This thesis consists of an overview and of the following publications which are referred to in the text by their Roman numerals.

I Ö. Bulakci, S. Redana, B. Raaf, J. Hämäläinen. Performance Enhancement in LTE-Advanced Relay Networks via Relay Site Planning. In *IEEE Vehicular Technology Conference (VTC Spring 2010)*, Taipei, Taiwan, pp. 1-5, May 2010.

II Ö. Bulakci, A. Bou Saleh, J. Hämäläinen, S. Redana. Performance Analysis of Relay Site Planning over Composite Fading/Shadowing Channels with Cochannel Interference. *IEEE Transactions on Vehicular Technology (TVT)*, vol. 62, no. 4, pp. 1692-1706, May 2013.

III Ö. Bulakci, J. Hämäläinen, A. Bou Saleh, S. Redana, B. Raaf. Impact of Preconditioning on the Convergence of Numerical Co-channel Interference Approximations in Heterogeneous Networks. In *IEEE International Wireless Communications and Mobile Computing Conference (IWCMC 2011)*, Istanbul, Turkey, pp. 119-124, July 2011.

IV Ö. Bulakci, S. Redana, B. Raaf, J. Hämäläinen. Impact of Power Control Optimization on the System Performance of Relay based LTE-Advanced Heterogeneous Networks. *Journal of Communications and Networks (JCN)*, Special Issue on Heterogeneous Networks, vol. 13, no. 4, pp. 345-359, August 2011.

V Ö. Bulakci, A. Awada, A. Bou Saleh, S. Redana, J. Hämäläinen. Auto-

mated Uplink Power Control Optimization in LTE-Advanced Relay Networks. *EURASIP Journal on Wireless Communications and Networking (WCN)*, [Highly Accessed] vol. 2013, no. 8, pp. 1-19, January 2013.

VI A. Bou Saleh, Ö. Bulakci, S. Redana, B. Raaf, J. Hämäläinen. Evaluating the Energy Efficiency of LTE-Advanced Relay and Picocell Deployments. In *IEEE Wireless Communications and Networking Conference (WCNC 2012)*, Paris, France, pp. 2335-2340, April 2012.

VII Ö. Bulakci, A. Bou Saleh, S. Redana, B. Raaf, J. Hämäläinen. Resource Sharing in LTE-Advanced Relay Networks: Uplink System Performance Analysis. *Transactions on Emerging Telecommunications Technologies (ETT)*, [Invited Paper] Special Issue on Multi-Carrier Transmission, LTE and LTE-Advanced, vol. 24, issue 1, pp. 32-48, January 2013.

VIII Ö. Bulakci, A. S. Nedelcu, A. Bou Saleh, S. Redana, J. Hämäläinen. Impact of Backhaul Subframe Misalignment on Uplink System Performance of LTE-Advanced Relay Networks. In *IEEE Vehicular Technology Conference (VTC Fall 2012)*, Quebec City, Canada, pp. 1-6, September 2012.

IX Ö. Bulakci, A. Bou Saleh, S. Redana, B. Raaf, J. Hämäläinen. Enhancing LTE-Advanced Relay Deployments via Relay Cell Extension. In *the 15th International OFDM Workshop (InOWo 2010)*, Hamburg, Germany, pp. 1-6, September 2010.

X A. Bou Saleh, Ö. Bulakci, S. Redana, J. Hämäläinen. On Cell Range Extension in LTE-Advanced Type 1 Inband Relay Networks. Accepted for publication in *Wireless Communications and Mobile Computing (WCM)*, December 2012.

XI D. W. Kifle, Ö. Bulakci, A. Bou Saleh, S. Redana, G. Fabrizio. Joint Backhaul Co-scheduling and Relay Cell Extension in LTE-Advanced Networks: Uplink Performance Evaluation. In *IEEE/VDE European Wireless Conference (EW 2012)*, Poznan, Poland, pp. 1-8, April 2012.

Author's Contribution

Publication I: "Performance Enhancement in LTE-Advanced Relay Networks via Relay Site Planning"

The author of this thesis had the lead role in this paper. The techniques provided in this paper have been developed in cooperation among the authors. Furthermore, the author of this thesis has analyzed the techniques, carried out the system-level simulations and has written the entire paper.

Publication II: "Performance Analysis of Relay Site Planning over Composite Fading/Shadowing Channels with Cochannel Interference"

The author of this thesis had the lead role in this paper. The general framework of this work has been developed in cooperation among the authors. The author of this thesis has deduced the closed-form expressions and has analyzed the techniques provided in this paper. Furthermore, the author of this thesis has carried out the system-level simulations and has written the entire paper.

Publication III: "Impact of Preconditioning on the Convergence of Numerical Co-channel Interference Approximations in Heterogeneous Networks"

The author of this thesis had the lead role in this paper. The author of this thesis has proposed the preconditioning techniques provided in this paper, where the general framework of the paper has been developed in cooperation among the authors. Furthermore, the author of this thesis

has analyzed the techniques, carried out the system-level simulations and has written the entire paper.

Publication IV: "Impact of Power Control Optimization on the System Performance of Relay based LTE-Advanced Heterogeneous Networks"

The author of this thesis had the lead role in developing and analyzing the techniques provided in this paper. The author has carried out the system-level simulations via MARS[1]. Furthermore, the author of this thesis has written the entire paper.

Publication V: "Automated Uplink Power Control Optimization in LTE-Advanced Relay Networks"

The author of this thesis had the lead role in this paper. The techniques provided in this paper have been developed in cooperation among the authors. The author of this thesis has proposed the performance steering concept and has carried out the system-level simulations via MARS[1]. The author of this thesis has written the entire paper except Sections 4.2 and 4.3.

Publication VI: "Evaluating the Energy Efficiency of LTE-Advanced Relay and Picocell Deployments"

The author of this thesis had one of the lead roles in this paper and has contributed to the development of energy efficiency modeling. In addition, the author of this thesis has conducted uplink analyses and has carried out the uplink system-level simulations via MARS[1]. The author of this thesis has written the uplink-related part entirely and has assisted in writing the paper.

[1]MARS, which stands for Matlab based Enhanced Relay Simulator, is a system-level snap-shot simulator which is developed by the author of this thesis for the doctoral studies.

Publication VII: "Resource Sharing in LTE-Advanced Relay Networks: Uplink System Performance Analysis"

The author of this thesis had the lead role in developing and analyzing the techniques provided in this paper. The author of this thesis has carried out the system-level simulations via MARS[1] and has written the entire paper.

Publication VIII: "Impact of Backhaul Subframe Misalignment on Uplink System Performance of LTE-Advanced Relay Networks"

The author of this thesis had the lead role in developing and analyzing the techniques provided in this paper. The author of this thesis has carried out the majority of the system-level simulations via MARS[1] and has written the entire paper.

Publication IX: "Enhancing LTE-Advanced Relay Deployments via Relay Cell Extension"

The author of this thesis had one of the lead roles in this paper and has contributed to the development of relay cell range extension modeling. In addition, the author of this thesis has conducted uplink analyses and has carried out the uplink system-level simulations via MARS[1]. The author of this thesis has written the uplink-related part entirely and had the main role in writing the paper.

Publication X: "On Cell Range Extension in LTE-Advanced Type 1 Inband Relay Networks"

The author of this thesis had one of the lead roles in this paper and has contributed to the development of relay cell range extension modeling. In addition, the author of this thesis has conducted uplink analyses and has carried out the uplink system-level simulations via MARS[1]. The author of this thesis has written the uplink-related part entirely and has assisted in writing the paper.

Publication XI: "Joint Backhaul Co-scheduling and Relay Cell Extension in LTE-Advanced Networks: Uplink Performance Evaluation"

The author of this thesis had one of the lead roles in this paper and has contributed to the development of the investigated techniques and the corresponding analyses. D. W. Kifle has carried out the uplink system-level simulations via MARS[1]. The author of this thesis has assisted in writing the paper.

List of Abbreviations and Symbols

Abbreviations

3GPP	Third Generation Partnership Project
4G	Fourth Generation
AIT-P	access instantaneous TP-proportional
AM	arithmetic mean
AMC	adaptive modulation and coding
AoF	amount of fading
ARTIST4G	Advanced Radio Interface Technologies for 4G Systems
ATB	adaptive transmission bandwidth
AUP	access UE proportional
BS	base station
CDF	cumulative distribution function
CDMA	Code Division Multiple Access
CoMP	coordinated multipoint
CRE	cell range extension
DeNB	donor eNB
DL	downlink
EARTH	Energy Aware Radio and Network Technologies
eNB	evolved Node B

FCPC	full compensation PC
FDD	frequency division duplex
FPC	fractional PC
HM	harmonic mean
HSPA	High Speed Packet Access
ID	identity
IEEE	Institute of Electrical and Electronics Engineering
IMT-Advanced	International Mobile Telecommunications - Advanced
IoT	Interference over Thermal noise
ISD	inter-site distance
ITU-R	International Telecommunication Union-Radiocommunication Sector
LOS	line-of-sight
LTE	Long-Term Evolution
LTE-Advanced	Long-Term Evolution-Advanced
MCS	modulation and coding scheme
MG distribution	mixture gamma distribution
MGF	moment generating function
MIMO	multiple-input multiple-output
MT	mobile terminal
MUE	macro-UE
NLOS	non-LOS
NOA	nearly orthogonal array
OA	orthogonal array
OAM	operations, administration, and maintenance
OFDMA	Orthogonal Frequency Division Multiple Access
OPEX	operational expenditure

PAPR	peak-to-average power ratio
PC	power control
PDCCH	Physical Downlink Control Channel
PDF	probability distribution function
PRB	physical resource block
PSD	power spectral density
PUCCH	Physical Uplink Control Channel
PUSCH	Physical Uplink Shared Channel
QAM	quadrature amplitude modulation
QoS	quality of service
Rel.	Release
RN	relay node
R-PDCCH	relay-specific PDCCH
R-PUSCH	relay-specific PUSCH
RRM	radio resource management
RSP	relay site planning
RSRP	reference signal received power
RUE	relay-UE
RV	random variable
Rx	reception
SC-FDMA	Single Carrier - Frequency Division Multiple Access
SDMA	Spatial Division Multiple Access
SINR	signal-to-interference-plus-noise ratio
SIR	signal-to-interference ratio
SNR	signal-to-noise ratio
SON	self-organizing networks

TP	throughput
TPC	TP power consumption
TTI	transmission time interval
Tx	transmission
UE	user equipment
UIT-P	UE instantaneous TP-proportional
UL	uplink
Un	the interface between DeNB and RN
Un subframe	backhaul subframe
Uu	the interface between access point and UE
Uu subframe	regular subframe
WCDMA	Wideband Code Division Multiple Access

Symbols

$2b_0$	average power of the scatter component in Rician fading
$\mathcal{C}$	set of candidate cells for cell association
$\mathcal{C}_{\mathrm{DeNB}}$	set of candidate DeNB cells for cell association
$\mathcal{C}_{\mathrm{RN}}$	set of candidate RN cells for cell association
d_1	distance between the serving BS and the midmost RN location
d_2	distance between the midmost RN location and a candidate location in RN location trellis 1
d_{cor}	shadowing de-correlation distance
$d_{m,k}$	distance between m^{th} potential relay location and k^{th} BS
$d_{m,n}$	distance between m^{th} and n^{th} potential relay locations
G	antenna gain
K	Rician factor

L	DL path loss estimate
$L_{m,k}$	path loss including shadowing at the m^{th} potential relay location toward the k^{th} BS
M	number of candidate RN locations in RSP
M_{r}	total number of PRBs in a Un subframe
M_{r}^{*}	total number of PRBs reserved for the relay link transmissions
M_u	number of PRBs allocated to a node u
m_{AL}	Nakagami parameter on the access link (AL)
m_{CL}	Nakagami parameter on a communication link (CL)
m_c	number of resources assigned to MUEs per Un subframe in a cell
m_i	resource share of RN i on the relay link
m_{ij}	resource share of RUE j served by RN i on the access link
m_{RL}	Nakagami parameter on the relay link (RL)
N_{b}	number of Un subframes out of 10
P_0	power offset
$P_{\max}$	maximum allowed transmit power
P_N	thermal noise power
P_{r}	radiated power
$P_{\text{Tx},k}$	transmit power of the k^{th} BS
P_u	transmit power of a node u
R_a	rate on the access link
$R_{e;m,k}$	end-to-end rate on the relay link at the m^{th} potential relay location in the k^{th} cell
R_{ijk}	per-PRB spectral efficiency on the access link of UE j to its serving RN i for PRB k
R_{ik}	per-PRB spectral efficiency of the RN i for PRB k
$R_{r;m,k}$	rate on the relay link at the m^{th} potential relay location in the k^{th} cell

$S^2_{m,k}$	power envelope of the multipath fading channel on the link between k^{th} BS and m^{th} potential relay location
$\text{TP}^{\text{a}}_{ij}$	user capacity of RUE j served by RN i on the access link
$\text{TP}^{\text{e}}_{ij}$	end-to-end TP of RUE j served by RN i
$\text{TP}^{\text{r}}_{ij}$	user capacity of RUE j served by RN i on the relay link
U_{c}	total number of all UEs in a cell
U_{RN}	total number of RUEs in a cell
u_i	number of UEs attached to RN i
α	path loss compensation factor
α_{p}	a propagation constant
β	path-loss exponent
γ	instantaneous SNR
$\bar{\gamma}$	average SNR
ε	effective biasing
$\zeta_{m,k}$	shadowing RV at the m^{th} potential relay location toward the k^{th} BS
ζ_{RN}	resource share of RNs per Un subframe
$\eta_{m,k}$	shadowing component at the m^{th} potential relay location toward the k^{th} BS
μ	shadowing mean
μ_{dB}	shadowing mean in decibels
ξ_m	shadowing component at the m^{th} potential relay location
ρ	shadowing correlation coefficient
ρ_{RN}	RUE fraction in the cell
σ	shadowing standard deviation
σ_{dB}	shadowing standard deviation in decibels
τ_a	time resources allocated for the access link
τ_r	time resources allocated for the relay link
τ_{UE}	UE time activity factor

$\Upsilon_{m,k}$	relay link SINR for the m^{th} potential relay location in the k^{th} cell
$\widetilde{\Upsilon}_{m,k}$	approximated relay link SINR for the m^{th} potential relay location in the k^{th} cell
$\Upsilon_{\hat{m},k}$	relay link SINR at the selected location
χ	power envelope of the shadowed Rician fading channel
Ω	average power of the LOS component in Rician fading

1. Introduction

1.1 Motivation

The number of mobile subscriptions has grown at an astonishingly rapid pace in recent years [1, 2]. This growth is coupled with an increasing number of data-intensive wirelessly-connected devices, such as smartphones and tablets. Additionally, next-generation applications and multimedia services, e.g., high-definition video, video chat, and real-time gaming, that require significant amount of data transfer are spreading and increasingly becoming part of everyday life. The result is a dramatic increase in the mobile data traffic and tremendous demand for mobile broadband access with the expectation of seamless connectivity along with high quality of service (QoS).

To address these challenges, International Telecommunication Union-Radiocommunication Sector (ITU-R) has specified the requirements to be satisfied by International Mobile Telecommunications-Advanced (IMT-Advanced) technologies for Fourth Generation (4G) mobile networks. Accordingly, ITU-R issued a circular letter in March 2008 calling for candidate radio access technologies [3]. The two official IMT-Advanced standards are Third Generation Partnership Project (3GPP) Long-Term Evolution (LTE) Release (Rel.) 10 and beyond (LTE-Advanced) and Institute of Electrical and Electronics Engineering (IEEE) 802.16m (wireless metropolitan area networks (WirelessMAN)- Advanced) [4]. For instance, LTE-Advanced fulfills and even exceeds the IMT-Advanced requirements [1, 5, 6].

The set of stringent requirements for future mobile networks necessitates a paradigm shift from conventional cellular network infrastructure consisting of costly high-power macrocell deployments toward cost-

efficient heterogeneous deployments comprising low-power nodes, such as picocells and relay nodes (RNs). In this context, multi-hop decode-and-forward relaying is a key enhancement technology [7] and, thus, is an integral part of both LTE-Advanced and WirelessMAN-Advanced [8, 9]. RNs are relatively small nodes which connect to the core network with wireless backhaul through a base station (BS). The wireless backhaul (a.k.a. backhaul link or relay link) enables deployment flexibility and eliminates the high costs of a fixed backhaul. Thanks to the compact physical characteristics and low power consumption, RNs can be mounted on structures, e.g., lamp posts with power supply facilities. Furthermore, RNs do not have strict installation guidelines with respect to radiation, visual disturbance, and planning regulation. Accordingly, it is shown that installing RNs involves lower operational expenditure (OPEX) [10] and faster network upgrade [11]. Further cost-efficiency evaluations of RNs are given in [12, 13, 14]. In addition, RNs promise to increase the network capacity [15, 16, 17] or alternatively extend the cell coverage area [15, 18, 19, 20, 21]. Nevertheless, relay deployments will require a more detailed dimensioning and planning than conventional single-hop networks. Besides, given the full frequency reuse in 4G mobile networks, RN cells can cause severe inter-cell interference especially when a large number of RNs are deployed in a cell. This, in turn, implies substantially different interference characteristics in relay deployments.

Consequently, in order to realize the potential benefits of relay deployments in a cost-efficient manner and to achieve further performance enhancements, proper radio resource management (RRM) is essential. In this regard, RRM concepts should factor in not only the links between mobile terminals (MTs) toward BSs or RNs, but also the relay link as it determines the end-to-end performance of MTs served by RNs. Moreover, a power control (PC) mechanism, which takes into account both channel variations and interference characteristics, is required for each link on the uplink (UL). However, a large part of the previous literature on relay deployments focuses on the downlink (DL) performance.

1.2 Scope of the Thesis and Research Questions

The focus of this thesis is on design and performance analysis of fixed inband RNs which control their own cells. RNs are deployed in the overlaying macrocell coverage area to improve the system performance while

targeting a more homogeneous user performance. Motivated by the importance of RRM, this thesis develops and verifies key RRM concepts for relay deployments to ensure the expected performance enhancements. In addition, a particular emphasis is put on the UL system performance that is not extensively investigated in the existing literature.

As a practical scenario, we consider LTE-Advanced Type 1 inband relay deployments [22]. Within this framework, we carry out analyses and provide system-level performance evaluations for the studied RRM strategies in different propagation environments. Moreover, a joint optimization of these RRM strategies is conducted, and various performance trade-offs are discussed. Further, recalling the vital role of the relay link for the overall system performance, we investigate means to improve its quality.

Accordingly, the following main research questions are addressed in this work.

1. How much can the performance of relay deployments be improved by simple site planning techniques?

2. How should UL PC parameters be selected when RNs are added to the network, and what are the performance impacts and trade-offs of the selected parameter settings?

3. How to design effective resource sharing for UL in relay deployments, and what is the available performance gain from the well-designed resource sharing?

4. How to effectively utilize the resource over-provisioning in RN cells?

1.3 Contributions and Structure of the Thesis

The work undertaken in this thesis contributes to the field of RRM for cellular networks enhanced by relay deployments. The performance of relay deployments significantly depends on the capacity of the relay link. Therefore, we utilize relay site planning (RSP) to improve the relay link by exploiting the deployment flexibility of RNs. We investigate the effect of RSP on the relay link signal-to-interference-plus-noise ratio (SINR) via system-level simulations and analytically. Both approaches indicate clear

gains in terms of the median relay link SINR. In the analysis, we demonstrate the performance of RSP over composite fading/shadowing channels with co-channel interference by deducing closed-form expressions for the relay link SINR, link rate, and end-to-end rate distributions. Consequently, we show that not only does RSP increase the median relay link SINR, but also decreases the severity of fading, which is critical for low SINR regime. We also present the achievable rate gains.

We then focus on RRM strategies for UL transmissions, where the gains on the relay link through RSP are already taken into account. In this context, we first analyze PC as an important means to compensate for channel variations, to mitigate inter-cell interference, and to increase the cell-edge performance or system capacity. Besides, PC can ensure that the receiver dynamic range does not exceed a predetermined level so that the orthogonality of the multiple access scheme is retained. Within the single-hop LTE Rel. 8 framework, the performance evaluation of PC has been well elaborated in the literature; however, for LTE-Advanced relay deployments it is not widely examined. Therefore, considering backward compatibility requirement, we show that LTE Rel. 8 compliant PC is, as well, appropriate for relay deployments. Further, we introduce propagation scenario-specific methods for PC parameter optimization on all links to enhance the system performance and to provide a comprehensive understanding of the impact of PC on the system performance. Nonetheless, to avoid skilled human intervention that is required in these methods during the optimization process, we propose an automated PC parameter optimization based on the introduced performance steering concept which employs novel performance metrics. The novel performance metrics can be easily adapted according to the operators' requirements. In addition, taking throughput (TP) per power consumption as the performance metric and considering transmit power levels, we illustrate the system-level energy efficiency of relay deployments from an MT point of view.

In the considered relay deployment, the relay link is time-division multiplexed with the access link (between RN-served MTs and RN), while macrocell-served MTs share the same resources with RNs at the serving BS. Hence, the system performance of relay deployments depends strongly on the resource sharing strategy among and within the links. Herein, we present a flexible resource split scheme between macrocell-served MTs and RNs to achieve the goal of obtaining a dynamic and efficient resource sharing. Next, considering resource sharing schemes on

individual links, we propose a combination of relay link scheduling based on the number of RN-served MTs and a TP throttling technique achieving max-min fairness in the end-to-end two-hop communications. In addition, the optimizations are carried out in conjunction with a PC strategy to guarantee system performance enhancement. The results reveal clear TP gains, high system fairness, and substantially increased flexibility in resource allocation. Finally, different degrees of inter-BS coordination for assigning the resource splits on the relay link are analyzed, and their impacts on the resultant system performance with different antenna configurations on the relay link are discussed.

Like other low-power node deployments, RN cells are characterized by small coverage areas in the overlaying macrocell. This is attributed to lower transmit power levels and limited antenna capabilities of RNs along with the conventional cell selection according to the DL received signal strength at MTs. Thus, load imbalances and inefficient resource utilization are observed when macrocell coverage area is overloaded implying high competition for resources, whereas the available resources in RN cells are not fully utilized. Another consequence on the UL is the increased inter-cell interference due to cell-edge macrocell-served MTs that transmit at high power levels. To tackle these issues, we employ backward-compatible cell range extension (CRE) in relay deployments. In the literature, most work on CRE has considered picocell deployments particularly focusing on the DL performance. Here, we conduct a joint optimization of CRE parameters, resource allocation, and PC parameters to enhance the UL system performance. Additionally, we present the impact of aligning DL and UL parameter settings associated with CRE.

This thesis is organized as follows. Chapter 2 presents the analyses pertaining to RSP and presents the achievable performance gains on the relay link SINR, link, and end-to-end rates. The work in Chapter 2 is mainly based on [PI]-[PIII]. In Chapter 3, an overview of the considered system model, which is used in the subsequent chapters, along with background knowledge and the simulation parameters are given. In Chapter 4, the proposed PC parameter optimization methods are considered. The rest of the chapter is devoted to the results on TP per power consumption. The work in Chapter 4 is based on [PIV]-[PVI], and on [23, 24, 25]. Chapter 5 focuses on the contributions regarding the resource sharing schemes and different inter-BS coordination scenarios for assigning the resource splits on the relay link. The work in Chapter 5 is mainly based on [PVII, PVIII],

and on [26, 27, 28]. Related work has been published in the Master's thesis [29], where the author of this thesis was the instructor. In addition, out of five patent applications that have been filed on some aspects of this thesis, [30, 31] are published in the course of this work and relate to the aspects presented in Section 5.4. Chapter 6 first introduces the CRE modeling and then presents the performance assessment of CRE. The work in Chapter 6 is based on [PIX]-[PXI], and on [32, 33]. Related work has been published in the Master's thesis [34], where the author of this thesis was the instructor. Finally, Chapter 7 summarizes the results and the contributions of this thesis. Moreover, some future research areas are outlined.

1.4 Summary of the Publications

This thesis consists of an introductory part and eleven original publications[1]. Publications [PI]-[PIII] study RSP. In [PI], performance evaluation of RSP is given via system-level simulations considering lognormal shadowing only along with co-channel interference, and the gains in terms of median relay link SINR are presented. In [PII], we build upon the concepts provided in [PI] and provide an analytical framework for RSP considering two-hop cellular relay networks operating over composite fading/shadowing channels in the presence of co-channel interference plus thermal noise. In this context, the Wilkinson preconditioning proposed in [PIII] is utilized. Consequently, relay link SINR, link rate, and end-to-end rate gains are shown, and a decrease in severity of fading on the relay link is demonstrated.

Publications [PIV]-[PVI] cover the PC-related contributions. Publication [PIV] presents propagation scenario-specific PC optimization methods and analyzes the impact of PC parameters on the system performance. To alleviate the burden due to skilled human intervention in these optimization methods, [PV] proposes automated PC optimization and explains the concept of performance steering based on novel performance metrics. Besides, [PVI] investigates the energy efficiency of relay and picocell deployments by focusing on the transmit power levels of MTs and the achieved TP, i.e., by employing TP power consumption (TPC) as the performance metric.

In [PVII, PVIII], we study various resource sharing schemes. Publica-

[1]Further relevant publications of the author of this thesis are listed in Bibliography.

tion [PVII] proposes a combination of relay link scheduling based on the number of RN-served MTs and a TP throttling scheme achieving max-min fairness in the end-to-end two-hop communications assuming a hard resource split between macrocell-served MTs and RNs. In addition, [PVII] presents further advantages of these schemes when a flexible resource split is applied instead of the hard resource split. In [PVIII], various inter-BS coordination scenarios for assigning the resource splits at BSs are presented, and the associated performance results are highlighted taking into account different antenna configurations on the relay link.

Publications [PIX]-[PXI] investigate RN CRE. In [PIX], we present practical CRE techniques, and considering ideal relay link, we show the maximum attainable performance through CRE. Publication [PX] extends the CRE analyses by including the impact of the inband relay link and applies a joint optimization of CRE parameters, resource allocation, and PC parameters. Moreover, the impact of aligning DL and UL parameter settings concerning CRE is addressed. In [PXI], the above-mentioned flexible resource split is also applied in case of CRE, and possible performance enhancements and trade-offs are outlined.

2. Performance Enhancement via Relay Site Planning

RNs are low-power nodes that connect to the core network through a BS by utilizing the wireless relay link between RNs and the BS. Furthermore, RNs do not have strict installation guidelines with respect to radiation, visual disturbance, and planning regulation. These features enable deployment flexibility, where RNs can be mounted on structures such as lamp posts with power supply facility.

Cell planning and site selection tools are routinely used by operators to improve the system performance and to provide a satisfactory service with minimal deployment expenditure. In this context, RSP exploits the deployment flexibility of RNs to enhance the system performance by means of improving the relay link. The performance of the relay link is also crucial for the users that are served by RNs. For example, in [15], the performance of inband RNs was investigated from both coverage extension and system capacity perspectives, and the limitations of the relay link were highlighted. Further, it was shown that there is a potential for significant gain if these limitations are relaxed. Accordingly, RSP is carried out by selecting RN deployment locations from a discrete set of alternatives based on a predefined criterion.

Performance evaluation of RSP within the LTE-Advanced context was first given in [PI] where we investigate the effect of RSP on the relay link SINR via system-level simulations considering lognormal shadowing only and co-channel interference. Performing RSP, random deployment of RNs is avoided, and an RN site is chosen from a set of different possible locations in order to optimize the relay link quality. Moreover, signal-to-noise ratio (SNR) based and SINR based selection criteria are utilized in RSP. It is shown that SINR based selection criterion outperforms the SNR based counterpart especially in interference-limited urban scenarios. In line with this study, the discussion on RSP modeling has also been carried

out in LTE-Advanced standardization [35, 36]. Consequently, a certain planning bonus has been added to the relay link channel model in 3GPP evaluation guidelines [22].

Motivated by [PI], a basic analytical model for RSP is deduced in [37], where a single dominant interfering BS is considered. In addition, the study aims at interference-limited scenarios and, hence, assumes a simplified SINR model based on signal-to-interference ratio (SIR), i.e., the thermal noise is neglected. Like [PI], the channel model in [37] considers lognormal shadowing on the relay link and presents the achievable gains through RSP. Besides, the channel model in [37] assumes Rayleigh fading on the access link and investigates the effectiveness of RSP in terms of increasing the relay link and end-to-end rates. We note that, in addition to location selection, serving cell selection is, as well, studied in [PI], [37] targeting a general framework for RSP. The analyses, therein, reveal that the gains via cell selection are notable when RNs are deployed at the cell edge. Nevertheless, these gains diminish in case of cell-center relay deployments, or substantially decrease as the number of candidate locations increases. That is, the improvement on the relay link quality from location selection becomes more prominent in such cases.

Fundamentally, composite fading/shadowing, where multipath fading is superimposed on shadowing, is frequently experienced especially in scenarios with low or no mobility [38, 39]. In addition, given the full-frequency reuse in 4G cellular networks, co-channel interference is another vital factor to be taken into account for accurate performance analysis. However, difficulties arise when considering co-channel interference, which is a sum of multiple interfering signals from different BSs that are subject to correlated composite fading/shadowing. In this context, in [PII], we build upon the concepts provided in [PI], [37] and present an analytical framework for RSP that can be used for planning and dimensioning of two-hop cellular relay networks operating over composite fading/shadowing channels in the presence of co-channel interference plus thermal noise. On this basis, we develop in this chapter a comprehensive analytical model for the impact of RSP on the performance of relay deployments, which explains and justifies RSP gains on the relay link and on the end-to-end user rates.

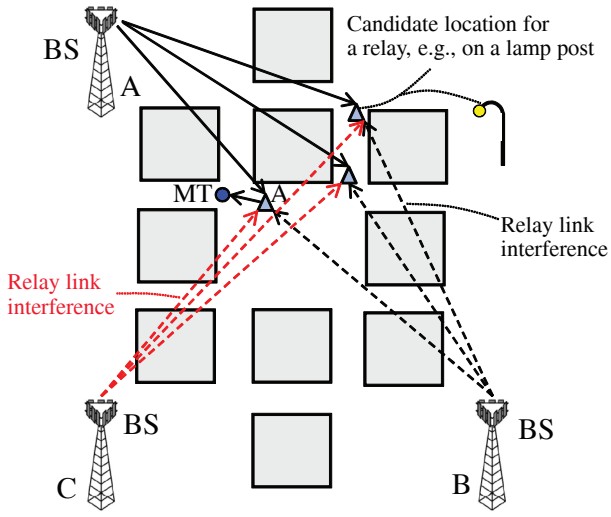

Figure 2.1. Exemplified relay deployment and RSP model for $M = 3$ RN candidate locations and two interfering BSs. ©2012 IEEE

2.1 Relay Site Planning Model

In this work, it is assumed that the original radio network planning has been done for a single-hop system (see, e.g., [40, Ch. 8] for High Speed Packet Access (HSPA) radio network planning and [41, Ch. 13] for LTE radio network planning). Then, half-duplex decode-and-forward RNs are introduced to improve the system performance. In the context of RSP, an RN location is chosen from a set of possible locations. As exemplified in Fig. 2.1 for three RN candidate locations, RSP takes into account the channel properties at different locations and considers their links' qualities toward the serving BS in order to optimize the relay link quality. Besides, as also shown in Fig. 2.1, it is assumed that a single MT is served by an RN. In this illustration, the MT is connected to RN A on the access link and is communicating via this RN with BS A. Moreover, two neighboring BSs B and C interfere with the serving BS transmission on the relay link. It is worth noting that the possible impact of so-called RN-to-RN interference is not included within the framework of RSP. RN-to-RN interference occurs on the DL when an RN transmits on its access link and interferes with a relay link reception of another RN. This type of interference may originate from, e.g., the misalignment of resource allocations on the relay link among different RNs. Further analysis on RN-to-RN interference is given in Section 5.4. Additionally, methods for RN-to-RN interference mitigation are provided in [30, 31].

In essence, we assume that there are M potential locations for RN deployment in cell k out of which we select the best location in terms of DL SINR on the relay link. In each location, RN is assumed to be served by a predefined BS solely as part of the network planning phase. Then, the SINR at the selected location is of the following form:

$$\Upsilon_{\hat{m},k} = \max\{\Upsilon_{m,k} : m = 1, 2, ..., M\}, \tag{2.1}$$

where $\Upsilon_{m,k}$ is the SINR for the m^{th} location in the k^{th} cell. In what follows, we first introduce the channel models on each link, which is followed by the system model.

2.1.1 Channel Models

The wireless channel is subject to simultaneous impairments by large-scale fading due to shadowing and by small-scale fading due to multipath propagation [38, 39]. Shadowing is usually modeled by a lognormal distribution with standard deviation σ and mean μ. As the parameters of lognormal distribution are often given in decibels, the mappings $\sigma = \lambda\sigma_{\text{dB}}$ and $\mu = \lambda\mu_{\text{dB}}$ with $\lambda = \ln(10)/10$ can be utilized for the conversion. Besides, the small-scale multipath fading is often characterized by Nakagami distribution with the fading parameter ($0.5 \leq m_{\text{CL}} \leq \infty$) on a communication link (abbreviated by CL in this notation), Rician or Rayleigh distribution.

The channel models to be derived pertain to a two-hop relay deployment where end-to-end performance is degraded also by interference on the relay link, as depicted in Fig. 2.1. Specifically, we model the relay and access links by Nakagami-lognormal and Rician-lognormal composite distributions, respectively, which are the two common models in the literature [38, 39, 42, 43]. As these composite distributions do not have closed-form expressions, we utilize mixture gamma distribution (MG distribution) [44] to accurately approximate them. In [44], it is shown that MG distribution can approximate Nakagami-lognormal more accurately than other existing models, and that it provides a unified framework without involving special functions. Besides, it is assumed that interfering signals on the relay link are subject to Rayleigh-lognormal (a.k.a. Suzuki) composite fading/shadowing, since RNs are not expected to have line-of-sight (LOS) links toward interfering BSs. Therefore, it can be inferred that different multipath fading characteristics are assumed for the desired and interfering signals provided that $m_{\text{CL}} \neq 1$ on the desired link. We note that

Nakagami distribution yields Rayleigh distribution when $m_{\mathrm{CL}} = 1$; thus, the distribution functions of Rayleigh-lognormal can be easily obtained once the distribution functions of Nakagami-lognormal are derived. In what follows, MG distribution is first outlined, and the composite SNR distributions on the relay and access links are then modeled in terms of MG distribution [PII]. The instantaneous SNR and the average SNR are denoted by γ and $\bar{\gamma}$, respectively.

MG Distribution

The probability distribution function (PDF) of the instantaneous SNR is approximated by MG distribution with N gamma components as [44], [PII]

$$f_\gamma(x) = \sum_{i=1}^{N} \alpha_i x^{\beta_i - 1} e^{-\zeta_i x}, \quad x \geq 0 \,, \tag{2.2}$$

where α_i, β_i and ζ_i are the parameters of the i^{th} gamma component. Furthermore, $\alpha_i = \theta_i / C$ where $C = \sum_{i=1}^{N} \theta_i \Gamma(\beta_i) \zeta_i^{-\beta_i}$ with $\Gamma(\cdot)$ being the gamma function is a normalization factor to ensure that $\int_0^\infty f_\gamma(x) = 1$. Accordingly, θ_i is a parameter of the i^{th} gamma component, as well. The number of components N determines the accuracy of the approximation and is obtained by matching the first r ($r = 3$ herein) moments of the approximation and the target distribution [44]. Next, the CDF of the approximation is given as

$$F_\gamma(x) = \sum_{i=1}^{N} \alpha_i \zeta_i^{-\beta_i} \boldsymbol{\gamma}(\beta_i, \zeta_i x) \,, \tag{2.3}$$

where $\boldsymbol{\gamma}(a, b) \triangleq \int_0^b t^{a-1} e^{-t} dt$ is the lower incomplete gamma function [45, eq. (8.350.1)]. Further, the r^{th} moment of MG distribution of the instantaneous SNR is given as

$$\mathrm{E}(\gamma^r) = \sum_{i=1}^{N} \alpha_i \Gamma(\beta_i + r) \zeta_i^{-(\beta_i + r)} \,, \tag{2.4}$$

where $\mathrm{E}(\cdot)$ denotes the statistical expectation. The amount of fading (AoF) can be then calculated from the first and the second moments of the SNR as [39]

$$AoF = \frac{\mathrm{var}(\gamma)}{[\mathrm{E}(\gamma)]^2} = \frac{\mathrm{E}(\gamma^2) - [\mathrm{E}(\gamma)]^2}{[\mathrm{E}(\gamma)]^2} = \frac{\mathrm{E}(\gamma^2)}{[\mathrm{E}(\gamma)]^2} - 1 \,, \tag{2.5}$$

where var$(\cdot)$ denotes variance. In addition, the moment generating function (MGF) of MG distribution, evaluated as $\Psi_\gamma(s) = \mathrm{E}(e^{-sx})$, is of the following form:

$$\Psi_\gamma(s) = \sum_{i=1}^{N} \alpha_i \Gamma(\beta_i)(s + \zeta_i)^{-\beta_i}. \tag{2.6}$$

The unified framework MG distribution implies that, once the parameters θ_i, β_i and ζ_i are determined, the performance metrics are readily available [44] or can be easily derived. In line with the derivations detailed in [PII], we provide these parameters for the relay and access link SNR distributions in the following.

SNR Distribution on the Relay Link

The instantaneous SNR on the relay link is modeled by a gamma- lognormal distribution (occurs over Nakagami-lognormal channel) [39, 44]. Then, the parameters of the i^{th} gamma component are expressed as [44]

$$\theta_i = \left(\frac{m_{\text{RL}}}{\bar{\gamma}}\right)^{m_{\text{RL}}} \frac{w_i e^{-m_{\text{RL}}(\sqrt{2}\sigma t_i + \mu)}}{\sqrt{\pi}\Gamma(m_{\text{RL}})}, \quad \beta_i = m_{\text{RL}}, \quad \zeta_i = \frac{m_{\text{RL}}}{\bar{\gamma}} e^{-(\sqrt{2}\sigma t_i + \mu)}, \tag{2.7}$$

where m_{RL} is the fading parameter of Nakagami distribution on the relay link (abbreviated by RL in this notation), and t_i and w_i are, respectively, abscissas and weight factors of N^{th} order Hermite integration. The AoF for the SNR distribution on the relay link can be then easily obtained through (2.4), (2.5) and (2.7). Moreover, a simplified expression of the AoF follows as [46]

$$AoF = \frac{\sqrt{\pi}(m_{\text{RL}}+1)}{m_{\text{RL}}} \frac{\sum_{i=1}^{N} w_i e^{2\sqrt{2}\sigma t_i}}{\left(\sum_{i=1}^{N} w_i e^{\sqrt{2}\sigma t_i}\right)^2} - 1. \tag{2.8}$$

As a reference, another simple expression for the AoF is provided in [39, eq. 2.60]:

$$AoF \;=\; \frac{m_{\text{RL}}+1}{m_{\text{RL}}} e^{\sigma^2} - 1. \tag{2.9}$$

SNR Distribution on the Access Link

An RN cell is typically characterized by small coverage area due to lower transmit power levels relative to the BSs [15, 22]. Hence, we assume that a direct LOS component along with many weak non-LOS (NLOS) scatter components exist on the propagation paths between an RN and an MT on the access link. Furthermore, the LOS component may be partially or completely blocked by surrounding objects, e.g., trees and buildings, which implies random shadowing [39]. Therefore, we model the access link by Rician-lognormal distribution. Accordingly, we obtain the parameters of the i^{th} gamma component [PII]:

$$\begin{aligned} \theta_i &= \frac{1+K}{\bar{\gamma}} \left(\frac{m_{\text{AL}}}{m_{\text{AL}}+K}\right)^{m_{\text{AL}}} \frac{(m_{\text{AL}})_{i-1}}{(\Gamma(i))^2} \left(\frac{K(1+K)}{\bar{\gamma}(m_{\text{AL}}+K)}\right)^{i-1}, \\ \beta_i &= i, \quad \zeta_i = \frac{1+K}{\bar{\gamma}}, \end{aligned} \tag{2.10}$$

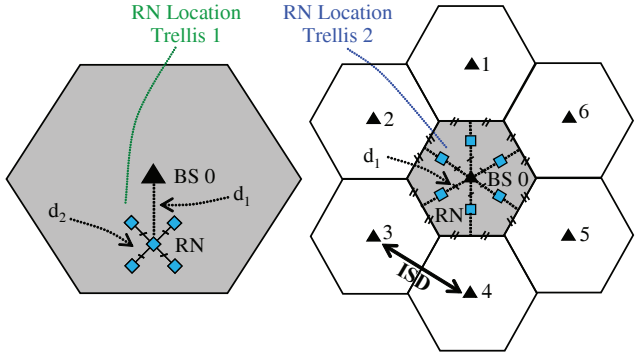

Figure 2.2. The multi-cellular network layout and RN location trellises considered for the RSP study. The distance between two neighboring BSs is referred to as inter-site distance (ISD). ©2012 IEEE

where $0 \leq m_{\mathrm{AL}} \leq \infty$ describes the severity of shadowing on the access link (abbreviated by AL in this notation), and $K \triangleq \Omega/2b_0$ is the Rician K factor where Ω is the average power of the LOS component and $2b_0$ is the average power of the scatter component. Besides, the simplified AoF expression is of the following form [PII]:

$$AoF = \frac{1}{C}\frac{(m_{\mathrm{AL}}+K)^{m_{\mathrm{AL}}-1}K}{{m_{\mathrm{AL}}}^{m_{\mathrm{AL}}}}\frac{\sum_{i=1}^{N}\frac{(m_{\mathrm{AL}})_{i-1}\Gamma(i+2)}{(\Gamma(i))^2}\left(\frac{K}{m_{\mathrm{AL}}+K}\right)^i}{\left(\sum_{i=1}^{N}\frac{(m_{\mathrm{AL}})_{i-1}\Gamma(i+1)}{(\Gamma(i))^2}\left(\frac{K}{m_{\mathrm{AL}}+K}\right)^i\right)^2} - 1\,. \quad (2.11)$$

As a reference, the AoF of the original model, which is provided in [39, eq. 2.67], can be obtained by using the transformation $\mathrm{E}(\gamma^r) = \mathrm{E}(\chi^r)A^r$, where $\chi = \gamma/A$ with $A = \frac{\bar{\gamma}}{2b_0+\Omega}$ is the power envelope of the shadowed Rician fading channel, and $\mathrm{E}(\chi^r)$ is given in [39, eq. 2.69]. After some manipulations, the AoF attains the following form:

$$AoF = 2\left(\frac{m_{\mathrm{AL}}+K}{m_{\mathrm{AL}}}\right)^{m_{\mathrm{AL}}}\frac{{}_2F_1(3, m_{\mathrm{AL}}, 1, K/(m_{\mathrm{AL}}+K))}{({}_2F_1(2, m_{\mathrm{AL}}, 1, K/(m_{\mathrm{AL}}+K)))^2} - 1, \quad (2.12)$$

where ${}_pF_q(\cdot,\cdot,\cdot,\cdot)$ is the generalized hypergeometric function for integer p and q [45, Sec. 9.14].

2.1.2 System Model for the Relay Site Planning Analysis

This section outlines the considered multi-cellular network model and the associated assumptions used in the analysis.

Network Layout and RSP Location Trellises

The considered network for this study is represented by a regular hexagonal layout with 7 BSs, where a suitable location for a single RN is sought in the k^{th} cell assuming M potential location candidates. Fig. 2.2 depicts

the network layout along with two *distinct* RN location trellises that are utilized for RSP. Here, RN location trellis 1 models a practical scenario where $M = 5$ candidate locations are confined in a target region. Moreover, d_1 denotes the distance between the serving BS and the midmost RN location. The outer candidate locations are at a distance of d_2 apart from the midmost candidate location (see also Fig. 2.1 for a similar scenario with $M = 3$ candidate RN locations). On the other hand, for RN location trellis 2, $M = 6$ candidate locations are selected such that each candidate location is at a distance of d_1 away from the serving BS, and, due to the symmetry of the network layout, the set of distances to neighboring BSs is the same for all candidate locations. In particular, RN location trellis 2 is utilized for determining AoF bounds.

Path-loss Model

The path loss, including the shadowing, is given by

$$L_{m,k} = \alpha_{\mathrm{p}} d_{m,k}^{\beta} 10^{\zeta_{m,k}/10}/G, \tag{2.13}$$

where $d_{m,k}$ is the distance between m^{th} potential relay location and k^{th} BS, $k = 0, 1, 2, ..., \mathcal{K}$. Further, α_{p} and β are, respectively, a propagation constant and the path-loss exponent, together which define the distance dependent path loss. G is dimensionless and reflects the impact of antenna gain, which is assumed to be the same for each BS noting that isotropic antenna gain patterns are employed at BSs. Moreover, $\zeta_{m,k}$ is a zero-mean Gaussian random variable (RV) that models the shadowing.

According to [47], RV $\zeta_{m,k}$ can be expressed as a sum of two independent zero-mean components, ξ_m and $\eta_{m,k}$, where the former corresponds to the near field of the m^{th} location and is the same for all BSs, and the latter variable is a BS-dependent variable, which is independent from one BS to another. Hence, we have

$$\zeta_{m,k} = \sqrt{\rho} \cdot \xi_m + \sqrt{1-\rho} \cdot \eta_{m,k}, \tag{2.14}$$

where ρ is the correlation coefficient related to any pair of BSs. In line with [47] and [PII], it is assumed that

$$\begin{aligned} &\mathbf{E}(\eta_{m,k}\eta_{m,j}) = 0,\ k \neq j, \\ &\mathbf{E}(\xi_m \eta_{m,k}) = 0, \\ &\mathrm{Var}\{\xi_m\} = \mathrm{Var}\{\eta_{m,k}\} = \sigma_{\mathrm{dB}}^2. \end{aligned} \tag{2.15}$$

Then, we obtain

$$\mathbf{E}(\zeta_{m,k}\zeta_{m,j}) = \rho\sigma_{\mathrm{dB}}^2,\ \mathbf{E}((\zeta_{m,k})^2) = \sigma_{\mathrm{dB}}^2,\ \mathbf{E}(\zeta_{m,k}) = 0. \tag{2.16}$$

In accordance with the Gudmundson model [48], the correlation between shadowing samples at different locations in the k^{th} cell is given by

$$\rho(\zeta_{m,k}, \zeta_{n,k}) = e^{-\frac{|d_{m,n}|}{d_{\text{cor}}} \ln 2}, \tag{2.17}$$

where $\zeta_{m,k}$ and $\zeta_{n,k}$ are the shadowing variables at locations m and n, respectively, $d_{m,n}$ is the distance between the two locations, and d_{cor} is the de-correlation distance. Given the proposed value for d_{cor}, e.g., 20 m in [49], shadowing correlation between potential RN positions with mutual distance of 50 m is neglected in the closed-form analysis. Also, due to the low correlation in shadowing between candidate locations, the correlation between SINR values is ignored.

2.2 Analysis of Relay Site Planning

2.2.1 Derivation of the Relay Link SINR

Following the formulation detailed in [PII], the SINR at the m^{th} location is given by

$$\Upsilon_{m,k} = \frac{S^2_{m,k} 10^{X_{m,k}/10}}{P_N + \sum_{j \neq k} S^2_{m,j} 10^{X_{m,j}/10}}, \tag{2.18}$$

where $S^2_{m,k}$ is the power envelope of the multipath fading channel on the desired link between k^{th} BS and m^{th} location, which is modeled by Nakagami distribution, $S^2_{m,j}$ is the power envelope of the multipath fading channel on the interfering link between j^{th} BS and m^{th} location, which is modeled by Rayleigh distribution, and P_N denotes the thermal noise. Further, $X_{m,k} \sim \mathcal{N}(\mu_{X_{m,k}}, \sigma^2_{\text{dB}})$ with $X_{m,k} = -\zeta_{m,k} + \mu_{X_{m,k}}$ and $X_{m,j} \sim \mathcal{N}(\mu_{X_{m,j}}, \sigma^2_{\text{dB}})$ with $X_{m,j} = -\zeta_{m,j} + \mu_{X_{m,j}}$ are Gaussian RVs, where means $\mu_{X_{m,k}}$ and $\mu_{X_{m,j}}$ comprise BS transmit power levels, and distance dependent path losses defined in (2.13). For example, we have $\mu_{X_{m,k}} = 10\log_{10}(P_{\text{Tx},k} G \alpha_{\text{p}}^{-1} d_{m,k}^{-\beta})$ with $P_{\text{Tx},k}$ being the transmit power of the k^{th} BS. Accordingly, the SINR expression attains the following form:

$$\Upsilon_{m,k} = \frac{S^2_{m,k} 10^{(\sqrt{\rho}\cdot\xi_m + \sqrt{1-\rho}\cdot\eta_{m,k} + \mu_{X_{m,k}})/10}}{P_N + \sum_{j \neq k} S^2_{m,j} 10^{(\sqrt{\rho}\cdot\xi_m + \sqrt{1-\rho}\cdot\eta_{m,j} + \mu_{X_{m,j}})/10}}. \tag{2.19}$$

It can be seen that, due to the common shadowing term ξ_m, the desired signal and interfering signals are mutually *dependent*. To derive an analytically tractable SINR expression, we need the distribution of the ther-

mal noise plus total co-channel interference. However, an exact closed-form expression for the distribution of the sum of multiple lognormal and/or Suzuki RVs is not available. In [50], the sum of a mixture of *independent* Suzuki and lognormal RVs is accurately approximated by a lognormal RV utilizing MGF-matching method. In this regard, the analytical modeling of the relay link SINR inherits two main difficulties. The first difficulty arises due to mutual dependence of the desired and interfering signals, and the second difficulty is due to constant thermal noise term P_N. In order to overcome these difficulties, we reformulate the SINR expression in (2.19) by dividing the numerator and denominator by the common shadowing term $10^{\sqrt{\rho}\cdot\xi_m/10}$ and obtain

$$\Upsilon_{m,k} = \frac{S_{m,k}^2 10^{(\sqrt{1-\rho}\cdot\eta_{m,k}+\mu_{X_{m,k}})/10}}{P_N 10^{-\sqrt{\rho}\cdot\xi_m/10} + \sum\limits_{j\neq k} S_{m,j}^2 10^{(\sqrt{1-\rho}\cdot\eta_{m,j}+\mu_{X_{m,j}})/10}}. \tag{2.20}$$

This form is particularly beneficial, since the RVs in this reformulated SINR expression are mutually *independent*. Furthermore, the newly introduced RV $P_N 10^{-\sqrt{\rho}\cdot\xi_m/10}$ follows a lognormal distribution with mean $10\log_{10}(P_N)$ and standard deviation $\sqrt{\rho}\cdot\sigma_{\text{dB}}$. Thus, the MGF-matching method can be applied. That is, the sum in the denominator of (2.20) is approximated by a new lognormal RV as

$$\begin{aligned} I &= P_N 10^{-\sqrt{\rho}\cdot\xi_m/10} + \sum_{j\neq k} S_{m,j}^2 10^{(\sqrt{1-\rho}\cdot\eta_{m,j}+\mu_{X_{m,j}})/10} \\ &= I_0 + \sum_{j\neq k} I_{m,j} \approx 10^{0.1Z} = \tilde{I}, \end{aligned} \tag{2.21}$$

where $Z \sim \mathcal{N}(\mu_Z, \sigma_Z^2)$. The aim of the approximation is then to determine μ_Z and σ_Z, both given in dB. Nonetheless, the MGF-matching method requires a numerical solution of a system of non-linear equations [PII]. Moreover, this numerical solution needs a starting point (μ_o, σ_o) to be able to initiate the solution process. To tackle this critical issue, Wilkinson preconditioning is shown to be an effective means through which the convergence of the numerical solution can be guaranteed, and the efficiency in terms of convergence rate and the total number of function evaluations in the numerical computations can be significantly enhanced [PIII]. We note that, in [PIII], Wilkinson preconditioning is applied for the case of a sum of lognormal RVs; hence, it is adapted for the aforementioned case of the sum of multiple lognormal and Suzuki RVs in [PII].

Consequently, after having determined the approximating lognormal RV $10^{0.1Z}$, the approximated SINR can be formulated by following the

expression in (2.20) as

$$\widetilde{\Upsilon}_{m,k} = S^2_{m,k} 10^{(\sqrt{1-\rho}\cdot\eta_{m,k} - Z + \mu_{X_{m,k}})/10} := S^2_{m,k} 10^{\Delta_{m,k}/10}\,, \tag{2.22}$$

where $\Delta_{m,k} \sim \mathcal{N}\left(\mu_{X_{m,k}} - \mu_Z, (1-\rho)\sigma^2_{\text{dB}} + \sigma^2_Z\right)$. Accordingly, the SINR distribution on the relay link follows a gamma-lognormal composite distribution which is characterized by (2.2)-(2.6), where the parameter expressions are provided by (2.7) in which $\bar{\gamma}$ is set to one. We note that considering the discussion on spatial shadowing correlation and the RN location trellises, we have $\mathrm{E}(\Delta_{m,k}\Delta_{n,k}) = 0$, if $m \neq n$; thus, variables $\left\{\widetilde{\Upsilon}_{m,k} : m \neq n\right\}$ are independent.

Therefore, when RSP is carried out in the k^{th} cell over M candidate locations, the cumulative distribution function (CDF) of the SINR becomes

$$F_{\hat{m},k}(\widetilde{\Upsilon}) = \prod_{m=1}^{M} F_{m,k}(\widetilde{\Upsilon}), \tag{2.23}$$

where $F_{m,k}(\widetilde{\Upsilon})$ is given by (2.3) following the discussion after (2.22). The PDF is then obtained by taking the derivative of (2.23) and reorganizing the terms, which yield

$$f_{\hat{m},k}(\widetilde{\Upsilon}) = \left(\prod_{m=1}^{M} F_{m,k}(\widetilde{\Upsilon})\right)\left(\sum_{m=1}^{M} \frac{f_{m,k}(\widetilde{\Upsilon})}{F_{m,k}(\widetilde{\Upsilon})}\right), \tag{2.24}$$

where $f_{m,k}(\widetilde{\Upsilon})$ is given by (2.2) following the discussion after (2.22). We further note that these expressions cover the general case, e.g., RN location trellis 1, where the SINR distribution may not be the same at different locations due to different mean received powers, i.e., $\mu_{X_{m,k}}$ and $\mu_{X_{m,j}}$. Nevertheless, in case where SINR distributions are the same at different locations, e.g., RN location trellis 2, these equations reduce to

$$F_{\hat{m},k}(\widetilde{\Upsilon}) = [F_{m,k}(\widetilde{\Upsilon})]^M, \tag{2.25}$$

and the PDF is given by

$$f_{\hat{m},k}(\widetilde{\Upsilon}) = M[F_{m,k}(\widetilde{\Upsilon})]^{M-1} f_{m,k}(\widetilde{\Upsilon}). \tag{2.26}$$

2.2.2 Relay Link AoF

An important performance measure in analysis of RSP is its impact on the resultant AoF on the relay link. The AoF after RSP can be evaluated using the definition (2.5) along with the PDFs given in (2.24) for RN location trellis 1, and in (2.26) for RN location trellis 2. In addition, to find out

the maximum achievable gains by RSP in terms of decrease in AoF on the relay link, i.e., lower bounds on the resultant AoF, we utilize RN location trellis 2 where each RN location is subject to the same SINR distribution [PII].

2.2.3 Link and End-to-end Rate Distributions

Once the distribution functions for SINR and SNR on relay and access links, respectively, are obtained, the corresponding link rate distributions can be easily derived by means of SINR or SNR to rate mappings as explained in [PII]. These mappings simulate the adaptive modulation and coding (AMC) functionality in the system [51, 52] and also account for, e.g., LTE overhead through reference symbols and control signaling.

Then, the end-to-end rate is given in terms of the link rates on the two hops. Specifically, the end-to-end rate experienced by a single user served by RN in the k^{th} cell and m^{th} location is defined as the minimum of the rates achieved on the relay and access links, i.e.,

$$R_{e;m,k} = \min\left(\tau_r \cdot R_{r;m,k}, \tau_a \cdot R_a\right), \tag{2.27}$$

where $R_{r;m,k}$ and R_a are the achievable rates on the relay and access links, respectively, which are independent RVs that are scaled by the portion of resources allocated to each. That is, recalling the half-duplex operation of RNs, time resources allocated for the relay link communication constitute τ_r of the total system resources, whereas access link communication is scheduled on τ_a of the total available resources, and resource normalization is given as $\tau_r + \tau_a = 1$. Furthermore, in practice, due to resource-allocation granularity in time, τ_r or τ_a takes discrete values, e.g., in LTE [22], from the set of $\{0.1, 0.2, \cdots, 0.9\}$. Subsequently, the distribution functions for the end-to-end rate can be formulated considering (2.27) and the distribution functions for the link rates [PII]. When RSP is performed, the distribution functions for the link and end-to-end rates are obtained similarly [PII].

2.3 Performance Evaluation and Discussions

Herein, we evaluate the effect of RSP on the relay link quality, on the resultant AoF on the relay link as well as on the end-to-end performance. All analytical results have been validated via simulations (denoted by *Empirical* in the figures) through which the accuracy of the deduced for-

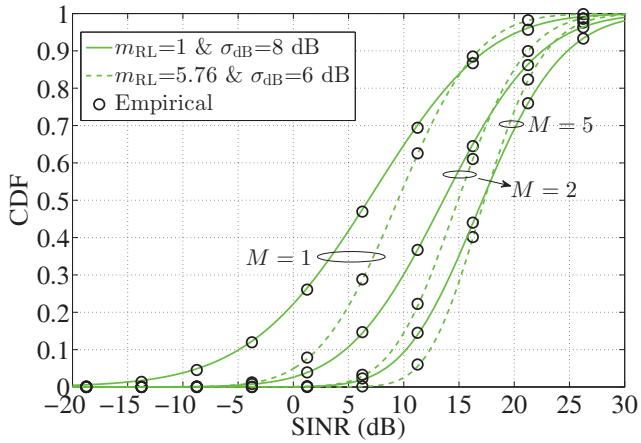

Figure 2.3. CDFs of SINR on the relay link with RSP ($M > 1$) and without RSP ($M = 1$). Two sets of channel parameters are depicted, namely, ($m_{\mathrm{RL}}; \sigma_{\mathrm{dB}}$)=$(1; 8)$ and ($m_{\mathrm{RL}}; \sigma_{\mathrm{dB}}$)=$(5.76; 6)$ illustrating a scenario with severe fading and a scenario with comparatively light fading, respectively. The CDF plots pertaining to analytical results (solid and dashed lines) are in good agreement with the simulation results (circular markers). ©2012 IEEE

mulations are, as well, presented. In particular, the simulation models follow the 3GPP guidelines given in [22] and are summarized in [PII]. It should be stressed that although spatial shadowing correlation between two candidate RN locations is ignored in analytical formulations (see the discussion on (2.17) in Section 2.1.2), this correlation is taken into account in the simulations. In addition, in the exemplified cellular network layout with ISD $= 500$ m, 6 neighboring cells cause co-channel interference with the relay link reception in the midmost cell. Furthermore, we focus on coverage-oriented planning, i.e., RNs are positioned at the cell edge with d_1=ISD$/\sqrt{3}$ m noting that, in 3GPP and IEEE, the main interest is on the coverage extension by relays [53]. RN location trellis 2 is analyzed only for the resultant AoF on the relay link, whereas RN location trellis 1 with $d_2 = 50$ m is employed for other results.

2.3.1 Relay Link SINR Distribution

The impact of RSP on the relay link SINR distribution is illustrated by CDF plots in Fig. 2.3 for different number of RN candidate locations along with two sets of channel parameters. These sets of channel parameters are:

1. ($m_{\mathrm{RL}}; \sigma_{\mathrm{dB}}$) = $(1; 8)$, which corresponds to a scenario with severe fading, and

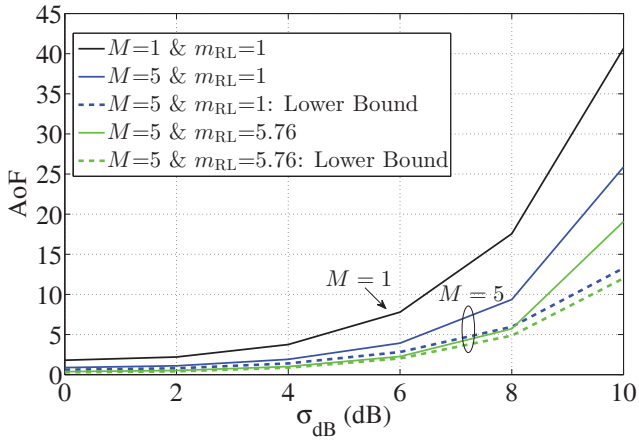

Figure 2.4. AoF on the relay link as a function of shadowing standard deviation. The solid lines are obtained by using RN location trellis 1 when $M = 5$, and $M = 1$ (no RSP). The dashed lines illustrate the lower bounds for AoF, which are obtained by using RN location trellis 2. For $m_{RL} = 5.76$ the multipath fading is not severe; hence, shadowing dominates. ©2012 IEEE

2. $(m_{RL}; \sigma_{dB}) = (5.76; 6)$, which corresponds to a scenario with comparatively light fading.

It is observed that RSP provides SINR gain particularly at lower CDF percentiles in both scenarios. The gain through RSP is more prominent for the first scenario where severe fading is experienced, which highlights the impact of RSP in alleviating the effects of severe fading. It can be inferred that as the number of RN candidate locations in RSP increases, the deviation of the SINR CDF plots reduces implying a decrease in the severity of fading, i.e., the resultant AoF on the relay link. It is worth noting that especially the cases with relatively more severe multipath fading component (here, the first set of channel parameters) reflect the maximum achievable gains from RSP in composite fading/shadowing environments.

2.3.2 Resultant AoF on the Relay Link

The AoF values on the relay link are plotted in Fig. 2.4 as a function of shadowing standard deviation when ($M = 5$). The case of no RSP ($M = 1$) is taken as a reference. It is seen that AoF on the relay link decreases clearly when RSP is performed and σ_{dB} is large, i.e., heavy shadowing. Thus, Fig. 2.4 illustrates the effectiveness of RSP in mitigating the deleterious impact of shadowing on the relay link. It is shown that RN location trellis 1 yields similar resultant AoF values with the lower bounds

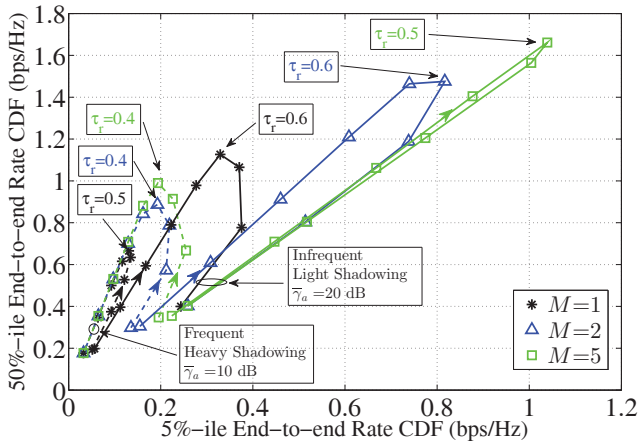

Figure 2.5. Achieved 5%-ile vs. 50%-ile end-to-end rates for different resource-allocation combinations on the access and relay links when $M = 1$ (no RSP) and $M > 1$ (with RSP). Each mark indicates a different τ_r, and the arrows on the curves indicate the direction of increase in τ_r. ©2012 IEEE

for $\sigma_{\text{dB}} \leq 6$ dB; however, the difference between the resultant AoF values of RN location trellis 1 and the lower bounds increases with σ_{dB}. We note that $\sigma_{\text{dB}} = 6$ dB is considered critical since it is a typical value for the shadowing standard deviation on the relay link, e.g., in the LTE-Advanced standard [22].

2.3.3 End-to-end Rates and Resource Allocation

Optimum resource allocation should take into account the qualities of both relay and access links, and should balance the achieved rates on them. In this context, Fig. 2.5 presents the achieved 5%-ile versus 50%-ile end-to-end rates for a range of relay and access link resource-allocation combinations (τ_r,τ_a). Here, τ_r, where $\tau_a = 1-\tau_r$, is varied within the range [0.1, 0.9] with a step size 0.1. In LTE, this step size implies one subframe out of ten potential subframes, equivalently an LTE radio frame. Note that, in Fig. 2.5, different resource-allocation combinations (τ_r,τ_a) can be used to maximize either the cell coverage (5%-ile end-to-end rate CDF level) or the median user performance (indicated by the 50%-ile end-to-end rate CDF level), or to decide on trade-off between both criteria.

The two cases of channel conditions on the access link provided in [PII] are applied in Fig. 2.5, where dashed and solid lines correspond to relatively moderate and good channel conditions, respectively. In both cases of channel conditions, the relay link channel parameters are ($m_{\text{RL}}; \sigma_{\text{dB}}$)= $(5.76; 6)$. The results depicted in Fig. 2.5 point out the importance of the

resource allocation for end-to-end rates. Moreover, the 50%-ile and 5%-ile end-to-end rate targets may lead to different optimum resource allocations. This is particularly observable under moderate access link conditions (dashed lines).

In the case of moderate access link channel conditions (dashed lines), performing RSP with $M = 5$ provides clear gains. For example, the maximum gain of 89% is achieved relative to no RSP at 5%-ile end-to-end rate CDF level when $\tau_r = 0.2$. Moreover, it can be seen that, due to improvement in relay link quality through RSP, the optimum gains are achieved with reduced resource shares on the relay link. If access link channel conditions are good (solid lines), the relay link quality lags behind the access link quality. Nevertheless, with RSP fewer resources are needed on the relay link when maximizing 5%-ile and 50%-ile end-to-end rates. This indicates that the relay link limitations can be eased by RSP yielding better overall end-to-end rates. As an example, in case of performing RSP with $M = 5$, the maximum gain relative to no RSP reads as 177% at 5%-ile end-to-end rate CDF level.

3. System Model

In this chapter, we outline the key features of the system model which comprises the general framework, background information, and the considered propagation scenarios. Since we consider LTE-Advanced as a practical scenario to demonstrate the concepts developed and investigated herein, the system model complies with the 3GPP specifications defined in [22]. LTE-Advanced utilizes Single Carrier - Frequency Division Multiple Access (SC-FDMA) and Orthogonal Frequency Division Multiple Access (OFDMA) as the UL and DL multiple access schemes, respectively. We note that the features of the system model given in this chapter have been utilized in the following chapters unless otherwise stated. We further note that, in line with the LTE-Advanced terminology, BS, serving BS for an RN, and MT are, respectively, referred to as evolved Node B (eNB), donor eNB (DeNB), and user equipment (UE) in the remainder of this thesis.

3.1 General Framework

In this section, we first recall the framework of LTE UL technology. Then, we present the constraints on the resource allocation.

3.1.1 LTE Uplink Technology and Frame Structure

LTE UL has adopted SC-FDMA [54] due to its low peak-to-average power ratio (PAPR) allowing low power consumption and high power efficiency at the UE. The bandwidth is divided into subbands, which are called physical resource blocks (PRBs). The PRB defines the resource allocation granularity in LTE. Herein, a transmission bandwidth of 10 MHz is allocated for UL; thus, there are 48 PRBs available for data transmission over the Physical Uplink Shared Channel (PUSCH), and 2 PRBs are reserved

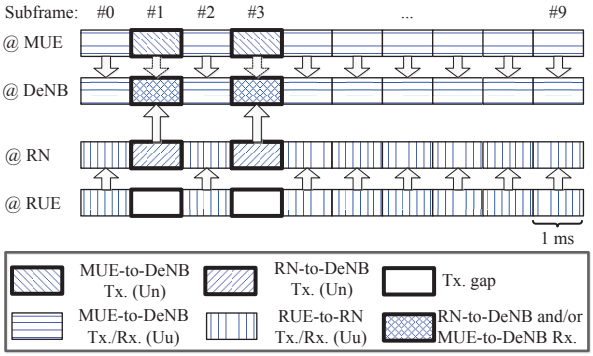

Figure 3.1. FDD LTE-Advanced frame structure considering Type 1 RNs. ©2012 Wiley

to the Physical Uplink Control Channel (PUCCH). Besides, frequency division duplex (FDD) mode is assumed. Given the frequency reuse one in LTE-Advanced networks, macro-UEs (MUEs) and relay-UEs (RUEs) are served on the same frequency bands by DeNBs and RNs, respectively. However, considering the resource allocation strategy defined for inband Type 1 RNs in [22], relay and access link transmissions are time-division multiplexed, i.e., half-duplex operation, to avoid self-interference. Moreover, users can be scheduled on a subset of the total available PRBs in each transmission time interval (TTI). A TTI (a.k.a. subframe) duration is 1 ms, and an LTE frame consists of 10 subframes. During the backhaul subframes (Un subframes[1]) for the relay link, RUEs are not scheduled on the access link; thus, they are experiencing transmission gaps (Tx. gaps). We note that both MUEs and RNs can be optionally co-scheduled during Un subframes. An example frame structure is given in Fig. 3.1, where two subframes are reserved for the relay link, and MUEs and RUEs are scheduled during regular subframes (Uu subframes[2]). In particular, a maximum of six Un subframes can be semi-statically allocated for the relay link [22, 55]. This subframe structure allows backward compatibility with LTE Rel. 8. Furthermore, unless otherwise stated, the subframe configuration is kept the same at all cells in the considered network in the following chapters. In this regard, a network-wide inter-DeNB synchronization is necessary, which can be managed by, e.g., the operations, administration, and maintenance (OAM) system.

[1]Un is the air interface between an RN and its DeNB [55], see also Fig. 3.3.
[2]Uu is the air interface between a UE and its serving cell [55], see also Fig. 3.3.

3.1.2 Constraints on Resource Allocation

The main difference of SC-FDMA compared to OFDMA is the single-carrier constraint, where only a set of *adjacent* PRBs can be allocated to a UE. Such a constraint impacts the frequency domain scheduler. We note that this constraint, which is defined in LTE Rel. 8, is considered for the sake of backward compatibility. Furthermore, the maximum number of the UEs that can be scheduled in each TTI is limited by the possible number of scheduling grants which can be carried by the Physical Downlink Control Channel (PDCCH), i.e., due to so-called PDCCH limitation [1, 56]. We note that a scheduling grant includes dedicated user information which is necessary to decode the data channel, e.g., data bandwidth allocation, and modulation and coding scheme (MCS). A typical number, which is eight [1], is considered herein. That is, if there are more than eight UEs accessing to an eNB, a DeNB or an RN, a subset of consisting of eight UEs will be scheduled in each TTI. The unscheduled UEs in a given TTI will be scheduled in other TTIs such that resource fairness is achieved in the time domain. Besides, no limitation is assumed on the relay-specific PDCCH (R-PDCCH) because the relay link experiences good channel conditions due to, e.g., higher antenna gains, and since a small number of RNs are deployed per cell, i.e., 4-RN and 10-RN deployments.

3.2 Multi-hop Relay Scenario

In this section, we present the essential features that pertain to the considered relay networks.

3.2.1 Relay Deployment and Network Layout

The considered network is represented by a regular hexagonal cellular layout with 19 tri-sectored sites, i.e., 57 cells in total. Targeting coverage improvements and a more homogeneous user performance over the cell area, which is the main interest for RNs in IMT-Advanced standards [53], we have systematically deployed RNs at the cell edge at fixed locations. An example network layout is shown in Fig. 3.2 considering an ISD of 500 m and 4-RN deployment. Relay deployment is performed in a way that no coverage gaps are left, and overlap between neighboring RN cells is minimized. In addition, in the two-hop relay based deployment, each

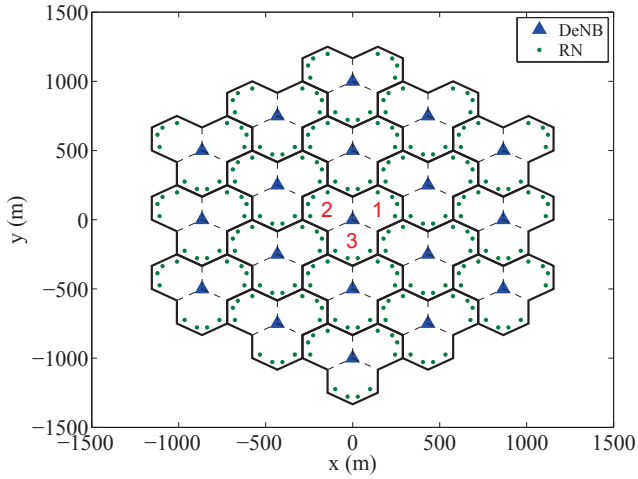

Figure 3.2. Example network layout for ISD=500 m and 4-RN deployment.

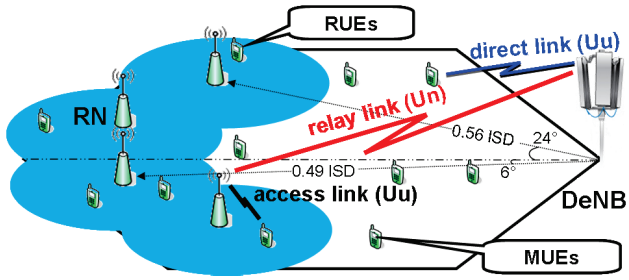

Figure 3.3. One-tier relay deployment shown in a sector along with the depicted links.

UE is either served directly by a DeNB or indirectly via an RN. This is depicted in Fig. 3.3 for 4-RN deployment along with the links. Besides, detailed RN locations for one-tier and two-tier RN deployments are provided in Fig. 3.4. Two antenna types are considered for RNs in this work, unless otherwise stated. Namely, directional antennas, which point toward their DeNBs, are assumed at the RNs for backhaul transmissions, while omni-directional antennas are assumed for the access link transmissions.

3.2.2 Propagation Scenarios and Implicit RSP Modeling

We consider urban (3GPP Case 1) and suburban (3GPP Case 3) scenarios with ISDs of 500 m and 1732 m, respectively [22]. These scenarios define the distance-dependent path losses on the depicted links as shown in Fig. 3.3 and as briefly explained in Section 2.1.2. Moreover, urban scenarios are interference-limited because of small ISD. On the contrary, suburban scenarios are coverage-limited because of large ISD. This highlights

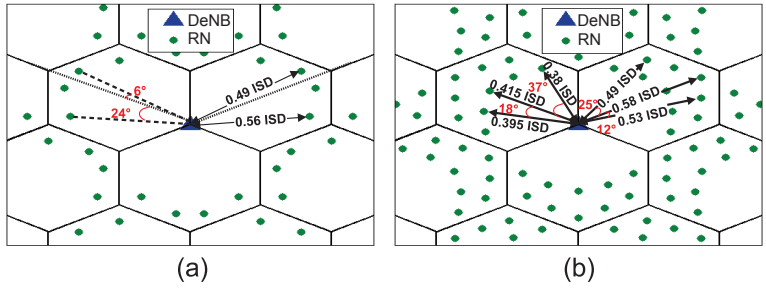

Figure 3.4. RN locations shown in a site; 4 RNs (a) and 10 RNs (b). ©2012 Wiley

one of the advantages of the relay deployment, which is the decreased radio distance to the serving cell. Both urban and suburban scenarios apply a probabilistic dual-slope channel model on all three links [22]. This channel model defines an LOS probability function versus the distance toward the serving cell. In particular, according to a random probability factor, a UE or an RN could be under either LOS or NLOS propagation conditions, and the probability of being in LOS increases as the distance to the serving cell decreases.

As discussed in Chapter 2, the end-to-end performance of the RUEs depends significantly on the capacity of the relay link. In this manner, RSP is shown to be an effective means to improve the relay link quality and, hence, to enhance the performance of relay deployments. The explicit modeling of RSP provided in Chapter 2 has presented notable gains and, thus, is included in the 3GPP guidelines [22]. Nevertheless, an implicit RSP modeling can be also applied [22]. In the implicit RSP modeling, the path loss formula is modified, which is to the benefit of the simulation run-time. Therefore, we employ the implicit RSP modeling in the following chapters. Specifically, an increased LOS probability is considered, and a planning bonus of 5 dB is added on the relay link when experiencing NLOS propagation conditions. Furthermore, if the RN experiences NLOS propagation conditions toward its DeNB, it is assumed that all other interfering links are in NLOS, as well. In addition, the interfering links can be under LOS conditions, only if the RN has LOS link toward its DeNB. Consequently, the parameters of the propagation scenarios are given in Table 3.1.

3.2.3 Shadowing Model

The lognormal shadowing model accounts for the fact that different locations with the same distance to the serving cell may exhibit differences in

Table 3.1. Propagation Scenarios

Distance	R [km]
Path Loss	PL [dB]
Direct Link	
PL(LOS): 103.4 + 24.2$\log_{10}$(R), PL(NLOS): 131.1 + 42.8$\log_{10}$(R)	
Urban Scenario - ISD 500 m	
Prob(LOS) = min(0.018 / R, 1) (1 - exp(-R / 0.063)) + exp(-R / 0.063)	
Suburban Scenario - ISD 1732 m	
Prob (LOS) = exp(-(R - 0.01) / 0.2)	
Access Link	
PL(LOS): 103.8 + 20.9$\log_{10}$(R), PL(NLOS): 145.4 + 37.5$\log_{10}$(R)	
Urban Scenario - ISD 500 m	
Prob(LOS) = 0.5 - min(0.5, 5exp(-0.156/R)) + min(0.5, 5exp(-R / 0.03))	
Suburban Scenario - ISD 1732 m	
Prob(LOS) = 0.5 - min(0.5, 3exp(-0.3/R)) + min(0.5, 3exp(-R / 0.095))	
Relay Link {a & b account for the RSP gain}	
$a = 3$ & $b = 5$ toward serving DeNB, while $a = 1$ & $b = 0$ toward other DeNBs.	
PL(LOS): 100.7 + 23.5$\log_{10}$(R), PL(NLOS): 125.2 + 36.3$\log_{10}$(R)-b	
Urban Scenario - ISD 500 m	
Prob(LOS) = 1 - (1 - (min(0.018 / R, 1) (1 - exp(-R / 0.072)) + exp(-R / 0.072)))^a	
Suburban Scenario - ISD 1732 m	
Prob(LOS) = 1 - (1 - exp(-(R - 0.01) / 0.23))^a	

average received signal levels. That is, the average received signal level changes with location due to shadowing process caused by different numbers of various obstructing large objects [38, 57, 58]. Accordingly, shadowing, as described in Section 2.1.2, is taken into account on all links for NLOS propagation conditions only.

Moreover, according to 3GPP guidelines [22], the shadowing correlation factors of 0.5 and 1.0 are assumed between sites and sectors, respectively. It is worth noting that this implies a shadowing correlation factor of 0.5 between DeNB sites and RN cells. In addition, shadowing standard deviation is $\sigma_{\text{DiL}} = 8$ dB on the direct link (abbreviated by DiL in this notation), $\sigma_{\text{AL}} = 10$ dB on the access link (abbreviated by AL in this notation), and $\sigma_{\text{RL}} = 6$ dB on the relay link (abbreviated by RL in this notation). When there is only a single value of standard deviation, e.g., in macrocell-only deployments and on the relay link in relay deployments, the shadowing model provided in [47] (see Section 2.1.2) can be directly used. However, attaining the aforementioned correlation factors along with the different

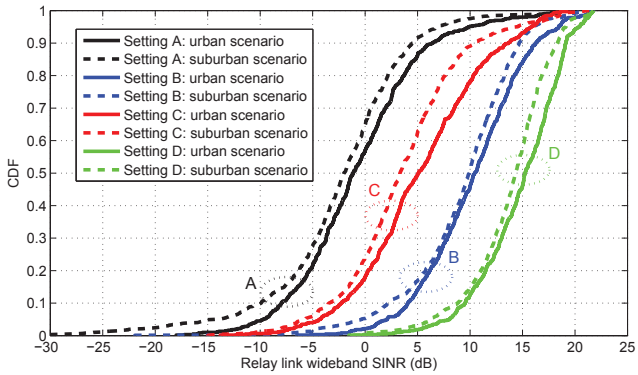

Figure 3.5. Relay link wideband SINR for urban and suburban scenarios under different configurations exemplified for 4-RN deployments. ©2011 KICS

standard deviations in relay deployments necessitates some further modifications in the shadowing model.

We start with the shadowing model in Section 2.1.2 where the shadowing RV on the direct link toward DeNB k can be stated in terms of two independent zero-mean Gaussian RVs ξ and η_k with the same standard deviation σ_{DiL} as

$$\zeta_k = \sqrt{\rho} \cdot \xi + \sqrt{1-\rho} \cdot \eta_k, \tag{3.1}$$

where $\rho = 0.5$. Here, we have $\mathrm{E}((\zeta_k)^2) = \sigma^2_{\text{DiL}}$. Further, the correlation factor between two different sites DeNB k and DeNB k' reads as

$$\mathrm{corr}(\zeta_k, \zeta_{k'}) = \frac{\mathrm{E}(\zeta_k \zeta_{k'})}{\sigma^2_{\text{DiL}}} = \frac{\rho \cdot \mathrm{E}(\xi^2)}{\sigma^2_{\text{DiL}}} = \rho, \tag{3.2}$$

where ξ, η_k, and $\eta_{k'}$ are mutually independent. In order to achieve the aforementioned relations, we introduce the shadowing RV on the access link toward RN l in terms of two independent zero-mean Gaussian RVs ξ and η_l with the same standard deviation σ_{DiL} as

$$\zeta_l = \Lambda \cdot \left(\sqrt{\rho} \cdot \xi + \sqrt{1-\rho} \cdot \eta_l \right), \tag{3.3}$$

where $\Lambda = \sigma_{\text{AL}}/\sigma_{\text{DiL}}$ is a scaling factor such that $\mathrm{E}((\zeta_l)^2) = \sigma^2_{\text{AL}}$. Then, the correlation factor between a DeNB site k and an RN cell l follows as

$$\mathrm{corr}(\zeta_k, \zeta_l) = \frac{\mathrm{E}(\zeta_k \zeta_l)}{\sigma_{\text{DiL}} \sigma_{\text{AL}}} = \frac{\Lambda \cdot \rho \cdot \mathrm{E}(\xi^2)}{\sigma_{\text{DiL}} \sigma_{\text{AL}}} = \rho, \tag{3.4}$$

where ξ, η_k, and η_l are mutually independent.

3.2.4 Wideband SINR Distribution

The wideband SINR (a.k.a. geometry or G-factor) is of particular interest for analyzing different implementations and deployments, and, thus, is

often utilized within the LTE framework, e.g., [22, 59, 60, 61, 62]. Then, the wideband SINR of a node (UE or RN) is determined on the DL in dB as

$$G_{\mathrm{SINR}} = \frac{P_{\mathrm{d}}}{\sum_n P_{\mathrm{i},n} + P_{\mathrm{N}}}, \tag{3.5}$$

where P_{d} is the received desired signal power, $P_{\mathrm{i},n}$ is the interference power caused by the n^{th} interfering node, and P_{N} is the thermal noise power over the whole bandwidth. We note that diversity gains via channel-aware scheduling and multiple-input multiple-output (MIMO) techniques are not included.

Herein, we explore the impact of directional antennas and RSP on the relay link wideband SINR. Hence, four settings are defined as follows.

- Setting A: No directional antennas on the relay link and no RSP (reference setting).
- Setting B: Only directional antennas on the relay link.
- Setting C: Only RSP.
- Setting D: Both directional antennas on the relay link and RSP.

The corresponding wideband SINR CDFs for urban and suburban scenarios are plotted in Fig. 3.5 for 4-RN deployments. It is observed that for all configurations, the relay link has higher wideband SINR in urban scenarios due to smaller ISD. Very low wideband SINR values are experienced when there is neither directional antennas installation nor RSP. This degradation is significant for suburban scenarios at low wideband SINR regime. Significant wideband SINR improvement is seen when directional antennas are installed, which results in lower interference levels. As expected, the best performance is obtained when both directional antennas are installed, and RSP is performed.

3.3 Simulation Parameters

Indoor UEs are assumed and, thus, a 20 dB penetration loss is added along with distance dependent path loss on direct and access links only. Yet, relays are located outdoors and, hence, there is no penetration loss on the relay link. Moreover, cell selection for UEs is based on the strongest

DL received signal power, whereas RNs are connected to the overlaying macrocells. Besides, 25 uniformly distributed UEs are dropped randomly per cell. For each UE drop, it is assumed that shadowing and distance-dependent path loss remain constant. The number of UE drops is selected to be large enough such that the difference between repeated tests is ignorable. Furthermore, simulations are carried out using a Matlab based system-level semi-static simulator, which is developed throughout this work and dubbed MARS (Matlab based Enhanced Relay Simulator). To ensure proper modeling of interference, results are collected from the midmost sector only (see sector 1 in Fig. 3.2). In addition, full buffer traffic model is employed, and all available resources in a cell are assumed to be used at all times provided that the considered resource allocation strategy permits.

The total RN coverage areas of 4-RN (one-tier) deployments in the overlaying macrocells read as 29.5% and 43.5% in urban and suburban scenarios, respectively. In case of 10-RN (two-tier) deployments, the total RN coverage areas become 45.5% and 67.0% in urban and suburban scenarios, respectively. We note that fast fading is not simulated in the following chapters. The main simulation parameters are then given in Table 3.2.

3.4 Rate Function

As briefly mentioned in Section 2.2.3, the SINR to link TP mapping is carried out by using the approximation:

$$\mathrm{TP} = S \cdot \begin{cases} 0, & \mathrm{SINR} < \mathrm{SINR}_{\min} \\ \mathrm{BW} \cdot \mathrm{SE}_{\max}, & \mathrm{SINR} \geq \mathrm{SINR}_{\max}, \\ \mathrm{BW} \cdot B_{\mathrm{eff}} \cdot \log_2\left(1 + A_{\mathrm{eff}} \cdot \mathrm{SINR}\right), & \text{otherwise} \end{cases} \tag{3.6}$$

where BW is the bandwidth per PRB, $\mathrm{SE}_{\max}$ is the maximum spectral efficiency depending on the highest available MCS for a given $\mathrm{SINR}_{\max}$, and B_{eff} and A_{eff} are, respectively, the so-called bandwidth and SINR efficiencies [51]. Besides, S is the overhead scaling which accounts for LTE UL overhead. Recall that the approximation in (3.6) models the AMC applied in the system [51, 52]. The utilized parameters are given in Table 3.2. Further, a minimum SINR level $\mathrm{SINR}_{\min}$ = -7 dB is considered, below which data detection is not possible. This limit is introduced due to control channel requirements.

Table 3.2. Simulation Parameters

System Parameters	
Carrier Frequency	2 GHz
Bandwidth	10 MHz
Number of PRBs	48 (data) + 2 (control channel)
PRB Bandwidth (BW)	180 kHz
Highest MCS	64-QAM, $\mathcal{R}$ = 9/10 ($\mathrm{SE}_{\max} = 5.4$ bps/Hz)
Bandwidth Efficiency (B_{eff})	0.88
SINR Efficiency (A_{eff})	1/1.25
Overhead Scaling (S)	0.75
Thermal Noise PSD	-174 dBm/Hz
Penetration loss	20 dB on direct and access links
eNB/DeNB Parameters	
Transmit Power	46 dBm
Maximum Antenna Gain	14 dBi
Antenna Configuration	Tx-2, Rx-2
Noise Figure	5 dB
Antenna Pattern (Horizontal)	A(θ) = $-\min[12(\theta/\theta_{3\mathrm{dB}})^2, A_m]$ $\theta_{3\mathrm{dB}}$=70° and A_m = 25 dB
UE Parameters	
Maximum Transmit Power	23 dBm
Antenna Configuration	Tx-1, Rx-2
Maximum Antenna Gain	0 dBi
Noise Figure	9 dB
RN Parameters	
Transmit Power	30 dBm
Antenna Configuration	Tx-2, Rx-2
Maximum Antenna Gain	7 dBi on relay link (directional) 5 dBi on access link (omni-directional)
Relay Link Antenna Pattern (Horizontal)	A(θ) = $-\min[12(\theta/\theta_{3\mathrm{dB}})^2, A_m]$ $\theta_{3\mathrm{dB}}$=70° and A_m = 20 dB
Noise Figure	5 dB
Shadowing	
Standard Deviation	8 dB (direct link) 10 dB (access link) 6 dB (relay link)
De-correlation Distance	50 m
Correlation Factor	0.5 (between sites) 1.0 (between sectors)

4. Uplink Power Control

Thanks to the orthogonality of SC-FDMA, intra-cell interference is not of main concern in LTE. The main task of PC mechanisms is then to maximize the received power of desired signals through compensating the channel variations while limiting the amount of the inter-cell interference generated. Besides, the receiver dynamic range[1] of eNBs/DeNBs and RNs should also be adjusted via PC to avoid intra-cell interference. In particular, PC can be used to decrease the deviation of the distribution of received power levels from different nodes, i.e., UEs or RNs, in the same cell ensuring that the receiver dynamic range does not exceed a predetermined level. We note that a high receiver dynamic range increases the susceptibility of SC-FDMA to the loss of orthogonality and, hence, can cause intra-cell interference [63].

Relay deployments will require a more detailed dimensioning and planning than conventional single-hop networks, e.g., RUEs can create severe inter-cell interference in particular when a large number of RNs are deployed in the cell with full frequency reuse. This is mainly due to additional interference imposed by RUEs within the same cell. Consequently, PC becomes a vital means to limit interference on the UL in relay deployments. In addition, in contrast to eNB-only networks, PC is necessary for the relay link because the end-to-end TP of RUEs depends on the qualities of both the access and relay links.

Within the single-hop LTE Rel. 8 framework, simulation-based performance evaluation of PC has been well elaborated in the literature [64, 65, 66, 67, 68, 69]. However, for LTE-Advanced relay deployments, PC parameter optimization problems were not widely examined. In [23], it is shown that LTE Rel. 8 compliant PC is also appropriate for relay networks, and

[1]The receiver dynamic range is defined as the difference in dB between the $5^{\text{th}}\%$-ile and $95^{\text{th}}\%$-ile of the CDF of the total UL received power.

that applying a heuristic optimization methodology, we can achieve a clear increase in the system performance. In [24], the PC optimization is done taking into account the imposed interference levels by MUEs and RUEs at DeNB, and we show that for the maximum performance enhancement, PC parameters should be optimized not only at RNs but also at DeNBs. Furthermore, in [23, 24], the PC optimization is carried out in urban scenarios for direct and access links only, and the relaying overhead is neglected. The impact of the relaying overhead is analyzed in [PIV] where two multi-step PC parameter optimization strategies are suggested for urban and suburban scenarios. Specifically, the PC parameters on one of the three links, i.e., the direct, access, and relay links, are tuned in each step according to the results obtained in the preceding step. This set of approaches is classified as *manual optimization method*, since a small number of values are logically selected for each PC parameter and evaluated against target performance metrics, e.g., 5%-ile user TP and 50%-ile user TP while targeting more ubiquitous user performance. Based on the simulation results, the best value is then selected for each PC parameter.

An advantage of the manual optimization method is that the impact of each PC parameter on the resultant system performance can be easily assessed [23, 24], [PIV]. On the other hand, as a subset of the search space is explored at each logical step, a nearly optimum solution may not be always achieved. Moreover, a change in the optimization target will require a direct skilled human intervention with high effort, which may incur additional costs, as well. Accordingly, the main goal of the *automated optimization method* is not only to explore the full search space but also, at the same time, to enable a flexible adaptation to changing optimization goals, thereby alleviating the burden in the manual optimization method. Such a flexible adaptation is achieved by the concept of *performance steering* as introduced in [PV], [25]. In this context, Taguchi's method based on nearly orthogonal array (NOA) and simulated annealing are utilized as two viable options for the automated optimization method.

In addition, in [PVI], we study the system-level energy efficiency of RN and picocell deployments from a UE point of view. In particular, we look at the energy efficiency at UE from a bit-per-power unit perspective by employing TP per power consumption as the performance measure.

4.1 Power Control Mechanism and Power Limitation

Motivated by the desired backward compatibility with LTE Rel. 8, i.e., legacy terminals should also support relay operations, the PC mechanism defined for the PUSCH in LTE [70] is used to determine the transmit power of UEs. Also, this mechanism is employed for the relay-specific PUSCH (R-PUSCH), which is the physical channel for the UL relay link data transmissions. Accordingly, the transmit power of a node u (UE or RN) is given in dBm as

$$P_u = \min\{P_{\max}, P_0 + 10 \cdot \log_{10} M_u + \alpha \cdot L + \Delta_{\mathrm{TF}}(i) + f(i)\}. \tag{4.1}$$

In this equation,

- $P_{\max}$ is the maximum allowed transmit power with an upper limit of 23 dBm for UE power class 3 [71] and 30 dBm for RN transmissions [22],
- P_0 is the power offset comprising cell-specific and node-specific components, which is used for controlling the received SNR target, and it can be set from -126 dBm to $P_{\max}$ with a step size of 1 dB,
- M_u is the number of PRBs allocated to an UE or an RN,
- α is a 3-bit cell-specific path loss compensation factor that can be set to 0.0 and from 0.4 to 1.0 with a step size of 0.1,
- L is the DL path loss estimate calculated by the node, and
- $\Delta_{\mathrm{TF}}(i)$ and $f(i)$ are the optional node-specific closed-loop correction and the MCS offset, respectively.

Since SC-FDMA is ideally an orthogonal system, and the cell-specific parameters have the main impact on the inter-cell interference, the optional closed-loop parameters in (4.1) are excluded. Omitting these parameters saves the overhead due to signaling especially when a large number of users are served in a cell. Also, we refer to [65] where the performances of open-loop PC and SINR-balancing closed-loop PC were compared. Therein, it was shown that closed-loop PC performs worse than open-loop PC especially when the cell load is high. Therefore, this work carries out the analyses based on open-loop PC. We note that depending

on the type of the QoS class, the service target can be met by open-loop PC along with fast link adaptation through frequency-domain scheduling and AMC, and bandwidth adaptation. Nevertheless, some UE-specific PC adjustment via optional closed-loop PC parameters can still be performed to attain a finer degree of control [6].

Open-loop PC compensates for slow channel variations, i.e., path loss including shadowing while limiting the inter-cell interference. If $\alpha = 1$ in (4.1), the path loss is fully compensated, and the resulting scheme is called full compensation PC (FCPC). For a given P_0 value, FCPC improves the cell-edge user performance at the cost of increased inter-cell interference due to higher transmit power levels. Yet, the inter-cell interference can be reduced by setting $\alpha < 1$, i.e., by using fractional PC (FPC), which increases the cell-center performance at the cost of penalizing the cell-edge performance [23, 24, 25, 64, 65] and [PIV, PV].

In addition, we apply the adaptive transmission bandwidth (ATB) functionality where the maximum number of PRBs which can be assigned to a UE depends on the difference between $P_{\max}$ and the *per-PRB* power spectral density (PSD) of that UE as described in [PIV, PV]. That is, power-limited UEs[2] will not be scheduled more resources than what they can effectively use, and, as a consequence, radio resources can be better utilized by other users resulting in more efficient bandwidth usage. Moreover, it is reported in [72] that ATB is particularly advantageous for suburban scenarios having large ISD. Thus, ATB is applied only for suburban scenarios in this work.

4.2 Optimization Methods

To enhance the overall system performance, the PC parameter optimization should be carried out on all links considering the interdependencies. In this task, however, a brute-force approach is infeasible due to high computational complexity given the PC parameter ranges discussed in Section 4.1 [PV]. To find a practically feasible solution, we formulate a PC parameter optimization problem. For that purpose, we define

$$x_1 = P_0^{\text{direct link}},\ x_2 = P_0^{\text{access link}},\ x_3 = P_0^{\text{relay link}},\ x_4 = P_{\max}^{\text{RUE}}, \tag{4.2}$$

where $P_0^{\text{direct link}}$, $P_0^{\text{access link}}$, and $P_0^{\text{relay link}}$ are the P_0 values on the direct, access, and relay links, respectively, and $P_{\max}^{\text{RUE}}$ is the maximum RUE

[2]These are the UEs that are transmitting at $P_{\max}$.

transmit power. We note that $P_{\max}^{\text{RUE}}$ is added to the configuration parameter set since it is shown in [PIV] and [23, 24] that further gain can be achieved by tuning it. Concretely, therein it is observed that for this gain the interference caused by RUEs should be reduced, and to achieve this either $P_0^{\text{access link}}$ or $P_{\max}^{\text{RUE}}$ can be decreased. The PC parameter optimization problem is then given by

$$(\hat{x_1}, \hat{x_2}, \hat{x_3}, \hat{x_4}) = \underset{(x_1,\, x_2,\, x_3,\, x_4)}{\arg\max}\; y(\text{TP}_1, \ldots, \text{TP}_C), \tag{4.3}$$

where y is the objective function based on the target performance metric, and C is the total number of UEs from which the statistics are collected.

Within the framework of *performance steering*, the system performance can be flexibly adjusted [PV] by using a proper performance metric as the objective function. In this context, the following key performance metrics are outlined:

- $\Gamma_{q\%}$: The *q^{th}%-ile level of the user TP CDF*, is a conventionally used performance metric in IMT-Advanced standardization. The objective function reads as

  $$y = \Gamma_{q\%} = F_s^{-1}(q/100), \tag{4.4}$$

  where $F_s^{-1}(q/100)$ is the inverse of the CDF at the $q/100$-quantile, called as q-percentile (%-ile).

- $\Gamma_{\text{HM}}^{Q\%}$: This is a performance metric proposed in [PV], which is related to the *harmonic mean (HM) of the user TP*. That is,

  $$y = \Gamma_{\text{HM}}^{Q\%} = \frac{C^*}{\sum_{\iota=1}^{C^*} \frac{1}{\text{TP}_\iota}} \text{ s.t. } \text{TP}_\iota > F_s^{-1}(Q/100), \tag{4.5}$$

  where $C^* \leq C$ is the total number of users whose TP values (TP_ι) satisfy the given condition, which depends on the cut-off percentile Q. In particular, Q should be adjusted such that too low TP levels, which can bias the performance metric, are omitted [PV].

- $\Gamma_{\text{AM}}^{(w_1,\, w_2, \ldots, w_L)}$: This is a performance metric obtained as a *weighted arithmetic mean (AM) of the normalized $\Gamma_{q_j\%}$ values as defined in* (4.4)*, for* $j = (1,\, 2, \ldots,\, L)$ [PV]. The objective function is given by

  $$y = \Gamma_{\text{AM}}^{(w_1,\, w_2, \ldots, w_L)} = \frac{\sum_{j=1}^{L} w_j \frac{\Gamma_{q_j\%}}{\kappa_{q_j\%}}}{\sum_{j=1}^{L} w_j}\,, \tag{4.6}$$

where κ_{q_j}% for $j = (1,\ 2, \ldots,\ L)$ is the normalization factor which corresponds to q_j%-ile of the user TP CDF of the reference eNB-only deployment. When targeting a more homogeneous user performance, we place the focus primarily on lower percentiles, e.g., we use $(q_1,\ q_2,\ q_3) = (5,\ 25,\ 50)$%-ile for computing $\Gamma_{\mathbf{AM}}^{(w_1,\ w_2,\ w_3)}$. Accordingly, a high parametric flexibility can be attained through the selection of the weights where a certain CDF percentile can be prioritized by means of increasing its corresponding weight.

4.2.1 Manual Optimization

Two manual PC parameter optimization methods are provided in [PIV] for urban and suburban scenarios . These methods differ in terms of adaptation to the considered deployment scenario.

Urban Scenario-specific Optimization Method

The inter-cell interference due to small ISD is the main limiting factor for the performance in urban scenarios; thus, it is of particular concern in the urban scenario-specific optimization method. The urban scenario-specific optimization method comprises two main parts. Concretely, the first part, which consists of four logical steps, tunes PC parameters on access and direct links, and ignores the impact of relay link. The impact of relay link is, in turn, considered in the second part of the optimization when PC parameter tuning is conducted. The four-step approach of the first part is given as follows.

1. In the first step, a PC parameter tuning is applied in eNB-only scenario. Specifically, a parameter sweep over P_0 range is applied for four different values of α. Obtained cell capacity (a.k.a. aggregate user TP) and 5%-ile user TP values are plotted in Fig. 4.1. Two parameter settings are selected depending on the prioritization strategy. Namely, the cell coverage-oriented setting (based on FCPC) prioritizes the 5%-ile user TP and the cell capacity-oriented setting (based on FPC) prioritizes the cell capacity at the cost of the reduced 5%-ile user performance.

2. In the second step, RNs are taken into account, and parameters resulting from Step 1 are applied for both MUEs and RUEs. It is then demonstrated in [PIV] that the relay deployment outperforms the eNB-

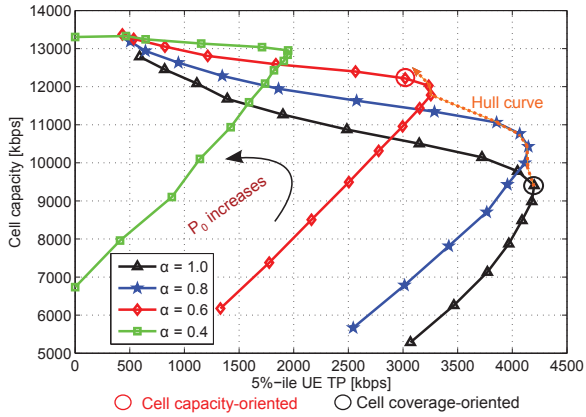

Figure 4.1. Cell capacity vs. 5%-ile user TP for different values of α in eNB-only deployment. The hull curve depicts the trade-off between cell coverage and cell capacity. ©2011 KICS

only deployment at all TP CDF percentiles. Simulation results of this step are used as a starting point for Steps 3 and 4 through which further performance enhancement can be achieved.

3. This step tackles the increased inter-cell interference due to the deployment of RNs. After RNs are deployed in the network, the inter-cell interference increases. More concretely, RUEs experience very high TP levels while causing interference to MUEs. As we focus on achieving a more homogeneous user performance over the whole cell area, the performance of MUEs is prioritized in this step. In particular, the interference imposed by RUEs is reduced by adequately adjusting their PC parameters such that the impact of the interference caused by RUEs on the performance of MUEs becomes minimal. In this regard, the total interference at DeNB is given in terms of a summation of the interferences caused by MUEs and RUEs, which are referred to as *Interference over Thermal noise (IoT) proportions* [PIV]. This approach is illustrated in Fig. 4.2 where the total mean IoT at DeNB is depicted using different PC settings in RN cells. It can be seen that the total mean IoT at DeNB decreases as P_0 and $P_{\max}$ values in RN cells decrease, which implies a decrease in the IoT proportion of RUEs. For both FPC and FCPC, the PC settings are then selected such that the total mean IoT at DeNB is dominated by the IoT proportion of MUEs (cf. black dash-dotted curves), and a further decrease of the IoT proportion of RUEs does not translate into notable decrease in the total mean IoT at DeNB. Also, the impact

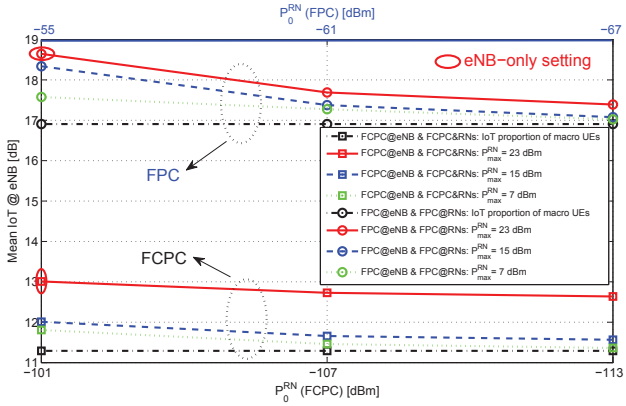

Figure 4.2. Mean IoT at DeNB vs. P_0 for different $P_{\max}$ values in RN cells. The simulation results are given for FPC and FCPC settings. The P_0 values pertaining to eNB-only settings are circumscribed. ©2011 KICS

on the receiver dynamic range at RNs and expected battery life time of RUEs are considered when selecting the PC settings.

4. In the final step, keeping PC parameters of the RUEs fixed to those found in Step 3, the PC parameters of MUEs are optimized. More concretely, the purpose of this step is to further improve the performance of MUEs by readjusting their PC parameters. Thus, a parameter sweep over P_0 set is applied similarly as in Step 1 while 50%-ile and 5%-ile user TP CDF levels are used as performance criteria. As a result, significant TP gains are achieved both at 50%-ile and 5%-ile user TP levels [PIV].

We note that due to stepwise optimization process in this method, after Step 4 the PC parameters for RUEs may not be optimal. Nevertheless, simulation results in Section 4.3.1 and further in [PV] show that automated optimization methods, which jointly optimize PC parameters, and this manual optimization method can achieve similar performances.

Following these steps, the PC parameters of MUEs and RUEs are tuned. In the second part of the optimization, the impact of relaying overhead on the system performance is addressed while PC parameter optimization is conducted on the relay link. The cell capacity-oriented setting found in Step 1 is taken as the starting point, and the P_0 value on the relay link is adjusted such that 50%-ile user TP level is maximized provided that the DeNB receiver dynamic range does not exceed the pre-determined level. Yet, as the relay link performance is highly interference-limited, the fine-tuning of the P_0 value does not yield a clear performance enhancement.

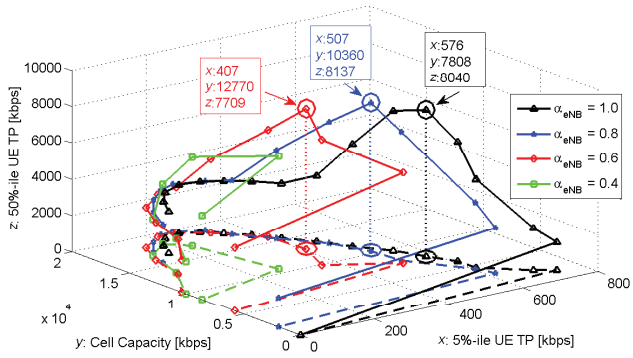

Figure 4.3. 5%-ile user TP vs. cell capacity vs. 50%-ile user TP for different values of α in eNB-only deployment. Out of the depicted candidate settings, the one with FPC ($\alpha = 0.6$) is selected. ©2011 KICS

Notable as well is the trade-off between resultant FPC-based and FCPC-based PC settings; the latter results in higher gains in low TP regime, whereas the former boosts the performance at higher TP regime [PIV].

Suburban Scenario-specific Optimization Method

Unlike urban scenarios, due to larger ISD, the impact of inter-cell interference decreases drastically in suburban scenarios. On the other hand, path loss of cell-edge UEs may not be compensated, and they can be easily driven to power limitation (see Section 4.1). The result is inhomogeneous TP distribution over the coverage area where cell-center UEs experience high TP levels because of reduced inter-cell interference when compared to urban scenario, and cell-edge UEs suffer from large path loss. Thus, this optimization method addresses the inhomogeneity of the TP distribution via jointly optimizing several performance metrics [PIV]. Similar to the urban-scenario specific method, this method comprises two main parts. Accordingly, the first part consists of three steps as follows.

1. In the first step, PC parameters of UEs in eNB-only scenario are tuned via jointly optimizing cell capacity, 50%-ile, and 5%-ile user TP CDF levels, as shown in Fig. 4.3. Then, a setting, which enables a good trade-off between the aforementioned performance metrics, is selected.

2. Here, RNs are considered, and parameters resulting from Step 1 are applied to both MUEs and RUEs for demonstration. Simulation results of this step are used as a starting point for Step 3.

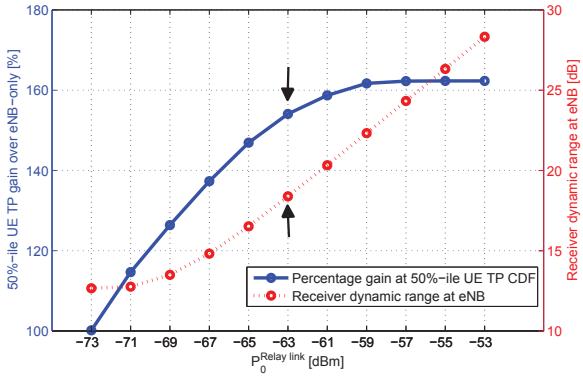

Figure 4.4. 50%-ile user TP gain w.r.t. eNB-only deployment, and DeNB receiver dynamic range vs. P_0 on the relay link. ©2011 KICS

3. In the final step, PC parameters of MUEs and RUEs are jointly reconfigured. Specifically, a fine tuning of parameter settings ($P_0^{\text{direct link}}$, $P_0^{\text{access link}}$, $P_{\max}^{\text{RUE}}$) is done around the PC setting found in Step 2. Further, 50%-ile and 5%-ile user TP levels are taken as the performance criteria, and the obtained PC setting is referred to as the *trade-off* setting.

After having found the PC configurations for MUEs and RUEs, the optimum parameter setting for the relay link is determined. The trade-off setting is used as the starting point, and the optimum P_0 value on the relay link is selected such that 50%-ile user TP level is maximized, and the DeNB receiver dynamic range does not exceed the pre-determined level, i.e., 20 dB (see Fig. 4.4 where arrows mark the selected setting). It is seen that, in contrast to urban scenarios, the fine tuning of P_0 on the relay link can yield notable performance enhancement.

4.2.2 Automated Optimization

Simulated annealing is a well known optimization method which has been extensively used in many engineering problems [73, 74, 75]. This meta-heuristic search method reduces significantly the complexity and network trial runs (a.k.a. evaluation runs), and still converges to a near-optimum system state. Besides, it is a local search-based optimization method that provides a means to escape local maxima [75]. Taguchi's method is another promising optimization method which was first developed for the optimization of manufacturing processes [76] and has been recently introduced in wireless communication field [76, 77, 78] and [PV], [25]. Unlike

simulated annealing that heuristically discovers the multi-dimensional parameter space of candidate solutions, Taguchi's method uses a so-called orthogonal array (OA) [79], where a reduced set of parameter combinations from the full search space is tested. The number of selected parameter combinations determines the number of experiments being carried out and evaluated using a performance metric. After considering all the results of the experiments, a candidate solution is found, and the process is repeated till a desired criterion is fulfilled. In this work, an NOA is used instead of an OA, like proposed in [80], to significantly reduce the computational complexity at the expense of a slight degradation in performance. The algorithms of these methods are provided in [PV]. We note that an advantage of Taguchi's method over simulating annealing is the comparatively simple initialization where the former requires three input parameters, whereas the latter requires six [PV]. Fundamentally, the performance steering concept, as introduced in Section 4.2, has a crucial role in the automated optimization.

4.3 Performance Assessment

The performance evaluation is carried out in 4-RN urban and suburban scenarios. Moreover, the eNB-only deployment is taken as a benchmark for performance comparisons. For the case of automated optimization method, in order to have a fair comparison between Taguchi's method and simulated annealing in terms of TP performance, the same computational complexity is applied [PV]. That is, they are run for the same number of evaluations, and the TP performances of their optimized configurations are compared. The number of evaluation runs, i.e., network trial runs, is set to 540 for automated optimization [PV]. Yet, automated optimization may converge to the final value before 540 evaluation runs are completed. On the other hand, in case of manual optimization, the number of evaluation runs is determined by the number of data points/markers on the curves for a given α value [PIV]. Urban scenario-specific manual optimization method and suburban scenario-specific manual optimization method require 51 and 65 evaluation runs, respectively. However, manual optimization requires direct skilled human intervention; hence, a complexity comparison between manual and automated optimizations is not relevant. Furthermore, an increase in the number of evaluation runs for manual optimization would decrease the step size between the PC param-

eter values that are simulated; this would in turn mean finer-tuning for manual optimization.

4.3.1 Urban Scenarios

In [PV], [25], a comparison of joint P_0 optimization (considering x_1, x_2, and x_3 in (4.3)), and joint P_0 and $P_{\max}$ optimization (considering x_1, x_2, x_3, and x_4 in (4.3)) is given. For both manual and automated optimizations, it is seen that relative to joint P_0 optimization, joint P_0 and $P_{\max}$ optimization achieves some improvement at 5%-ile UE TP CDF level where the improvement is more pronounced for FCPC, while it is marginal for FPC.

Thanks to small ISD, power limitation (see Section 4.1) and, thus, user outage are less pronounced in urban scenarios, which translates into a more homogeneous user performance over the cell area. In essence, the performance metrics which consider a specific UE TP CDF level, i.e., $\Gamma_{q\%}$, can be utilized to steer the performance toward the desired performance level without causing significant performance degradation at other performance levels. This is depicted in Fig. 4.5 where joint P_0 optimization is considered in case of FPC. It is observed that, via $\Gamma_{50\%}$, the 50%-ile UE TP can be further increased at the cost of performance degradation at low TP regime, whereas, via $\Gamma_{5\%}$, the best 5%-ile UE TP can be achieved with worse performance at higher percentiles. Furthermore, using $\Gamma_{\text{HM}}^{Q\%}$ for $Q > 0$ higher percentiles can be prioritized. For example, $\Gamma_{\text{HM}}^{10\%}$ yields higher gains at high TP regime but lower gains at low TP regime. Besides, a trade-off between lower and higher UE TP CDF percentiles can be achieved when $\Gamma_{\text{AM}}^{(1,\,1,\,1)}$ is used. More crucially, the graphs pertaining to manual optimization, which aims at the same trade-off, and automated optimization using $\Gamma_{\text{AM}}^{(1,\,1,\,1)}$ are broadly similar.

4.3.2 Suburban Scenarios

A comparison between joint P_0 optimization, and joint P_0 and $P_{\max}$ optimization is provided in [PV], where it is shown that both of them yield similar results. Thus, the primary focus is put on joint P_0 optimization, and the high inhomogeneity of user performance due to large ISD is tackled by performance steering.

For demonstration, the performance difference between conventional performance metrics, namely, $\Gamma_{5\%}$, $\Gamma_{25\%}$, and $\Gamma_{50\%}$, and the proposed performance metric $\Gamma_{\text{AM}}^{(1,\,1,\,1)}$ is illustrated in Fig. 4.6. We note that Taguchi's

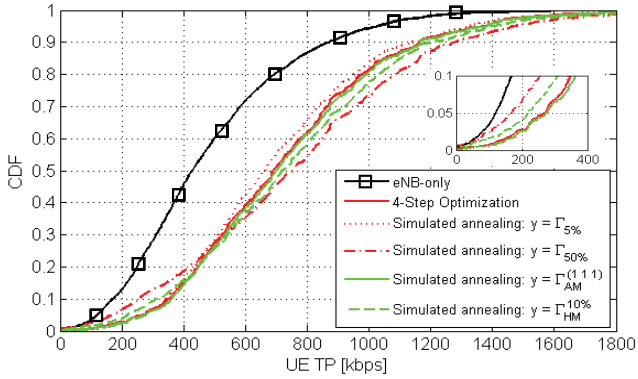

Figure 4.5. The UE TP CDFs using FPC and different performance metrics for joint P_0 optimization considering manual optimization (4-Step Optimization) and automated optimization (Simulated Annealing); urban scenario.

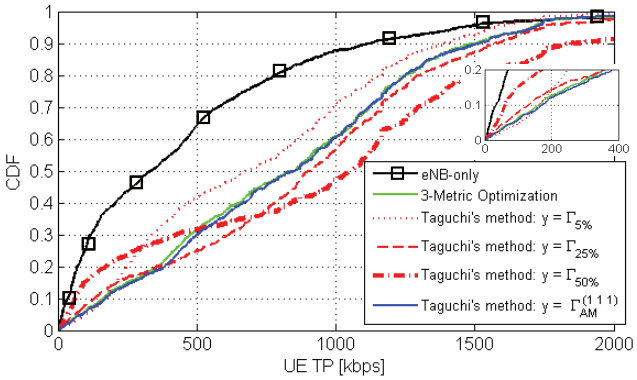

Figure 4.6. The UE TP CDFs for manual optimization (3-Metric Optimization), and automated optimization (Taguchi's method) using $\Gamma_{\text{AM}}^{(1,\,1,\,1)}$ and conventional performance metrics; suburban scenario.

method and simulated annealing exhibit similar performances in this analysis. It can be seen that the conventional performance metrics optimize the targeted UE TP CDF levels. However, performance degradation is observed at other levels, and when $\Gamma_{\text{AM}}^{(1,\,1,\,1)}$ is employed, the three UE TP CDF percentiles are equally prioritized, and a trade-off can be reached. In addition, the performance results of manual optimization, which already targets a trade-off between different UE TP CDF percentiles, and Taguchi's method using $\Gamma_{\text{AM}}^{(1,\,1,\,1)}$ are in agreement.

Within the performance steering context, the impact of utilizing different weights for $\Gamma_{\text{AM}}^{(w_1,\,w_2,\,w_3)}$ is addressed through Fig. 4.7. It is shown that increasing a given weight relative to other weights, the performance of the corresponding UE TP CDF percentile can be increased. For instance, $\Gamma_{\text{AM}}^{(2,\,1,\,1)}$ maximizes the 5%-ile UE TP CDF while yielding a per-

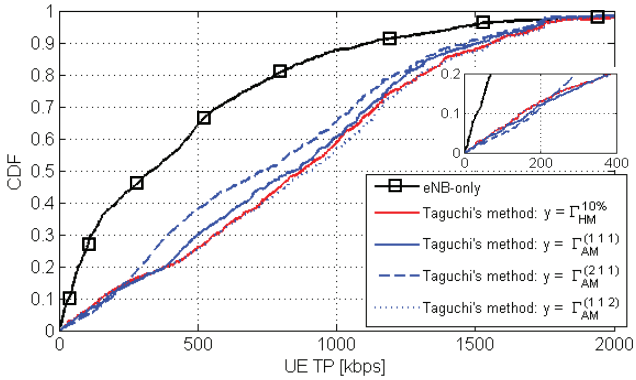

Figure 4.7. The UE TP CDFs for automated optimization (Taguchi's method) using $\Gamma_{\text{AM}}^{(w_1,\, w_2,\, w_3)}$ as the performance metric with different weights; suburban scenario.

formance degradation at higher percentiles, whereas $\Gamma_{\text{AM}}^{(1,\, 1,\, 2)}$ maximizes the 50%-ile UE TP CDF at the cost of performance degradation at low percentiles. Crucially, it is noted that compared to conventional metrics, using $\Gamma_{\text{AM}}^{(w_1,\, w_2,\, w_3)}$ results in small performance degradation at less prioritized percentiles since their performances are, as well, taken into account. In addition, $\Gamma_{\text{HM}}^{10\%}$ prioritizes higher UE TP CDF percentiles by focusing on the UEs that contribute to as of 10%-ile UE TP CDF. Besides, the advantages of selecting a cut-off percentile of $Q = 10\%$-ile over $Q = 0\%$-ile are identified in [PV].

4.4 Throughput Power Consumption

Energy consumption has become one of the crucial issues in the wireless industry. Example efforts for enabling green radio networks include the European Commission research project Energy Aware Radio and Network Technologies (EARTH) [81, 82, 83], and a privately financed consortium called the Green Touch Initiative [84, 85]. With regards to UL transmissions, energy saving mechanisms are of particular interest for supporting the mobility and extending the battery life time of a UE.

Here, in line with [PVI], we study the energy efficiency of RN and picocell deployments by means of TPC. We note that the same channel models are assumed for both deployments, where the key difference between the two is that picocells require a costly fixed backhauling. Next, we define the radiated power P_{r} in terms of the UE time activity factor τ_{UE} and the

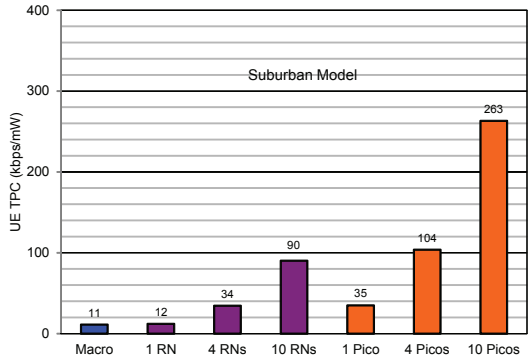

Figure 4.8. TPC_{UL} values for suburban RN and picocell deployments. ©2012 IEEE

transmit power level of the UE P_u (see (4.1)) as

$$P_{\mathrm{r}} = \tau_{\mathrm{UE}} \cdot P_u, \tag{4.7}$$

where τ_{UE} reflects the portion of the time during which the UE is scheduled. Hence, for RNs, as the UEs are not scheduled during the Un subframes on the UL, τ_{UE} inherently includes the impact of the half-duplex operation of RNs. Also, the PDCCH limitation introduced in Chapter 3 is reflected by τ_{UE}. Then, TP per power consumption on the UL TPC_{UL} is given in kbps/mW considering the average radiated power $\mathrm{E}(P_{\mathrm{r}})$ and the mean user TP TP_{avg} as

$$TPC_{\mathrm{UL}} = \frac{TP_{\mathrm{avg}}}{\mathrm{E}(P_{\mathrm{r}})}. \tag{4.8}$$

We note that the focus is on the transmit power levels of the UEs because the UE power consumption dramatically increases when the transmit power exceeds a certain level (cf. [40, Fig. 20.30] and the discussion thereon). For demonstration, we present TPC_{UL} values for different RN and picocell deployments in Fig. 4.8 for suburban scenarios. First, it is observed that significant gains are achieved over the reference eNB-only deployment when RNs or picocells are deployed. This stems from the fact that mean user TP increases in RN and picocell deployments, and, at the same time, the average radiated power decreases because of reduced path loss toward the serving cells. Moreover, it is seen that the picocell deployments outperform the RN deployments. This is because the mean user TP levels experienced by the UEs in picocell deployments are significantly higher. Nevertheless, due to half-duplex operation of RNs, the average radiated power levels of UEs are lower in RN deployments.

5. Resource Sharing

System performance of relay deployments depends strongly on the resource sharing strategy among and within the links. In particular, depending on target performance criteria, a proper balance should be maintained between links which compete for DeNB resources that usually form the bottleneck. In this context, the resource split at DeNB aims at finding not only the optimum number of Un subframes but also the resource shares of RNs and MUEs. A common assumption in the literature, e.g., [15, 18, 24, 86, 87, 88] and [PIV], is that Un subframes are exclusively assigned for relay link transmissions (see Fig. 5.1.a). In this case, the resource split determines both the resource shares of RNs and MUEs, and the number of Un subframes. For example, in [86], the number of Un subframes is selected to maximize TP or fairness on DL. Nevertheless, as the set of subframes assigned for the relay link transmissions is semi-statically configured, a dynamic reconfiguration to adapt to fast-changing system conditions, e.g., RN cell load, is not viable in case of exclusive resource allocation to RNs. Furthermore, such an exclusive allocation, in turn, reduces the resource utilization efficiency at the DeNB. For instance, when there are no RUEs within the coverage area in a given LTE frame, the subframes allocated to RNs cannot be utilized by the DeNB for MUEs. Therefore, a flexible resource split is desirable, which can be achieved by co-scheduling RNs and MUEs during Un subframes (see Fig. 5.1.b). Such an approach has been considered in [89, 90] where the impact of co-scheduling on the DL performance of relay deployments was investigated. These studies provide the resultant system performance by applying a parameter sweep for the number of Un subframes.

In [PVII], [26, 27] various resource sharing techniques are investigated for UL transmissions taking into account PC as discussed in Chapter 4. Herein, we first describe two resource sharing schemes for the resource

split at DeNB between RNs and MUEs. Namely, we present *hard resource split* [PVII], [26], where RNs are exclusively allocated all resources during Un subframes, and *flexible resource split* [PVII], [27], where Un subframes are over-provisioned, and MUEs and RNs are co-scheduled during these subframes. In the latter approach, the goal is to achieve a dynamic and efficient resource sharing which can instantaneously adapt to the changes in the system conditions, rather than relying on semi-static Un subframe allocation. Accordingly, the required number of Un subframes is determined for these schemes. Second, we focus on resource sharing schemes on individual links and analyze two models. The first model is the reference model which is adopted from [87, 88]. In the *reference model*, the resource share of an RN is proportional to the total instantaneous TP achieved on the access link of this RN. Further, the end-to-end TP of an RUE is proportional to its instantaneous access TP also considering the capacity of the relay link. The second model, which is referred to as the *hop-optimization model* [PVII], [26], applies a combination of relay link scheduling based on the number of RUEs, and a TP throttling technique achieving max-min fairness in the end-to-end two-hop communications (see Fig. 5.2). We note that adapted versions of the reference and hop-optimization models are, as well, studied for DL system performance in [91, 92].

Like in the rest of this work, one common assumption in the performance evaluation of relay deployments is that inter-DeNB synchronization is assumed, and a network-wide Un subframe configuration is applied. In this context, in [PVIII], we analyze the impact of Un subframe misalignment on the UL system performance of relay deployments. That is, we consider the case where DeNBs in the network can independently configure the set of Un subframes, and/or a system-wide Un subframe configuration is not possible.

5.1 Resource Split at DeNB

The number of Un subframes should be selected such that balance between the resource shares of relay and direct links is attained. As RUEs experience transmission gaps during the Un subframes, increasing the number of the Un subframes may render access link a bottleneck on the two-hop communications. This should be factored in, as well. The following two schemes are studied in this context.

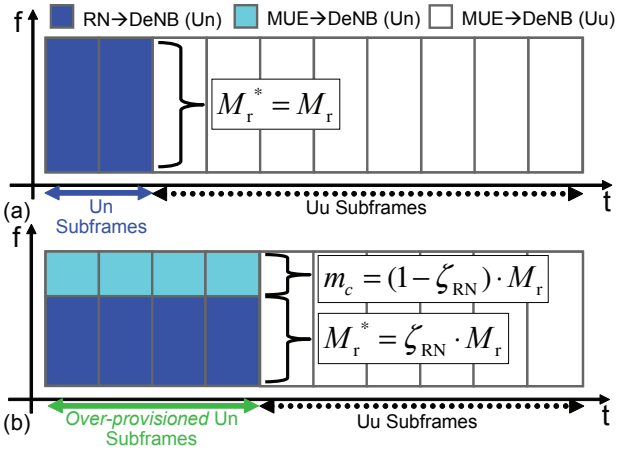

Figure 5.1. Resource split at DeNB; hard resource split (a), flexible resource split (b). ©2012 Wiley

5.1.1 Hard Resource Split

In this benchmark scheme, Un subframes are exclusively assigned for the relay link transmissions as illustrated in Fig. 5.1.a where the resource allocation at DeNB is depicted on the time-frequency plane. Due to the exclusive resource allocation, MUEs experience the same transmission gaps as RUEs. Moreover, the optimal number of Un subframes is selected according to the long-term average demand of UEs; thus, it may not be optimal on a short-term basis.

5.1.2 Flexible Resource Split

In this scheme, the Un subframes are over-provisioned such that MUEs can be scheduled during Un subframes. An example resource allocation is shown in Fig. 5.1.b where the Un subframes are depicted to be consecutive for illustration purposes. In this figure, m_c, the number of resources assigned to MUEs per Un subframe in cell c, is provided in terms of ζ_{RN}, the resource share of RNs per Un subframe, and M_r, the total number of PRBs in a Un subframe. Furthermore, ζ_{RN} is given in terms of ρ_{RN}, the RUE fraction in the cell, and N_b, the number of Un subframes out of 10, as

$$\zeta_{RN} = \min\{1, \rho_{RN}\frac{10}{N_b}\} \text{ with } \rho_{RN} = \frac{U_{RN}}{U_c}, \quad (5.1)$$

where U_{RN}, and U_c are the total number of RUEs, and the total number of all UEs in the cell, respectively. For a given N_b, the RN and MUE resource shares per Un subframe are, respectively, proportional to the total

number of RUEs U_{RN} and the total number of MUEs $U_{\mathrm{c}} - U_{\mathrm{RN}}$, provided that $\rho_{\mathrm{RN}} \leq N_{\mathrm{b}}/10$. Thus, the selection of N_{b} yields a trade-off, where, e.g., a larger N_{b} means a higher flexibility in adapting to system conditions but it leads to a reduced access link capacity since RUEs experience transmission gaps during Un subframes.

5.2 Resource Sharing Models

Here, we introduce two models, which comprise the strategies of allocating resources to different RNs and TP throttling techniques for the RUEs. Recalling from Section 2.2.3 that the end-to-end TP of the RUEs depends on the qualities of both the access and relay links, the end-to-end TP of RUE j served by RN i is obtained as

$$\mathrm{TP}^{\mathrm{e}}_{ij} = \min(\mathrm{TP}^{\mathrm{a}}_{ij}, \mathrm{TP}^{\mathrm{r}}_{ij}),\ j = 1, \cdots, u_i,\ i = 1, \cdots, N, \tag{5.2}$$

where the user capacity on the access link is defined as $\mathrm{TP}^{\mathrm{a}}_{ij}$ and that on the relay link as $\mathrm{TP}^{\mathrm{r}}_{ij}$. We note that a resource fair round robin scheduler is utilized for MUEs on the direct link, and for RUEs on the access link.

5.2.1 Reference Model

In the reference model, RNs are assigned resources on a demand basis, where the RN with more demand on the access link will be assigned more resources on the relay link. This allocation scheme is referred to as *access instantaneous TP-proportional (AIT-P)*. Then, the resource share of RN i is set as

$$m_i = \frac{\sum_{j=1}^{u_i} \sum_{k=1}^{m_{ij}} R_{ijk}}{\sum_{i=1}^{N} \sum_{j=1}^{u_i} \sum_{k=1}^{m_{ij}} R_{ijk}} M^*_{\mathrm{r}}, \quad i = 1, \cdots, N, \tag{5.3}$$

where N is the number of active RNs in the overlaying macrocell, m_{ij} is the number of resources assigned to RUE j served by RN i, and u_i is the number of UEs attached to RN i. Further, M^*_{r} (see Fig. 5.1) is the total number of PRBs reserved for the relay link transmissions in a Un subframe, and R_{ijk} is defined as the *per-PRB* spectral efficiency on the access link of UE j to its serving RN i for PRB k [PVII], [26].

Next, within the context of *UE instantaneous TP-proportional (UIT-P)* scheme, the end-to-end TP of UE j attached to RN i is expressed by

$$\mathrm{TP}^{\mathrm{e}}_{ij} = \min\left(\sum_{k=1}^{m_{ij}} R_{ijk}, \frac{\sum_{k=1}^{m_{ij}} R_{ijk}}{\sum_{j=1}^{u_i} \sum_{k=1}^{m_{ij}} R_{ijk}} \sum_{k=1}^{m_i} R_{ik}\right), \quad j = 1, \cdots, u_i, \quad i = 1, \cdots, N, \tag{5.4}$$

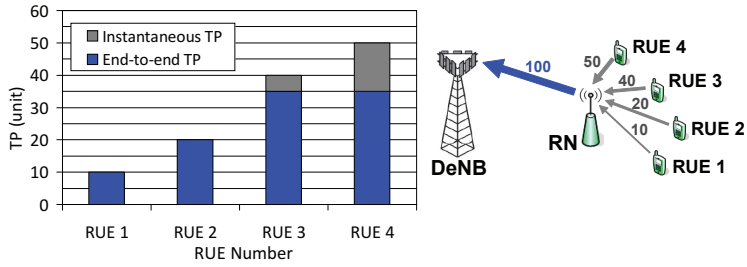

Figure 5.2. Example realization of the max-min fairness based TP throttling algorithm.

where R_{ik} is the per-PRB spectral efficiency of the RN i for PRB k.

5.2.2 Hop-optimization Model

In line with the *access UE proportional (AUP)* scheme, the resource share of RN i is set as

$$m_i = \frac{u_i}{U_{\mathrm{RN}}} M_{\mathrm{r}}^*, \quad i = 1, \cdots, N. \tag{5.5}$$

Then, the *max-min fairness* scheme is applied as the TP throttling technique. Following the algorithm presented in [PVII], [26], the end-to-end TP levels of RUEs are obtained. In this scheme, the users with worse link qualities are prioritized which, in turn, improves the performance of the users in low TP regime. An example scenario is illustrated in Fig. 5.2 where a water-filling analogy can be observed.

5.3 Performance Evaluation and Analysis

Here, the selection of the number of Un subframes is demonstrated considering aforementioned resource sharing approaches at DeNB. We first analyze the system assuming the hard resource split, and, then, further performance enhancements are presented utilizing the flexible resource split.

5.3.1 Selection of the Number of Un subframes

In case of hard resource split at DeNB, the number of Un subframes is selected with the help of so-called *proportional CDFs* as proposed in [PVII], [26]. By means of proportional CDFs, the impact of an optimization technique on the individual performances of RUEs and MUEs can be easily inferred. Namely, the system UE TP CDF is decomposed into the scaled CDFs of RUEs and MUEs. An example is illustrated in Fig. 5.3 where UE

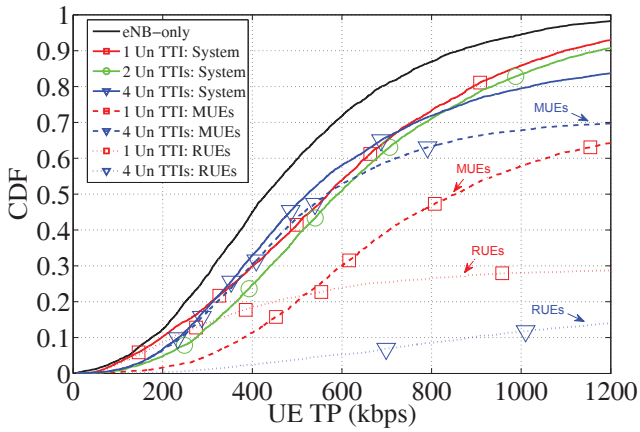

Figure 5.3. UE TP CDFs considering different Un subframe (TTI) configurations in 4-RN deployment; urban scenario. ©2012 Wiley

TP CDFs for different Un subframe configurations are plotted for a 4-RN urban scenario assuming the reference model. The FPC-based PC setting, as discussed in Chapter 4, is employed. When an insufficient number of Un subframes, i.e., 1 Un TTI, is set, the system performance is mainly limited by the performance of RUEs due to the backhaul bottleneck. On the other hand, the MUE performance becomes the limitation when four Un subframes are used because only six subframes are available for the MUEs. In this case, the RUE performance is significantly increased resulting in a higher TP gain at high percentiles. In addition, when two Un subframes are set, the best gain is achieved at the low TP regime. As the emphasis in LTE-Advanced is a more homogeneous user performance within the network, the optimum number of Un subframes is chosen to be two.

When flexible resource split at DeNB is utilized, the CDF of RN cell load, which is defined as RUE fraction ρ_{RN}, is considered as discussed in [PVII], [27]. The resultant number of Un subframes, N_{b}, is then determined taking the upper bound $\rho_{\mathrm{RN}} \leq N_{\mathrm{b}}/10$ into account as

$$N_{\mathrm{b}} = \min\left(\mathrm{round}\left(10 \cdot F^{-1}(\lambda)\right), 6\right) \ , \ N_{\mathrm{b}} \in \mathbb{N}^{+}, \tag{5.6}$$

where λ=90%-ile is the target percentile up to which the resource split is aimed to be flexibly tuned. In Fig. 5.4, CDFs of ρ_{RN} are plotted for the considered scenarios. Consequently, the values of $N_{\mathrm{b}} = \{4, 6, 6, 6\}$ for {Urban 4-RN, Urban 10-RN, Suburban 4-RN, Suburban 10-RN} deployments, respectively, are obtained. Due to the constraints on N_{b}, the target λ level cannot be exactly achieved for these scenarios. In this regard, the achievable percentiles $\lambda^{*} = F(N_{\mathrm{b}}/10)$ are depicted in Fig. 5.4. We note that the

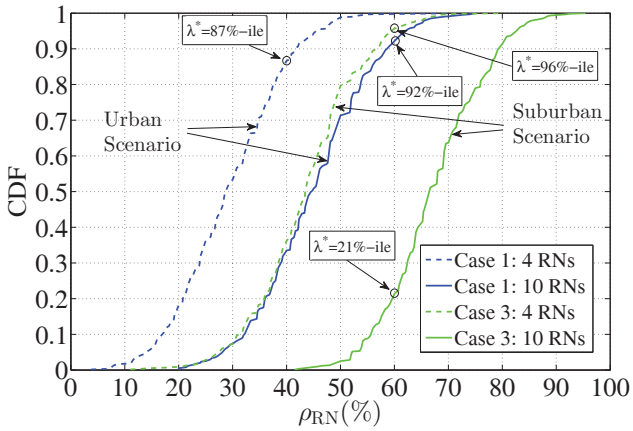

Figure 5.4. The CDFs of RUE fraction (ρ_{RN}) for urban and suburban scenarios. ©2012 Wiley

access link capacity is also considered in the selection of N_{b} such that the access link does not render a bottleneck [PVII], [27].

5.3.2 Performance Assessment

Assuming the hard resource split at DeNB, we evaluate the performance of the resource sharing models. The simulation results for urban scenarios are shown in Fig. 5.5. The relative gains at depicted percentiles of UE TP CDFs are presented with respect to the eNB-only deployment for the 4-RN and 10-RN deployments. It is seen that, when the resultant FPC-based PC setting (see Chapter 4) is utilized, the hop-optimization model achieves significant gains at the 5%-ile UE TP CDF and moderate gains at the 50%-ile UE TP CDF without degrading the cell capacity (cf. Cell TP in the figure) relative to the reference model. Moreover, the 5%-ile TP gain can be further increased at the expense of slightly reduced 50%-ile TP gain and a small degradation in cell capacity, when the the resultant FCPC-based PC setting (see Chapter 4) is utilized. In addition, as depicted in [PVII], [26], using Jain's fairness index as a metric to reflect the fairness in the system, it is shown that the hop-optimization model yields substantially higher fairness compared to both eNB-only deployment and the reference model.

The achieved gains are depicted for 4-RN and 10-RN suburban deployments in Fig. 5.6 considering FPC (see Chapter 4). The gains observed at the 5%-ile UE TP CDF prove that relay deployments can effectively tackle coverage issues due to large ISD in suburban scenarios. It is seen that

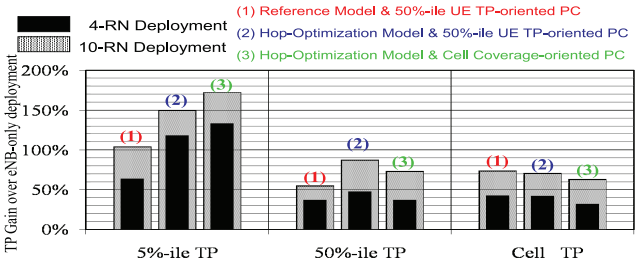

Figure 5.5. Relative TP gains over eNB-only in 4- and 10-RN deployments; urban scenario. ©2011 IEEE

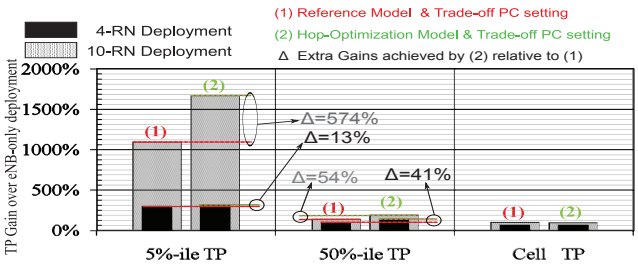

Figure 5.6. Relative TP gains over eNB-only in 4- and 10-RN deployments; suburban scenario. ©2012 Wiley

the hop-optimization model outperforms the reference model both at 5%-ile and 50%-ile UE TP. The extra gains achieved by the hop-optimization model over the reference model at 5%-ile UE TP are less pronounced in 4-RN deployment. The reason is twofold. First, the cell-edge MUEs mainly determine the 5%-ile UE TP. Second, the performance of these MUEs does not change notably via the applied resource sharing strategies, which primarily target RN cells. Moreover, like in urban deployments, the hop-optimization model yields significantly higher fairness in the system compared to both eNB-only deployment and the reference model [PVII], [26].

Targeting a more uniform user performance in the cell, the preceding results have shown that the hop-optimization model outperforms the reference model in all considered scenarios. Accordingly, the hop-optimization model is taken as the resource sharing scheme in the analysis of the flexible resource split. In addition to the aforementioned advantages, the possibility of MUE selection for co-scheduling increases the degree of freedom in optimization strategies; thus, various trade-offs can be attained. That is, as will be discussed in greater detail in the following, different schemes can be employed for the MUE selection for co-scheduling such as depending on the link quality. Nevertheless, the co-scheduling of MUEs and RNs implies different interference characteristics for Uu and Un subframes. Specifically, the total mean IoT at DeNB is lower during Un subframes

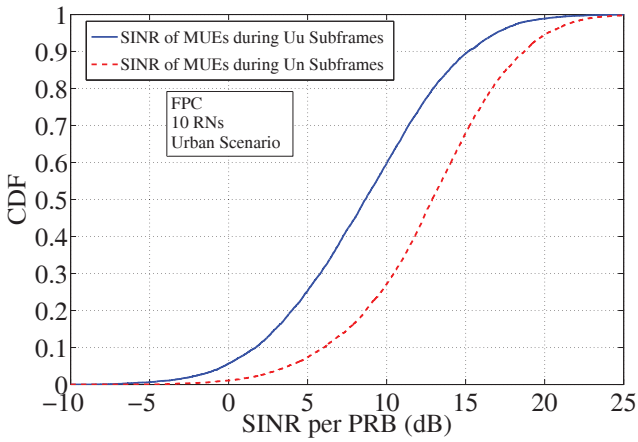

Figure 5.7. SINR CDFs for MUEs during Uu and Un subframes in 10-RN deployment utilizing FPC; urban scenario.

than that during Uu subframes, thanks to decreased interference levels due to, e.g., directional antennas at RNs for the relay link [PVII]. Then, the experienced SINR values of co-scheduled MUEs can be substantially higher during Un subframes provided that proper PC settings are applied. This is exemplified in Fig. 5.7 for 10-RN urban deployment where PC parameter settings are selected based on the results of [PVII]. Hence, the PC parameters of MUEs and RNs should be fine-tuned depending on the applied MUE selection scheme.

In [PVII], [26], it is shown that the flexible resource split scheme yields higher gains in a wide range of UE TP CDF percentiles relative to the hard resource split both in urban and suburban scenarios, when random MUE selection is considered. Therein, the importance of PC parameter tuning is also analyzed. For example, when FCPC is employed in urban scenarios, the P_0 value of MUEs in Un subframes is set to be 16 dB higher than that in regular subframes (Uu subframes) to cope with different interference characteristics. This is illustrated in Fig. 5 of [28]. An example set of results are plotted in Fig. 5.8 for 10-RN urban deployment utilizing FCPC, and two MUE selection schemes, namely, cell-edge and cell-center MUE selection schemes. The MUE selection schemes follow the algorithm that employs reference signal received power (RSRP) measurements as described in [PVII]. It is first noticed that the flexible resource split utilizing random MUE selection scheme has superior performance up to 74%-ile UE TP CDF level. As depicted by the mean IoT indicators (see insets in Fig. 5.8), co-scheduling cell-edge or cell-center MUEs has different impacts on the interference characteristics for Uu and Un

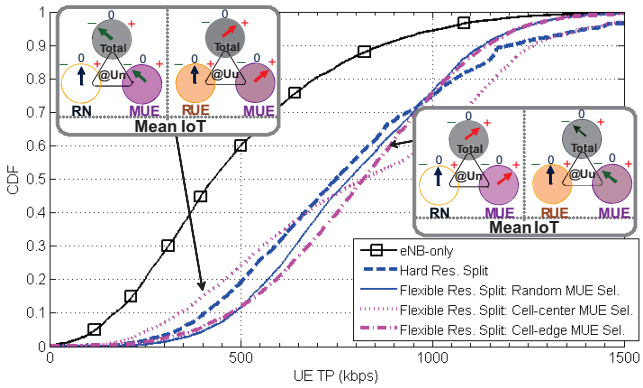

Figure 5.8. UE TP CDFs in flexible resource split shown for 10-RN deployment utilizing FCPC and different MUE selection schemes; urban scenario. Resource and selection are abbreviated by Res. and Sel., respectively. ©2012 Wiley

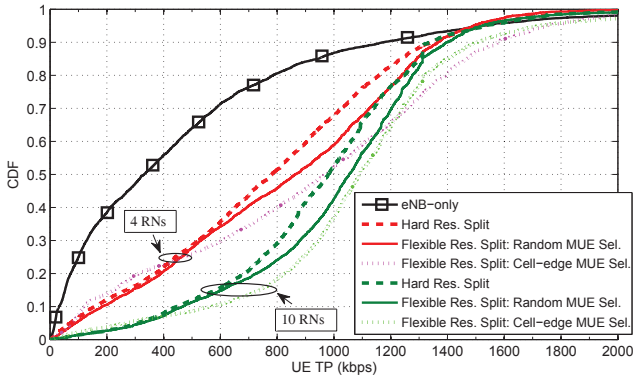

Figure 5.9. UE TP CDFs in 4- and 10-RN deployments; suburban scenario. Resource and selection are abbreviated by Res. and Sel., respectively. ©2012 Wiley

subframes. This is, in turn, reflected in the resultant TP performance. Specifically, cell-center MUE selection scheme favors co-scheduled MUEs and RNs (cf. performance increase at high TP regime), whereas it decreases the performance of cell-edge MUEs scheduled in Uu subframes (cf. performance decrease at low TP regime) which stems from the increased interference levels. When cell-edge MUE selection scheme is applied, reversed effects are observed. Then, a gain is observed at mid TP regime at the cost of a loss at low TP regime.

Fig. 5.9 presents UE TP CDFs for 4-RN and 10-RN suburban deployments. There, it can be seen that the flexible resource split with random MUE selection outperforms the hard resource split up to the 94%-ile CDF level. Unlike urban scenario, MUE selection schemes use the path loss as the selection criterion because the received SNR is of main concern and not the inter-cell interference. We focus on the cell-edge MUE selection

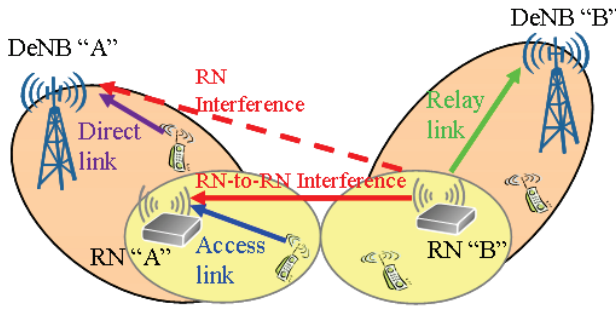

Figure 5.10. UL RN-to-RN interference due to Un subframe misalignment. ©2012 IEEE

since the cell-center MUE selection does not provide a good trade-off between high and low TP regimes. As depicted in Fig. 5.9, the cell-edge MUE selection can further improve the performance at higher UE TP CDF percentiles at the expense of a loss at low TP regime.

5.4 Impact of Un Subframe Misalignment on the System Performance

In line with [PVIII], we study the impact of Un subframe misalignment on the UL system performance. For DL performance, such a scenario is also investigated in the LTE-Advanced standardization, e.g., in [93], and a more comprehensive evaluation is provided in [94, 95, 96]. In addition, some insights into UL performance are given in [88] where 4-RN deployments are studied, and a partially misaligned Un subframe configuration is employed in the whole network.

In case of Un subframe misalignment, UL interference characteristics will be clearly different compared to the fully synchronized configuration because the transmissions of RNs and UEs will interfere with each other. A similar case occurs within the context of flexible resource split as exemplified in Fig. 5.7 (for a more detailed analysis, see [29]). Moreover, a new type of interference, referred to as RN-to-RN interference, is introduced as depicted in Fig. 5.10. Such interference occurs on the UL when a relay link transmission of an RN interferes with an access link reception at another RN. In essence, the work in [PVIII] demonstrates the impacts of directional antennas, the number of deployed RNs, and propagation conditions in case of Un subframe misalignment. The outcome from [PVIII] is summarized in the following.

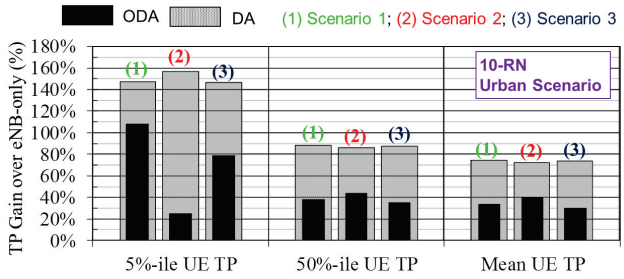

Figure 5.11. TP gain over eNB-only when directional antennas (abbreviated by DA) and omni-directional antennas (abbreviated by ODA) are used for backhauling. ©2012 IEEE

5.4.1 Inter-DeNB Coordination Scenarios

We consider three inter-DeNB coordination scenarios as follows [PVIII].

- *Scenario 1 (System-wide Alignment)*: This scheme assumes coordination among all network DeNBs for the Un subframe configuration.

- *Scenario 2 (Fixed Intra-cell Alignment)*: In this scheme, the Un subframe configuration is the same for the RNs in the midmost sector, while all other sectors have another misaligned configuration. This scenario is studied to illustrate the bounds of the impact of such a misalignment.

- *Scenario 3 (Random Intra-cell Alignment)*: In this scheme, the Un subframe configurations are randomly selected by DeNBs for different cells.

5.4.2 Simulation Results and Discussion

According to the results detailed in [PVIII] for 4-RN and 10-RN urban and suburban deployments, it is seen that when the PC parameters found in Scenario 1 (see Chapter 4) are applied in Scenarios 2 and 3, and directional antennas are available for backhauling, misalignment does not degrade system performance. However, if omni-directional antennas are used for backhauling, the misalignment causes severe performance degradation at low TP regime in suburban and 10-RN urban deployments; therefore, additional optimization strategies are necessary as highlighted in [PVIII]. For demonstration, the results pertaining to 10-RN urban deployment are provided in Fig. 5.11. We note that utilizing directional antennas decreases the interference imposed by RNs at other access nodes.

6. Relay Cell Range Extension

As mentioned in Chapter 3, relay cell coverage is conventionally defined according to the received signal strength at a UE on the DL. When using this approach, RN cells tend to have small coverage areas. This stems mainly from the lower transmit power of an RN and limited antenna capabilities, e.g., low antenna gain. If RN coverage area is small, then only a small number of UEs will be served by RNs, i.e., RN coverage area admits low cell load relative to that of the overlaying macrocell. More concretely, the available resources in the RN cells may not be fully exploited, whereas in the macrocell, the load and, hence, the competition for the resources remains high. This, in turn, leads to load imbalance and inefficient resource utilization. Furthermore, another issue to be relaxed is the resulting imbalance between the DL and UL, which is typical to low-power node deployments. In particular, some UEs will connect to the DeNBs, though they experience smaller path losses toward the nearby RNs. Considering the PC mechanism described in Chapter 4, these UEs will transmit on the UL at high power due to path loss compensation toward DeNB, which increases the UL inter-cell interference level in the network.

The aforementioned issues can be tackled by expanding the coverage area of small cells in general, i.e., via CRE, and, hence, off-loading MUEs to RN cells. CRE has been mainly investigated for picocell deployments, e.g., [97, 98, 99, 100, 101] and references therein, particularly targeting the DL system performance. Nonetheless, as opposed to picocell deployments, where a fixed backhaul exists, CRE in relay deployments should take into account the impact of the wireless relay link, and the associated PC and resource sharing mechanisms as discussed in Chapter 4 and Chapter 5, respectively.

Within the framework of relay deployments, in [PIX], [32], two basic and practically feasible CRE techniques were investigated assuming ideal re-

lay link and taking into account the backward compatibility with LTE Rel. 8. In essence, studies presented in [PIX], [32] aimed at showing the maximum attainable performance for the investigated CRE techniques. Specifically, in [32], a bias is added to the cell selection and handover thresholds noting that the applicable value of the bias is limited by the pre-defined lower SINR bound (-7 dB) on the DL. This bound is introduced since UEs should be able to reliably detect DL control channels. Therein, it is shown that CRE yields UL system performance enhancement even without a CRE-specific PC optimization. Moreover, in [PIX], DeNB transmission power reduction is, as well, performed on the DL, which enables a further RN coverage area increase especially in urban scenarios. Besides, a CRE-specific PC optimization, which adapts to the new system conditions, is applied, and the performance benefits of such an optimization on the UL system performance are highlighted. A similar analysis including the impact of the inband relay link bottleneck is carried out in [PX]. In addition, as mentioned before, joint optimizations of CRE, resource sharing, and PC parameters are performed based on various key performance metrics. Furthermore, the impact of aligning DL and UL parameter settings associated with CRE is addressed. Then, the use of Taguchi's method (see Chapter 4) to reduce the network trial runs required to optimize the system performance is analyzed. In order to achieve a higher resource utilization efficiency and to further improve the system performance, the flexible resource split scheme, as discussed in Chapter 5, is employed along with CRE in [PXI], [33], and [34], where possible UL system performance gains and trade-offs are presented. Further, a combination of CRE and interference coordination is investigated in [102, 103] within the DL framework.

6.1 Cell Range Extension Modeling

The cell association of a UE is conventionally based on periodic DL measurements of RSRP s_i from different candidate cells. Accordingly, the cell ID of the serving cell $\hat{i}$ is determined as

$$\hat{i} = \arg\max_{i \in \mathcal{C}} s_i, \tag{6.1}$$

where $\mathcal{C}$ is the set of candidate cells. Here, for simplicity, we assume that hysteresis and offset values are set to 0 dB in cell reselection and handover procedures [1]. Therefore, the cell border between a DeNB and

an RN will be defined by the point where the RSRP levels from both are equal. CRE is then attained by biasing the cell selection and handover decisions along with the DeNB power reduction. Specifically, we model a reduction of DeNB transmission power by X dB and biasing by Y dB as a common parameter $\varepsilon := 10^{(X+Y)/10}$ which is referred to as the *effective biasing* (a.k.a. *extension factor*, see [PX]). We note that both techniques have the same effect on cell selection when applied to all nodes in the network. Thus, we obtain

$$\hat{i} = \arg\max_{i \in \mathcal{C}} s_i^*, \tag{6.2}$$

$$s_i^* = \begin{cases} s_i, & i \in \mathcal{C}_{\mathrm{DeNB}} \\ \varepsilon \cdot s_i,\ \varepsilon > 1 & i \in \mathcal{C}_{\mathrm{RN}} \end{cases}, \tag{6.3}$$

where $\mathcal{C}_{\mathrm{DeNB}} \subset \mathcal{C}$ and $\mathcal{C}_{\mathrm{RN}} \subset \mathcal{C}$ with $\mathcal{C}_{\mathrm{DeNB}} \cup \mathcal{C}_{\mathrm{RN}} = \mathcal{C}$ are, respectively, the sets of candidate DeNB cells and RN cells. Further, the impact of DeNB power reduction on cell selection is modeled as a boost of RN power. In line with this formulation, CRE is illustrated in Fig. 6.1, where RSRP levels from the DeNB and RN along with the corresponding coverage areas are depicted. As exemplified in this figure, before CRE, the UE 2 and UE 3 are served by the DeNB, and, due to large path losses, they transmit at high power; therefore, they increase inter-cell interference in the network. After CRE, these UEs are served by the nearby RN and, hence, are subject to smaller path losses. Assuming a proper PC setting in the RN cells[1], the inter-cell interference decreases.

Fig. 6.2 shows the increase in total RN coverage area for different effective biasing values. We note that the total RN coverage area defines the percentage of UEs served by RNs considering a uniform distribution of users. An expansion in coverage area versus increasing effective biasing values is observed in urban scenarios. However, a comparatively low increase is noticed in suburban scenarios. For example, a 10-dB effective biasing expands the RN coverage area by 22% and 6.5% in 4-RN urban deployment and 4-RN suburban deployment, respectively. Such behavior is related to the different characteristics of the propagation models in these scenarios.

[1]Recall from Chapter 4 that the P_0 value of MUEs is higher than that of RUEs, and the same α value is applied in both macrocells and RN cells.

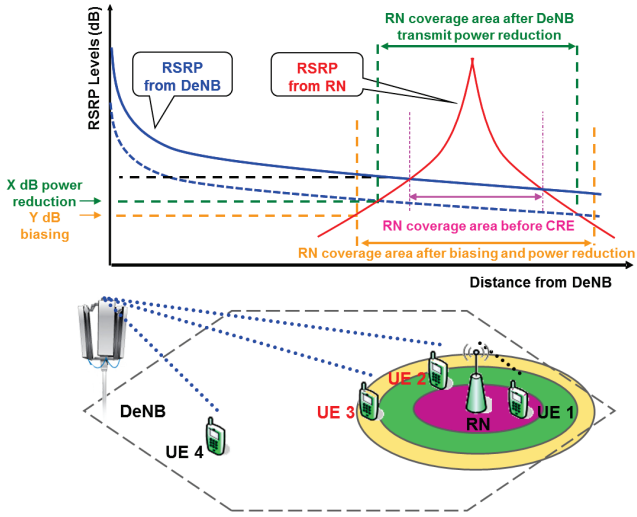

Figure 6.1. CRE via DeNB power reduction and biasing: RSRP levels from the DeNB and RN (top) and corresponding coverage areas (bottom). Dotted lines represent the desired signal links before CRE. ©2012 Wiley

6.2 Performance Assessment

Parameter optimizations in CRE for the UL involve a selection of the effective biasing value, the number of Un subframes, and UL PC settings within the parameter ranges as given in [PX]. When co-scheduling of RNs and MUEs[2] is performed along with CRE, the parameter tuning presented in Chapter 5 should be applied [PXI], [33], which calls for a more sophisticated analysis. Thus, the performance evaluation of CRE is carried out in 4-RN and 10-RN deployments in urban and suburban scenarios, where the eNB-only deployment is taken as the reference to clarify the relative gains. In particular, in each scenario, the impact of CRE on SINR distributions is investigated. Then, the parameter tuning is performed such that the target performance based on UE TP distributions is maximized. Concretely, $K1$ (best 5%-ile UE TP), $K2$ (best 50%-ile UE TP), and $K3$ (best mean UE TP) are utilized as the optimization metrics. Also, further gains and trade-offs are shown considering the co-scheduling of RNs and MUEs. Thereafter, Taguchi's method is applied as an effective tool in achieving nearly optimum results with a smaller number of network trials. Recall that urban scenarios with relatively small ISD are mostly limited by inter-cell interference, whereas in suburban scenarios due to large ISD the inter-cell interference is not of main concern.

[2]Random selection of MUEs for co-scheduling is considered herein (see Chapter 5).

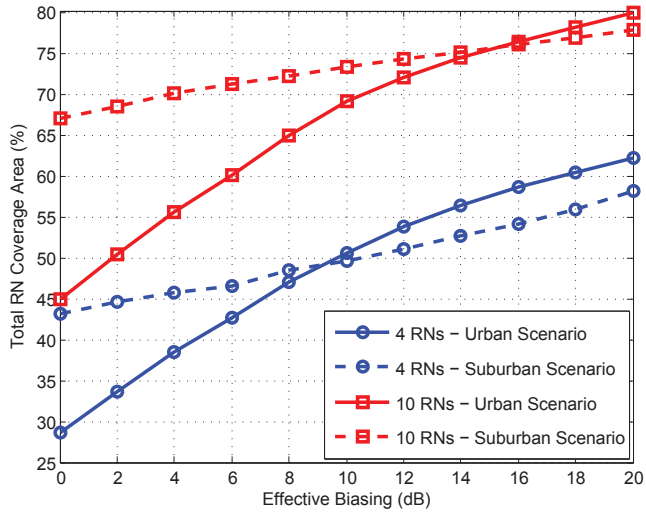

Figure 6.2. Expansion of total RN coverage area in terms of effective biasing in urban and suburban scenarios. ©2012 Wiley

6.2.1 Urban Scenarios

Along with the selection of the effective biasing value and the number of Un subframes, following the PC optimization methodologies in Chapter 4, the cell coverage-oriented setting based on FCPC ($\alpha = 1.0$) is applied in relay deployments, and the P_0 value of MUEs during Uu subframes is tuned [PX]. Moreover, the cell capacity-oriented PC setting is applied in the eNB-only deployment. In addition, when co-scheduling is enabled, the P_0 values of RNs and MUEs during Un subframes are tuned considering FPC [PXI].

The SINR CDFs of 4-RN deployment are depicted in Fig. 6.3. The SINR values of the cell-center MUEs are degraded because of interference from close-by RUEs. This effect is reflected by a performance deterioration at the high SINR regime. On the other hand, low SINR regime, which is mainly determined by RUEs, improves with CRE. Specifically, as effective biasing increases, more cell-edge MUEs are admitted by RNs. Hence, the interference imposed by such MUEs on the RN cells is eliminated via CRE.

The UE TP CDF plots for 4-RN deployment are depicted in Fig. 6.4 taking into account different performance metrics and no CRE. First, a clear performance enhancement over the eNB-only deployment is observed when RNs are deployed (no CRE). The performance of relay deployments can be further enhanced when CRE with $K1$ (best 5%-ile UE

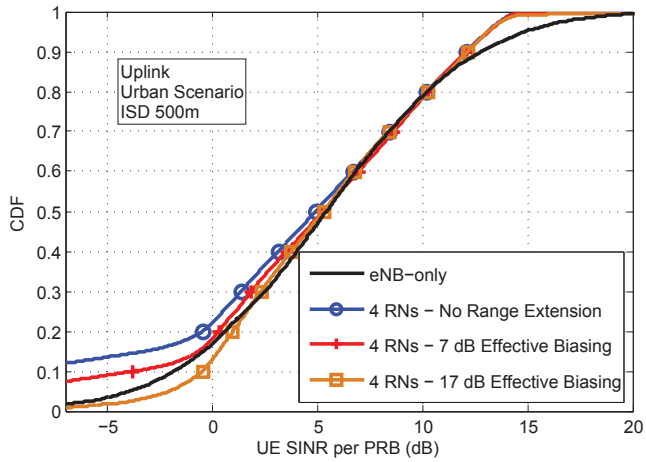

Figure 6.3. UL SINR distributions in 4-RN urban scenario. ©2012 Wiley

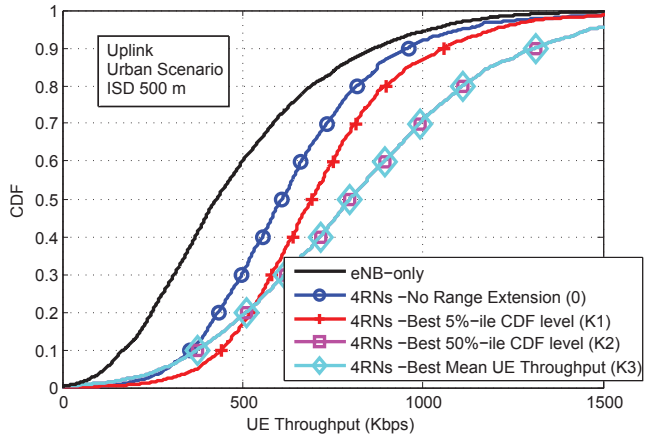

Figure 6.4. UE TP distributions considering different optimization metrics in 4-RN urban scenario. ©2012 Wiley

TP) is utilized. The TP performance at higher CDF percentiles can be improved at the cost of reduced 5%-ile TP performance when either $K2$ (best 50%-ile UE TP) or $K3$ (best mean UE TP) is used as the optimization metric. The TP gains achieved by CRE on the UL are due to increased SINR values and decreased competition for the DeNB resources. The achievable gains via CRE are further outlined in [PX]. We note that, on both the UL and DL, a UE is associated to the same serving cell, and the number of Un subframes should be the same. Nevertheless, according to the results of [PX], CRE brings notable gains on the UL even if the DL-defined settings are employed.

Additional resource utilization efficiency and performance enhancement can be attained by co-scheduling RNs and MUEs along with CRE [PXI].

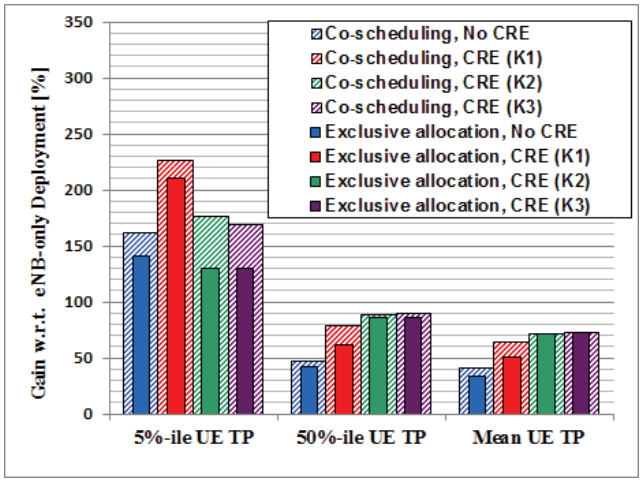

Figure 6.5. Achieved UE TP gains considering different optimization metrics and co-scheduling of RNs and MUEs in 4-RN urban scenario. ©2012 VDE

For demonstration, relative gains with respect to eNB-only deployment are shown for 4-RN urban scenario in Fig. 6.5 considering the aforementioned optimization metrics. It is seen that enabling co-scheduling brings additional gains at all levels when compared to the exclusive backhaul resource allocation, i.e., hard resource split scheme.

6.2.2 Suburban Scenarios

Like in urban scenarios, a parameter tuning for the effective biasing, the number of Un subframes, and the UL PC is carried out in suburban scenarios. Specifically, the trade-off setting found in Chapter 4 based on FPC ($\alpha = 0.6$) is applied in the eNB-only deployment as well as in relay deployments. Moreover, a parameter sweep is performed for the P_0 value of MUEs during Uu subframes [PX]. Besides, when co-scheduling is performed, the P_0 values of RNs and MUEs during Un subframes are adjusted [PXI].

The corresponding SINR CDFs are plotted in Fig. 6.6. It is first observed that the SINR values increase significantly when RNs are deployed. This is mainly due to the substantially decreased radio distances between UEs and serving nodes after RN deployment. On the other hand, the impact of CRE on the SINR distributions of the relay deployments is less pronounced. For instance, even with 17-dB effective biasing, only a slight degradation is observed on the low SINR regime. In part, this is because PC can effectively compensate for path losses thanks to reduced radio distances, and in part because low interference levels are experienced.

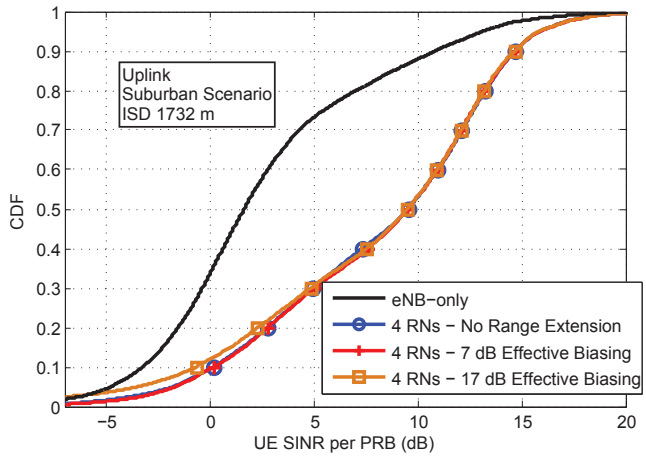

Figure 6.6. UL SINR distributions in 4-RN suburban scenario. ©2012 Wiley

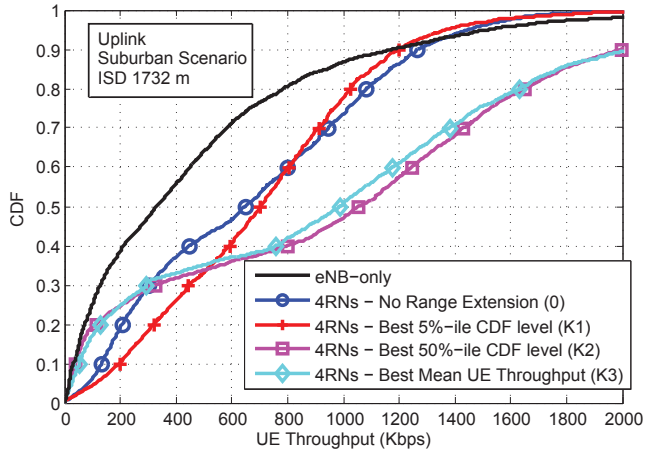

Figure 6.7. UE TP distributions considering different optimization metrics in 4-RN suburban scenario. ©2012 Wiley

The UE TP CDF plots for 4-RN deployment are given in Fig. 6.7 taking into account different optimization metrics and no CRE. We first notice the drastic performance enhancement over the eNB-only deployment after RNs are deployed in case of no CRE. Second, it is seen that CRE with $K1$ (best 5%-ile UE TP) increases the performance at low to mid TP levels at the cost of marginal performance degradation at high TP regime. Moreover, CRE with $K2$ (best 50%-ile UE TP) and $K3$ (best mean UE TP) can significantly enhance the performance at higher TP levels; however, notable performance degradation is observed at low TP regime. Also, the impact of UL-DL alignment is investigated in [PX], and still notable gains are shown on the UL even if the DL-defined settings are employed.

Next, the performance evaluation of co-scheduling of RNs and MUEs

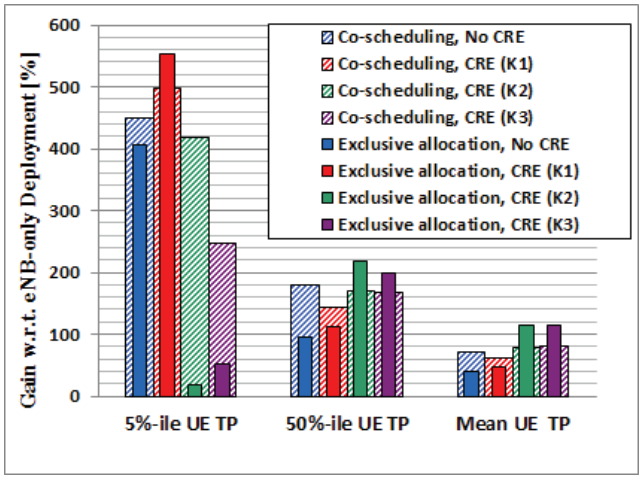

Figure 6.8. Achieved UE TP gains considering different optimization metrics and co-scheduling of RNs and MUEs in 4-RN suburban scenario. ©2012 VDE

along with CRE is conducted [PXI]. Accordingly, relative gains with respect to eNB-only deployment are exemplified for 4-RN suburban deployment in Fig. 6.8 considering the aforementioned optimization metrics. Overall, various trade-offs can be achieved when co-scheduling is enabled. For example, in case of $K1$ (best 5%-ile UE TP), co-scheduling provides additional gains at 50%-ile UE TP and mean UE TP at the cost of a loss at 5%-ile UE TP as compared to no co-scheduling, i.e., exclusive allocation of backhaul resources to RNs. It is worth noting that this degradation is around 9 kbps (from 114 kbps to 105 kbps) in absolute values; hence, the practical performances are almost the same. As another example, by improving the resource utilization efficiency, the co-scheduling enables a more homogeneous TP distribution when $K2$ (best 50%-ile UE TP) and $K3$ (best mean UE TP) are utilized.

6.2.3 Realization Considerations

The joint parameter optimization above requires a large number of network trial runs. Namely, up to 17 dB effective biasing and up to 6 Un subframes along with 31 alternative P_0 values for MUEs during Uu subframes with ranges of $[-143, -113]$ dB (FCPC, $\alpha = 1.0$) and $[-106, -76]$ dB (FPC, $\alpha = 0.6$) require 3348 network trial runs. This number of combinatorial possibilities grows substantially when the co-scheduling is enabled since P_0 values for RNs and MUEs during Un subframes should also be tuned jointly. This may prove time-intensive and costly for operators. In this regard, Taguchi's method, which is also utilized for automated PC op-

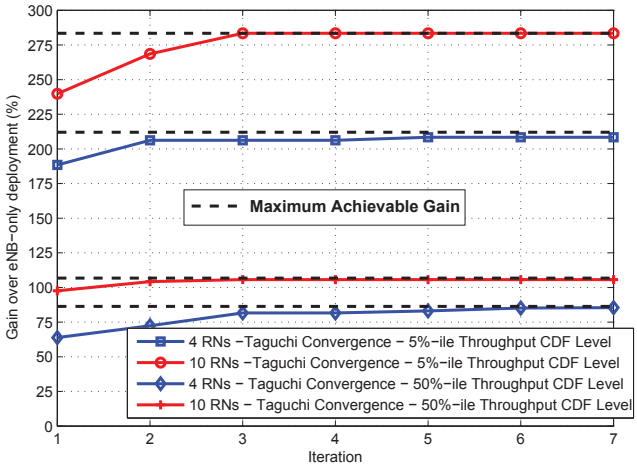

Figure 6.9. Convergence of Taguchi's method in optimizing the 5%-ile and 50%-ile UE TP levels in 4-RN and 10-RN urban deployments. ©2012 Wiley

timization in Chapter 4, can be used to automate the optimization and to significantly reduce the number of network trial runs required during network planning or offline optimization. In [PX], we show the efficiency of Taguchi's method for CRE without co-scheduling, while, in [PXI], [33], it is shown for CRE with co-scheduling. Therein, it is presented that Taguchi's method can converge to the nearly optimum values with a smaller number of network trial runs.

For demonstration, considering no co-scheduling, we optimize the 5%-ile UE TP and 50%-ile UE TP in 4-RN and 10-RN urban deployments via Taguchi's method for CRE. The corresponding convergence curves along with the maximum achievable gains obtained via brute-force optimization are depicted in Fig. 6.9. As can be seen, e.g., for 10-RN deployment, the performance increase saturates after 3 iterations, i.e., 54 network trial runs, at both 5%-ile and 50%-ile UE TP levels. Consequently, via Taguchi's method nearly optimum values are achieved in less than 2% of the total network trial runs needed in the brute-force optimization [PX].

7. Conclusion

Multi-hop decode-and-forward relaying is a promising and cost-efficient enhancement for future mobile networks. Relay deployments are of particular interest for increasing the network capacity or extending the cell coverage. At the same time, relay deployments incur low OPEX and enable a fast network upgrade when operators aim to improve the QoS. In this regard, relaying is an integral part of the 4G standards.

In particular, being cognizant of the importance of RRM in realizing the promised benefits of relay deployments, we have developed and analyzed RRM concepts, and have shown the potential for performance improvements. Moreover, as a practical scenario, we have considered the framework of LTE-Advanced Type 1 inband half-duplex relay deployments. The analyses and concepts are verified by carrying out system-level performance evaluations. Since most work in the literature focuses on the DL performance, we have placed the particular focus on the UL performance analyses noting that various relevant aspects studied in this thesis are, as well, investigated taking into account the impact on the DL performance.

We first improved the relay link quality by employing practical RSP. The analyses have been carried out to assess the performance of RSP in terms of relay link SINR, link rate, and end-to-end rate distributions considering, e.g., shadowing only and composite fading/shadowing channels in the presence of co-channel interference. Consistent numerical and analytical results have revealed that performing even a simple RSP provides significant gains on the relay link SINR on a wide range. Also, using AoF as the performance measure, a substantial decrease in the severity of fading has been observed. Moreover, achieved gains on the relay link are shown to translate into clear improvements in end-to-end rates provided that a proper resource allocation is applied, and that the access link is not the bottleneck.

Within the UL framework, we have studied PC in relay deployments considering urban and suburban scenarios. First, taking into account backward compatibility requirement in LTE-Advanced, we have demonstrated that LTE Rel. 8 PC mechanism is also appropriate for relay deployments. Basically, PC is found to be crucial not only to compensate for channel variations and to mitigate inter-cell interference, but also to ensure that the receiver dynamic range does not exceed a pre-determined level. Then, we have introduced propagation scenario-specific optimization methods which provide a comprehensive understanding of the impact of PC on the system performance, and justify that through a proper PC optimization relay deployments can clearly outperform conventional macrocell-only deployments. For instance, it is observed that poor cell-edge performance of macrocell-only deployments in suburban scenarios can be effectively tackled by relay deployments. In addition, we have proposed automated PC parameter optimization to avoid skilled human intervention during the optimization process. More concretely, we have introduced the performance steering concept along with the novel performance metrics which can be easily adapted according to the performance targets. Furthermore, relay deployments are shown to be more efficient than the macrocell-only deployments in terms of TP per power consumption performance especially when a large number of RNs are deployed in a cell.

As for resource sharing, we have investigated different techniques taking into account PC optimization. On this basis, we have proposed a combination of relay link scheduling based on the number of RUEs, and a TP throttling scheme achieving max-min fairness in the end-to-end two-hop communications. Besides, we have demonstrated a flexible resource split at DeNB based on over-provisioning of Un subframes and co-scheduling of MUEs, which enables a fast adaptation to dynamic system conditions and enhances the resource utilization efficiency. Results show significant TP enhancements and high fairness. Additionally, we have analyzed the impact of Un subframe misalignment on the resultant system performance by studying different inter-DeNB coordination schemes and different antenna configurations on the relay link. Results show that if directional antennas are available for backhauling, the misalignment does not degrade the system performance. On the other hand, if omni-directional antennas are used on the relay link, the misalignment causes performance degradation and, thus, should be addressed. Such performance degradation can

be fully alleviated by the proposed joint optimization strategies in urban scenarios, while there are performance trade-offs in suburban scenarios.

The work on backward compatible CRE in relay deployments overcome the challenges, e.g., load imbalance, and increased inter-cell interference on the UL, which are due to small RN coverage area caused by low transmit power levels and limited antenna capabilities of RNs. Accordingly, we have conducted a joint optimization of CRE, resource allocation, and PC parameters. Results demonstrate clear gains in urban scenarios, whereas gains decrease considerably in suburban scenarios. Further, the limitations faced when aligning UL and DL parameter configurations have been highlighted. Yet, it has been shown that after the alignment, CRE still brings notable gains on the UL. In addition, Taguchi's method has proven to be an efficient way of performing the joint parameter optimization during, e.g., network planning.

Some possible areas for future research can be outlined as follows.

- Mobile (a.k.a. moving) RNs can be used for enhancing user experience on, e.g., high-speed trains, where mobile RNs are mounted on vehicle carriages. Specifically, mobile RNs promise to overcome challenges arising from severe Doppler shift due to high speed, high penetration loss due to carriage shield, and, thus, reduced handover rates and high UE power consumption. The framework and several use cases of mobile RNs have been studied in LTE-Advanced [104]. Accordingly, various aspects investigated in this thesis, such as PC and resource sharing techniques, can be adapted for scenarios with mobile RNs.

- The work can be extended considering the framework of self-organizing networks (SON). Self-organizing features have attracted great attention. The goal is to minimize operational effort and cost by employing automated mechanisms, e.g., self-configuration, self-optimization, and self-healing [105]. In this regard, mobility management in relay deployments would be an essential research field. For instance, mobility load balancing, of which task is to optimally distribute the traffic demand among the same or different radio access technologies, should factor in the capacity of the relay link along with that of the access link.

- One of the observations in this work is the pivotal role of the relay link in relay deployments. The relay link performance can be substantially

improved by applying Spatial Division Multiple Access (SDMA) as exemplified in [106]. Moreover, we have seen that the relay link performance can be severely interference limited particularly in urban scenarios, see, e.g., [PIV]. Therefore, coordinated multipoint (CoMP) principles can be effectively utilized to mitigate interference on the relay link noting that fixed RN locations and, thus, comparatively less varying channels on the relay link can be efficiently exploited. CoMP operation, where multiple transmission/reception points dynamically coordinate mainly to alleviate the detrimental effects of interference, has been studied in LTE-Advanced [107, 108, 109]. Besides, performance improvements in case of employing CoMP principles for the relay link have been demonstrated in the Advanced Radio Interface Technologies for 4G Systems (ARTIST4G) project [110]. On this basis, various aspects presented herein can be further investigated. For instance, the work on RSP can be extended by taking into account CoMP schemes applied for the relay link.

Bibliography

[1] H. Holma and A. Toskala, *LTE for UMTS–Evolution to LTE-Advanced*, 2nd ed. John Wiley & Sons Ltd., Chichester, UK, 2011.

[2] A. Fehske, G. Fettweis, J. Malmodin, and G. Biczok, "The global footprint of mobile communications: The ecological and economic perspective," *IEEE Communications Magazine,*, vol. 49, no. 8, pp. 55 –62, August 2011.

[3] Circular Letter, "Invitations for submission of proposals for candidate radio interface technologies for the terrestrial components of the radio interface(s) for IMT-Advanced and invitation to participating in their subsequent evaluation," ITU-R, Tech. Rep. 5/LCCE/2, March 2008. [Online]. Available: www.itu.int

[4] Recommendation ITU-R, "Detailed specifications of the terrestrial radio interfaces of International Mobile Telecommunications Advanced (IMT-Advanced)," ITU-R, Tech. Rep. M.2012, January 2012. [Online]. Available: www.itu.int

[5] E. Dahlman, P. S., and J. Sköld, *4G LTE/LTE-Advanced for Mobile Broadband*. Academic Press, Elsevier Ltd., Oxford, UK, 2011.

[6] S. Sesia, T. I., and M. Baker, *LTE- The UMTS Long Term Evolution: From Theory to Practice*, 2nd ed. John Wiley & Sons Ltd., Chichester, UK, 2011.

[7] R. Pabst, B. Walke, D. Schultz, P. Herhold, H. Yanikomeroglu, S. Mukherjee, H. Viswanathan, M. Lott, W. Zirwas, M. Dohler, H. Aghvami, D. Falconer, and G. Fettweis, "Relay-based deployment concepts for wireless and mobile broadband radio," *IEEE Communications Magazine*, vol. 42, no. 9, pp. 80 – 89, September 2004.

[8] C. Wijting, K. Doppler, K. KallioJarvi, T. Svensson, M. Sternad, G. Auer, N. Johansson, J. Nystrom, M. Olsson, A. Osseiran, M. Dottling, J. Luo, T. Lestable, and S. Pfletschinger, "Key technologies for IMT-Advanced mobile communication systems," *IEEE Wireless Communications*, vol. 16, no. 3, pp. 76 –85, June 2009.

[9] K. Loa, C.-C. Wu, S.-T. Sheu, Y. Yuan, M. Chion, D. Huo, and L. Xu, "IMT-advanced relay standards [WiMAX/LTE update]," *IEEE Communications Magazine*, vol. 48, no. 8, pp. 40 –48, August 2010.

[10] E. Lang, S. Redana, and B. Raaf, "Business impact of relay deployment for coverage extension in 3GPP LTE-Advanced," in *IEEE International*

Conference on Communications Workshops (ICC 2009), Dresden, Germany, June 2009, pp. 1 –5.

[11] K. Doppler, S. Redana, M. Wodczak, P. Rost, and R. Wichman, "Dynamic resource assignment and cooperative relaying in cellular networks: Concept and performance assessment," *EURASIP Journal on Wireless Communications and Networking*, vol. 2009, pp. 1–14, 2009.

[12] P. Moberg, P. Skillermark, N. Johansson, and A. Furuskar, "Performance and cost evaluation of fixed relay nodes in future wide area cellular networks," in *IEEE International Symposium on Personal, Indoor and Mobile Radio Communications (PIMRC 2007)*, Athens, Greece, September 2007, pp. 1 –5.

[13] B. Timus, "Cost analysis issues in a wireless multihop architecture with fixed relays," in *IEEE Vehicular Technology Conference (VTC 2005-Spring)*, Stockholm, Sweden, May, June 2005, pp. 3178 – 3182.

[14] D. Soldani and S. Dixit, "Wireless relays for broadband access [radio communications series]," *IEEE Communications Magazine*, vol. 46, no. 3, pp. 58 –66, March 2008.

[15] A. Bou Saleh, S. Redana, J. Hämäläinen, and B. Raaf, "On the coverage extension and capacity enhancement of inband relay deployments in LTE-Advanced networks," *Journal of Electrical and Computer Engineering*, vol. 2010, pp. 1–12, 2010, article ID 894846. [Online]. Available: http://www.hindawi.com/journals/jece/2010/894846/

[16] A. Bou Saleh, S. Redana, B. Raaf, and J. Hämäläinen, "Comparison of relay and pico eNB deployments in LTE-Advanced," in *IEEE Vehicular Technology Conference Fall (VTC 2009-Fall)*, Anchorage, USA, September 2009, pp. 1 –5.

[17] A. So and B. Liang, "Effect of relaying on capacity improvement in wireless local area networks," in *IEEE Wireless Communications and Networking Conference (WCNC 2005)*, New Orleans, USA, March 2005, pp. 1539 – 1544, Vol. 3.

[18] R. Schoenen, W. Zirwas, and B. H. Walke, "Capacity and coverage analysis of a 3GPP-LTE multihop deployment scenario," in *IEEE International Conference on Communications Workshops (ICC 2008)*, Beijing, China, May 2008, pp. 31 –36.

[19] R. Schoenen, R. Halfmann, and B. H. Walke, "An FDD multihop cellular network for 3GPP-LTE," in *IEEE Vehicular Technology Conference (VTC 2008-Spring)*, Marina Bay, Singapore, May 2008, pp. 1990 –1994.

[20] T. Beniero, S. Redana, J. Hämäläinen, and B. Raaf, "Effect of relaying on coverage in 3GPP LTE-Advanced," in *IEEE 69th Vehicular Technology Conference, 2009. VTC 2009-Spring*, Barcelona, Spain, April 2009, pp. 1 –5.

[21] R. Irmer and F. Diehm, "On coverage and capacity of relaying in LTE-advanced in example deployments," in *IEEE International Symposium on Personal, Indoor and Mobile Radio Communications (PIMRC 2008)*, September 2008, pp. 1 –5.

[22] Technical Specification Group (TSG) Radio Access Network, "Evolved Universal Terrestrial Radio Access (E-UTRA); Further advancements for E-UTRA physical layer aspects (Release 9)," 3GPP, Tech. Rep. 36.814 v9.0.0, March 2010. [Online]. Available: http://www.3gpp.org/ftp/Specs/archive/36_series/36.814

[23] A. Karaer, Ö. Bulakci, S. Redana, B. Raaf, and J. Hämäläinen, "Uplink performance optimization in relay enhanced LTE-Advanced networks," in *IEEE International Symposium on Personal, Indoor and Mobile Radio Communications (PIMRC 2009)*, Tokyo, Japan, September 2009, pp. 360–364.

[24] Ö. Bulakci, S. Redana, B. Raaf, and J. Hämäläinen, "System optimization in relay enhanced LTE-Advanced networks via uplink power control," in *IEEE Vehicular Technology Conference (VTC Spring 2010)*, Taipei, Taiwan, May 2010, pp. 1–5.

[25] Ö. Bulakci, A. Awada, A. Bou Saleh, S. Redana, J. Hämäläinen, B. Wegmann, B. Raaf, and I. Viering, "Joint optimization of uplink power control parameters in LTE-Advanced relay networks," in *IEEE International Wireless Communications and Mobile Computing Conference (IWCMC 2011)*, Istanbul, Turkey, July 2011, pp. 2064–2069.

[26] Ö. Bulakci, A. Bou Saleh, Z. Ren, S. Redana, B. Raaf, and J. Hämäläinen, "Two-step resource sharing and uplink power control optimization in LTE-Advanced relay networks," in *IEEE Multi-Carrier Systems & Solutions (MC-SS 2011)*, Herrsching, Germany, May 2011, pp. 1–6.

[27] Ö. Bulakci, A. Bou Saleh, S. Redana, B. Raaf, and J. Hämäläinen, "Flexible backhaul resource sharing and uplink power control optimization in LTE-Advanced relay networks," in *IEEE Vehicular Technology Conference (VTC Fall 2011)*, San Francisco, USA, September 2011, pp. 1–6.

[28] Ö. Bulakci, A. Bou Saleh, S. Redana, B. Raaf, and J. Hämäläinen, "Uplink radio resource management challenges in LTE-Advanced relay networks," in *the 16. VDE/ITG Workshop on Mobile Communications*, Osnabrück, Germany, May 2011, pp. 45–50.

[29] A. S. Nedelcu, *Impact of Backhaul Subframe Misalignment on Uplink System Performance of Relay Enhanced LTE-Advanced Networks*. Master's thesis, Technische Universität München, Munich, Germany, September 2011, (instructed by Ö. Bulakci).

[30] Ö. Bulakci, A. Bou Saleh, S. Redana, and B. Raaf, "Relay-to-relay interference coordination in a wireless communication network," International Patent Application WO/2012/089 269 A1, July 2012. [Online]. Available: http://patentscope.wipo.int/search/en/WO2012089269

[31] A. Bou Saleh, Ö. Bulakci, S. Redana, and B. Raaf, "Divide-and-conquer approach to mitigating relay-to-relay interference," International Patent Application WO/2012/119 636 A1, September 2012. [Online]. Available: http://patentscope.wipo.int/search/en/WO2012119636

[32] A. Bou Saleh, Ö. Bulakci, S. Redana, B. Raaf, and J. Hämäläinen, "Enhancing LTE-Advanced relay deployments via biasing in cell selection and handover decision," in *IEEE International Symposium on Personal Indoor and*

Mobile Radio Communications (PIMRC 2010), Istanbul, Turkey, September 2010, pp. 2277–2281.

[33] Ö. Bulakci, A. Bou Saleh, S. Redana, and J. Hämäläinen, "Uplink system performance of LTE-Advanced relay deployments in different propagation environments," in *the 17. VDE/ITG Workshop on Mobile Communications*, Osnabrück, Germany, May 2012, pp. 7–12.

[34] D. W. Kifle, *Relay Cell Coverage Extension and Uplink Performance Optimization in Relay-enhanced LTE-Advanced Networks*. Master's thesis, Università Degli Studi Di Trento, Trent, Italy, October 2011, (instructed by Ö. Bulakci).

[35] Nokia Siemens Networks (NSN) and Nokia, "Selection criteria for relay site planning," 3GPP Technical Specification Group Radio Access Network Working Group 1, Los Angeles, USA, Tech. Rep. R1-092563, June 2009. [Online]. Available: www.3gpp.org/ftp/tsg_ran/wg1_rl1/TSGR1_57b/Docs/

[36] China Mobile Communications Corporation (CMCC), "Text proposal for relay backhaul link, macro-UE link channel model and relay evaluation methodologies for TR 36.814," 3GPP Technical Specification Group (TSG) Radio Access Network Working Group 1 (RAN1), Los Angeles, USA, Tech. Rep. R1-092976, June 2009. [Online]. Available: http://www.3gpp.org/ftp/tsg_ran/wg1_rl1/TSGR1_57b/Docs

[37] A. Bou Saleh, Ö. Bulakci, J. Hämäläinen, S. Redana, and B. Raaf, "Analysis of the impact of site planning on the performance of relay deployments," *IEEE Transactions on Vehicular Technology (TVT)*, vol. 61, no. 7, pp. 3139 –3150, September 2012.

[38] G. L. Stüber, *Principles of Mobile Communication (3rd Edition)*. Springer, New York, USA, 2011.

[39] M. Simon and M. Alouini, *Digital communication over fading channels*. 2nd ed. John Wiley & Sons Inc., New York, USA, 2005.

[40] H. Holma and A. Toskala, *WCDMA for UMTS–HSPA Evolution and LTE*, 5th ed. John Wiley & Sons Ltd, Chichester, UK, 2010.

[41] J. T. J. Penttinen, *The LTE/SAE Deployment Handbook*. John Wiley & Sons Ltd, Chichester, UK, 2011.

[42] A. Abdi, W. Lau, M.-S. Alouini, and M. Kaveh, "A new simple model for land mobile satellite channels: First- and second-order statistics," *IEEE Transactions on Wireless Communications*, vol. 2, no. 3, pp. 519 – 528, May 2003.

[43] J. Paris, "Closed-form expressions for Rician shadowed cumulative distribution function," *Electronics Letters*, vol. 46, no. 13, pp. 952 –953, 2010.

[44] S. Atapattu, C. Tellambura, and H. Jiang, "A mixture gamma distribution to model the SNR of wireless channels," *IEEE Transactions on Wireless Communications*, vol. 10, no. 12, pp. 4193 –4203, December 2011.

[45] I. Gradshteyn and I. Ryzhik, *Table of Integrals, Series and Products*. 7th ed. Academic Press, Burlington, Massachusetts, USA, 2007.

[46] S. Atapattu, C. Tellambura, and H. Jiang, "Representation of composite fading and shadowing distributions by using mixtures of gamma distributions," in *Wireless Communications and Networking Conference (WCNC), 2010 IEEE*, Sydney, Australia, April 2010, pp. 1 –5.

[47] A. J. Viterbi, A. M. Viterbi, K. Gilhousen, and E. Zehavi, "Soft handoff extends CDMA cell coverage and increases reverse link capacity," *IEEE Journal on Selected Areas in Communications*, vol. 12, no. 8, pp. 1281 – 1288, October 1994.

[48] M. Gudmundson, "Correlation model for shadow fading in mobile radio systems," *Electronics Letters*, vol. 27, no. 23, pp. 2145–2146, Nov. 1991.

[49] Broadband Wireless Access Working Group, "Multi-hop relay system evaluation methodology (channel model and performance metric)," IEEE 802.16m, Tech. Rep. 06/013r3, Feb. 2007. [Online]. Available: http://www.ieee802.org/16/relay/docs/80216j-06_013r3.pdf

[50] N. Mehta, J. Wu, A. Molisch, and J. Zhang, "Approximating a sum of random variables with a lognormal," *IEEE Transactions on Wireless Communications*, vol. 6, no. 7, pp. 2690 –2699, July 2007.

[51] P. Mogensen, W. Na, I. Z. Kovacs, F. Frederiksen, A. Pokhariyal, K. I. Pedersen, T. Kolding, K. Hugl, and M. Kuusela, "LTE capacity compared to the Shannon bound," in *IEEE 65th Vehicular Technology Conference, 2007. VTC 2007-Spring*, Dublin, Ireland, April 2007, pp. 1234 –1238.

[52] Technical Specification Group (TSG) Radio Access Network, "Evolved Universal Terrestrial Radio Access (E-UTRA); Radio frequency (RF) system scenarios (Release 10)," 3GPP, Tech. Rep. 36.942 v10.3.0, June 2012. [Online]. Available: http://www.3gpp.org/ftp/Specs/archive/36_series/36.942

[53] K. Loa, C.-C. Wu, S.-T. Sheu, Y. Yuan, M. Chion, D. Huo, and L. Xu, "IMT-Advanced relay standards [WiMAX/LTE update]," *IEEE Communications Magazine*, vol. 48, no. 8, pp. 40–48, August 2010.

[54] Technical Specification Group (TSG) Radio Access Network, "Evolved Universal Terrestrial Radio Access (E-UTRA) and Evolved Universal Terrestrial Radio Access Network (E-UTRAN); Overall description; Stage 2 (Release 10)," 3GPP, Tech. Rep. 36.300 v10.8.0, June 2012. [Online]. Available: http://www.3gpp.org/ftp/Specs/archive/36_series/36.300

[55] H. Holma and A. Toskala, *LTE-Advanced: 3GPP Solution for IMT-Advanced*. John Wiley & Sons Ltd., Chichester, UK, 2012.

[56] D. Laselva, F. Capozzi, F. Frederiksen, K. Pedersen, J. Wigard, and I. Kovacs, "On the impact of realistic control channel constraints on QoS provisioning in UTRAN LTE," in *IEEE Vehicular Technology Conference (VTC 2009-Fall)*, Anchorage, USA, September 2009, pp. 1 –5.

[57] T. S. Rappaport, *Wireless Communications: Principles and Practice*. Prentice-Hall, New Jersey, USA, 2002.

[58] W. H. Tranter, K. S. Shanmugan, T. S. Rappaport, and K. L. Kosbar, *Principles of Communication Systems Simulation with Wireless Applications*. Prentice-Hall, New Jersey, USA, 2003.

[59] N. Wei, A. Pokhariyal, T. Sorensen, T. Kolding, and P. E. Mogensen, "Performance of spatial division multiplexing MIMO with frequency domain packet scheduling: From theory to practice," *IEEE Journal on Selected Areas in Communications (JSAC)*, vol. 26, no. 6, pp. 890 –900, August 2008.

[60] S. Kumar, G. Monghal, J. Nin, I. Ordas, K. Pedersen, and P. Mogensen, "Autonomous inter cell interference avoidance under fractional load for downlink Long Term Evolution," in *IEEE Vehicular Technology Conference (VTC Spring-2009)*, Barcelona, Spain, April 2009, pp. 1 –5.

[61] M. Simsek, H. Wu, B. Zhao, T. Akbudak, and A. Czylwik, "Performance of different cell selection modes in 3GPP-LTE macro-/femtocell scenarios," in *Wireless Advanced (WiAd 2011)*, London, UK, June 2011, pp. 126 –131.

[62] H. Wang, C. Rosa, and K. Pedersen, "Performance analysis of downlink inter-band carrier aggregation in LTE-Advanced," in *IEEE Vehicular Technology Conference (VTC Fall-2011)*, San Francisco, USA, September 2011, pp. 1 –5.

[63] B. Priyanto, T. Sorensen, and O. Jensen, "In-band interference effects on UTRA LTE uplink resource block allocation," in *IEEE Vehicular Technology Conference (VTC Spring 2008)*, Marina Bay, Singapore, May 2008, pp. 1846 –1850.

[64] C. Castellanos, D. Villa, C. Rosa, K. Pedersen, F. Calabrese, P.-H. Michaelsen, and J. Michel, "Performance of uplink fractional power control in UTRAN LTE," in *IEEE Vehicular Technology Conference (VTC Spring 2008)*, Marina Bay, Singapore, May 2008, pp. 2517 –2521.

[65] A. Simonsson and A. Furuskar, "Uplink power control in LTE - overview and performance," in *IEEE Vehicular Technology Conference (VTC Fall 2008)*, Calgary, Canada, September 2008, pp. 1 –5.

[66] C. Castellanos, F. Calabrese, K. Pedersen, and C. Rosa, "Uplink interference control in UTRAN LTE based on the overload indicator," in *IEEE Vehicular Technology Conference (VTC Fall 2008)*, Calgary, Canada, September 2008, pp. 1 –5.

[67] R. Müllner, C. Ball, K. Ivanov, J. Lienhart, and P. Hric, "Contrasting open-loop and closed-loop power control performance in UTRAN LTE uplink by UE trace analysis," in *IEEE International Conference on Communications (ICC 2009)*, Dresden, Germany, June 2009, pp. 1 –6.

[68] M. Boussif, C. Rosa, J. Wigard, and R. Müllner, "Load adaptive power control in LTE uplink," in *IEEE/VDE European Wireless Conference (EW 2010)*, Lucca, Italy, April 2010, pp. 288 –293.

[69] R. Müllner, C. F. Ball, M. Boussif, J. Lienhart, P. Hric, H. Winkler, K. Kremnitzer, and R. Kronlachner, "Enhancing uplink performance in UTRAN LTE networks by load adaptive power control," *European Transactions on Telecommunications (ETT)*, vol. 21, no. 5, pp. 458 –468, August 2010.

[70] Technical Specification Group (TSG) Radio Access Network, "Evolved Universal Terrestrial Radio Access (E-UTRA); Physical layer procedures (Release 8)," 3GPP, Tech. Rep. TS 36.213 v8.5.0, December 2009. [Online]. Available: http://www.3gpp.org/ftp/Specs/archive/36_series/36.213

[71] Technical Specification Group (TSG) Radio Access Network, "Evolved Universal Terrestrial Radio Access (E-UTRA); User Equipment (UE) radio transmission and reception (Release 8)," 3GPP, Tech. Rep. TS 36.101 v8.4.0, December 2008. [Online]. Available: http://www.3gpp.org/ftp/Specs/archive/36_series/36.101

[72] F. Calabrese, C. Rosa, M. Anas, P. Michaelsen, K. Pedersen, and P. Mogensen, "Adaptive transmission bandwidth based packet scheduling for LTE uplink," in *IEEE Vehicular Technology Conference (VTC Fall 2008)*, September 2008, pp. 1 –5.

[73] D. Henderson, S. Jacobson, and A. Johnson, "The theory and practice of simulated annealing," in *Handbook of Metaheuristics*, ser. International Series in Operations Research and Management Science. Springer New York, 2003, vol. 57, pp. 287–319, Chapter 10.

[74] S. Hurley, "Planning effective cellular mobile radio networks," *IEEE Transactions on Vehicular Technology (TVT)*, vol. 51, no. 2, pp. 243 –253, March 2002.

[75] I. Siomina and D. Yuan, "Enhancing HSDPA performance via automated and large-scale optimization of radio base station antenna configuration," in *IEEE Vehicular Technology Conference (VTC Spring 2008)*, Marina Bay, Singapore, May 2008, pp. 2061 –2065.

[76] R. Roy, *Design of Experiments Using the Taguchi Approach: 16 Steps to Product and Process Improvement*. John Wiley & Sons Ltd., New York, USA, 2001.

[77] Y. Cai and D. Liu, "Multiuser detection using the Taguchi method for DS-CDMA systems," *IEEE Transactions on Wireless Communications*, vol. 4, no. 4, pp. 1594 – 1607, July 2005.

[78] A. Awada, B. Wegmann, I. Viering, and A. Klein, "Optimizing the radio network parameters of the Long Term Evolution system using Taguchi's method," *IEEE Transactions on Vehicular Technology*, vol. 60, no. 8, pp. 3825 –3839, October 2011.

[79] A. Hedayat, N. Sloane, and J. Stufken, *Orthogonal Arrays: Theory and Applications*. Springer Verlag New York, USA, 1999.

[80] A. Awada, B. Wegmann, I. Viering, and A. Klein, "A joint optimization of antenna parameters in a cellular network using Taguchi's method," in *IEEE Vehicular Technology Conference (VTC Spring 2011)*, Budapest, Hungary, May 2011, pp. 1–5.

[81] Energy Aware Radio and neTwork tecHnologies (EARTH). (January 2010 - June 2012) EU funded research project FP7-ICT-2009-4-247733-EARTH. [Online]. Available: https://www.ict-earth.eu

[82] L. Correia, D. Zeller, O. Blume, D. Ferling, Y. Jading, I. Gódor, G. Auer, and L. Van Der Perre, "Challenges and enabling technologies for energy aware mobile radio networks," *IEEE Communications Magazine*, vol. 48, no. 11, pp. 66 –72, November 2010.

[83] G. Auer, V. Giannini, C. Desset, I. Godor, P. Skillermark, M. Olsson, M. Imran, D. Sabella, M. Gonzalez, O. Blume, and A. Fehske, "How much energy is needed to run a wireless network?" *IEEE Wireless Communications*, vol. 18, no. 5, pp. 40 –49, October 2011.

[84] Green Touch Initiative. (August 2012). [Online]. Available: http://www.greentouch.org

[85] O. Blume, D. Zeller, and U. Barth, "Approaches to energy efficient wireless access networks," in *International Symposium on Communications, Control and Signal Processing (ISCCSP 2010)*, Limassol, Cyprus, March 2010, pp. 1 –5.

[86] S. Roth, J. Gan, and D. Danev, "Subframe allocation for relay networks in the LTE-Advanced standard," in *IEEE Personal Indoor and Mobile Radio Communications (PIMRC 2010)*, Istanbul, Turkey, September 2010, pp. 1758 – 1763.

[87] J. Han and H. Wang, "Uplink performance evaluation of wireless self-backhauling relay in LTE-Advanced," in *IEEE Wireless Communications Networking and Mobile Computing (WiCOM 2010)*, Chengdu, China, September 2010, pp. 1 –4.

[88] W. Hong, J. Han, and H. Wang, "Full uplink performance evaluation of FDD/TDD LTE-Advanced networks with Type-1 relays," in *IEEE Vehicular Technology Conference (VTC Fall 2011)*, San Francisco, USA, September 2011, pp. 1 –5.

[89] Motorola, "Relay performance evaluation with backhaul subframe dynamic partitioning and enhancement techniques - system simulations," 3GPP Technical Specification Group Radio Access Network Working Group 1, Tech. Rep. R1-102131, April 2010. [Online]. Available: http://www.3gpp.org/ftp/tsg_ran/WG1_RL1/TSGR1_60b/Docs/

[90] Panasonic, "Downlink relay performance evaluation," 3GPP Technical Specification Group (TSG) Radio Access Network Working Group 1 (RAN1), Tech. Rep. R1-101273, Feb. 2010. [Online]. Available: http://www.3gpp.org/ftp/tsg_ran/WG1_RL1/TSGR1_60/Docs/

[91] A. Bou Saleh, Ö. Bulakci, Z. Ren, S. Redana, B. Raaf, and J. Hämäläinen, "Resource sharing in relay-enhanced 4G networks," in *IEEE/VDE European Wireless Conference (EW 2011)*, Vienna, Austria, April 2011, pp. 1 –8.

[92] Z. Ren, *LTE-Advanced DL Performance Analysis considering Relay Link Bottleneck*. Bachelor's thesis, Technische Universität München, Munich, Germany, September 2010, (co-supervised by Ö. Bulakci).

[93] ZTE, "Simulation study on downlink RN to RN interference," 3GPP Technical Specification Group Radio Access Network Working Group 1, Tech. Rep. R1-102918, May 2010. [Online]. Available: http://www.3gpp.org/ftp/tsg_ran/WG1_RL1/TSGR1_61/Docs/

[94] A. Bou Saleh, Ö. Bulakci, S. Redana, B. Raaf, and J. Hämäläinen, "A divide-and-conquer approach to mitigate relay-to-relay interference," in *IEEE Personal International Symposium on Indoor and Mobile Radio Communications (PIMRC 2011)*, Toronto, Canada, September 2011, pp. 1889 –1893.

[95] A. Bou Saleh, Ö. Bulakci, S. Redana, B. Raaf, and J. Hämäläinen, "Addressing radio resource management challenges in LTE-Advanced relay networks: Downlink study," in *the 16. VDE/ITG Workshop on Mobile Communications*, Osnabrück, Germany, May 2011, pp. 39 –44.

[96] A. Bou Saleh, Ö. Bulakci, S. Redana, B. Raaf, and J. Hämäläinen, "Impact of relay-to-relay interference on the performance of LTE-Advanced relay networks," in *the 17. VDE/ITG Workshop on Mobile Communications*, Osnabrück, Germany, May 2012, pp. 13 –18.

[97] A. Khandekar, N. Bhushan, J. Tingfang, and V. Vanghi, "LTE-Advanced: Heterogeneous networks," in *IEEE/VDE European Wireless Conference (EW 2010)*, Lucca, Italy, April 2010, pp. 978 –982.

[98] J. Sangiamwong, Y. Saito, N. Miki, T. Abe, S. Nagata, and Y. Okumura, "Investigation on cell selection methods associated with inter-cell interference coordination in heterogeneous networks for LTE-Advanced downlink," in *IEEE/VDE European Wireless Conference (EW 2011)*, Vienna, Austria, April 2011, pp. 1 –6.

[99] S. Strzyz, K. Pedersen, J. Lachowski, and F. Frederiksen, "Performance optimization of pico node deployment in LTE macro cells," in *Future Network Mobile Summit (FutureNetw 2011)*, Warsaw, Poland, June 2011, pp. 1 –9.

[100] I. Guvenc, "Capacity and fairness analysis of heterogeneous networks with range expansion and interference coordination," *IEEE Communications Letters*, vol. 15, no. 10, pp. 1084 –1087, October 2011.

[101] I. Guvenc, M.-R. Jeong, I. Demirdogen, B. Kecicioglu, and F. Watanabe, "Range expansion and inter-cell interference coordination (ICIC) for picocell networks," in *IEEE Vehicular Technology Conference (VTC Fall 2011)*, San Francisco, USA, September 2011, pp. 1 –6.

[102] Z. Ren, A. Bou Saleh, Ö. Bulakci, S. Redana, B. Raaf, and J. Hämäläinen, "Joint interference coordination and relay cell expansion in LTE-Advanced networks," in *IEEE Wireless Communications and Networking Conference (WCNC 2012)*, Paris, France, April 2012, pp. 2874 –2878.

[103] Z. Ren, *Relay Cell Expansion and Interference Coordination in LTE-Advanced Systems*. Master's thesis, Technische Universität München, Munich, Germany, April 2011, (co-supervised by Ö. Bulakci).

[104] Technical Specification Group (TSG) Radio Access Network, "Mobile Relay for Evolved Universal Terrestrial Radio Access (E-UTRA) (Release 11)," 3GPP, Tech. Rep. TR 36.836 v1.0.0, May 2012. [Online]. Available: http://www.3gpp.org/ftp/Specs/archive/36_series/36.836

[105] S. Hämäläinen, H. Sanneck, and C. Sartori, *LTE Self-Organising Networks (SON): Network management automation for operational efficiency*. John Wiley & Sons Ltd., Chichester, UK, 2012.

[106] CMCC, “Relay performance evaluation,” 3GPP Technical Specification Group Radio Access Network Working Group 1, Miyazaki, Japan, Tech. Rep. R1-094041, October 2009. [Online]. Available: http://www.3gpp.org/ftp/tsg_ran/wg1_rl1/TSGR1_58b/Docs/

[107] P. Marsch and G. P. Fettweis, *Coordinated Multi-Point in Mobile Communications*. Cambridge University Press, Cambridge, UK, 2011.

[108] D. Lee, H. Seo, B. Clerckx, E. Hardouin, D. Mazzarese, S. Nagata, and K. Sayana, “Coordinated multipoint transmission and reception in LTE-advanced: deployment scenarios and operational challenges,” *IEEE Communications Magazine*, vol. 50, no. 2, pp. 148 –155, February 2012.

[109] X. Tao, X. Xu, and Q. Cui, “An overview of cooperative communications,” *IEEE Communications Magazine*, vol. 50, no. 6, pp. 65 –71, June 2012.

[110] ARTIST4G, “Enhancements to Type-1 Relay Implementation,” ARTIST4G deliverable, Tech. Rep. D3.5a v2.0.0, June 2012. [Online]. Available: https://ict-artist4g.eu/projet/deliverables

Errata

Publications VI, VIII, and XI

- Under Simulation Parameters, in the expression of LOS probability for the relay link channel model in suburban scenario, 1.15 should be replaced by 0.23.

  The error is a typo and does not have any effect on either the results or conclusions.

Publication XI

- In Fig. 3, the legend elements should be swapped, i.e., the gray curve corresponds to non-backhaul subframes.

  The error is a typo and does not have any effect on either the results or conclusions.

Relaying is a promising cost-efficient enhancement to existing mobile networks to fulfill the challenging coverage and capacity requirements. Yet, to fully exploit the potential benefits of relay deployments, proper radio resource management (RRM) is necessary. Also, the quality of the wireless backhaul is crucial for the end-to-end user performance. In this dissertation, relay site planning is first investigated as an effective means to improve the wireless backhaul substantially. Further, key RRM concepts with a particular focus on uplink system performance are developed and verified for relay deployments to ensure the expected performance enhancements. In particular, uplink power control optimization, resource sharing, and cell range extension techniques are investigated by taking 3GPP LTE-Advanced Type 1 relaying as a practical framework. Significant system performance improvements are shown while achieving a more ubiquitous user performance.

ISBN 978-952-60-5222-9
ISBN 978-952-60-5223-6 (pdf)
ISSN-L 1799-4934
ISSN 1799-4934
ISSN 1799-4942 (pdf)

Aalto University
School of Electrical Engineering
Department of Communications and Networking
www.aalto.fi

BUSINESS + ECONOMY

ART + DESIGN + ARCHITECTURE

SCIENCE + TECHNOLOGY

CROSSOVER

DOCTORAL DISSERTATIONS

Aalto-DD 103/2013